Synthesis and evaluation of D-cycloserine analogues against *Mycobacterium tuberculosis*

Dissertation presented for the degree of Master of Science

Department of Chemistry, University of Cape Town

by

Shoneeze Simone Renga

Supervisor: Prof. Kelly Chibale

Co-Supervisor: Dr Vinayak Singh

Department of Chemistry

University of Cape Town

Rondebosch, 7700

South Africa

January 2020

Declaration

I testify that the thesis titled **"*Synthesis and evaluation of D-cycloserine analogues against Mycobacterium tuberculosis*"** is my authentic work and has not been granted for the award for any degree at any university. I apprehend the meaning of plagiarism and declare that all the work in the dissertation, expect for that which is properly acknowledged, is my own.

Signed by candidate

Shoneeze S. Renga
January 2020

Acknowledgements

To my supervisors, Prof. Kelly Chibale and Dr Vinayak Singh, I would like to sincerely thank you for taking a chance on me. Your exceptional scientific guidance, mentorship, and friendship throughout this journey has helped shape and mould me into the researcher I am today. Your constant advice, patience, and belief in me helped me navigate through the constant challenges of this project. You have redefined what resilience and grit is for me. Ashante!

To my mentors Dickson Mambwe, Peter Cheuka, Antonina Wasuna, Tando Ntsabo, and Ronnet Sheldon, thank you for your time and patience in mentoring me. You have enhanced my skills as a medicinal chemist by teaching me the finer details of synthesis and assay techniques. You are examples of what belief, determination, and resilience can achieve. Thank you for making the lab a second home, a place filled with support, friends, and laughter.

A special thank you to Mrs Elaine-Rutherfoord, Mrs. Deidre Van Rooyen, Miss Saroja Naicker, and Miss Amina Sayed. Thank you for always being so willing to help and provide support. You have helped me to succeed on this journey, whether it was administrative or laboratory-related, to being a shoulder I could lean on when I wasn't sure of my own capabilities.

To the members of the academic group, thank you for your generosity, problem-solving ideas, and overall for creating an enjoyable working environment.

To my parents, thank you for always being my cheerleaders. Your unconditional love and support is unwavering. Lastly, to my partner Seamus Hennessy, your constant belief in my potential is enduring, thank you for helping me on this journey to achieve this milestone.

Conferences

American Society of Tropical Medicine and Hygiene, 68th Annual Meeting, Gaylord National Resort and Convention Center National Harbor, Maryland, USA, 20-24,November 2019.

Poster presentation: *Potential antimycobacterial pro-drugs of D-cycloserine*

Abstract

Tuberculosis (TB) continues to be the leading cause of death from a single infectious agent worldwide. The rapid emergence of multidrug-resistant and extremely drug-resistant underpin the urgent need for novel, safe and efficacious drugs. D-Cycloserine (DCS) is an oral bacteriostatic anti-tubercular drug used for the treatment of drug-resistant TB. Despite attractive properties, DCS displays significant toxicity at effective dosages. However, a synthetic analogue of DCS, terizidone, has shown an improved safety profile.

This study focused on the synthesis of two new classes of DCS analogues: isoxazolidin-3-one-imines (ISIs) and 3-isoxazolidin-4-yl amides (ISAs). These analogues were designed to act as potential prodrugs. In an effort to explore structure-activity-relationships, a total of 17 compounds were synthesized, fully characterized, and evaluated *in vitro* for their antimycobacterial activity against the drug-susceptible *Mtb* H37Rv strain cultured in 7H9/ADC media. Of these, two compounds displayed noteworthy antimycobacterial activity ($MIC_{99} \leq 10$ µM). In addition to this, all 17 compounds manifested low cytotoxicity ($IC_{50} > 25$ µM) when tested *in vitro* against the chinese hamster ovarian cells and the human hepatocytes cells. Furthermore, a selected potent compound displayed high microsomal metabolic stability in rat, mouse and human liver microsomes.

The kinetic solubility of the target compounds was determined using a HPLC-based method. The solubility data obtained was then correlated with melting point, tPSA and cLogP in order to establish structure-solubility relationships across the two compounds series. Solubility was strongly correlated to melting point in the IZAs series ($R^2 = 0.9318$) and moderately correlated to tPSA for IZIs ($R^2 = 0.164$, whereas there was no correlation between solubility and cLogP (lipophilicity) in either class of compounds ($R^2 = 0.085$ for IZIs and $R^2 = 0.0004$ for ISA).

Contents

List of Abbreviations

Alanine racemase	Alr
Analytical grade	AR
Antiretroviral drugs	ARVs
Central nervous system	CNS
Chinese hamster ovary	CHO
Correlation spectroscopy	COSY
Cytochrome P450	CYP 450
D-alanine:D-alanine ligase	Ddl
D-cycloserine	DCS
Dimethyl sulfoxide	DMSO
Directly observed treatment Short-Course	DOTS
Drug-susceptible TB	DTS-TB
Ethambutol	ETB
Extensively drug-resistant	XDR
Food & Drug Administration	FDA
Hertz	Hz
Heteronuclear single-quantum correlation	HSQC
High-performance liquid chromatography	HPLC
Human hepatic	Hep2G
Human immunodeficiency virus	HIV
Human liver microsomes	HLM
Isoniazid	INH
3-Isoxazolidin-4-yl amides	ISA
Isoxazolidine-3-one-imines	ISI
Latent tuberculosis infection	LTBI
Lipinski's rule of five	RO5
Mycobacterium smegmatis	*M. smeg*
Mass spectrometry	ms
Mechanism of action	MoA
Minimum inhibitory concentration	MIC
Mouse liver microsomes	MLM
Multi-drug resistant	MDR
M*ycobacterium tuberculosis*	*Mtb*
N-methyl-D-aspartate	NMDA

Nuclear magnetic resonance	NMR
Para-aminosalicylic acid	PAS
Pathogen-associated molecular patterns	PAMPS
Pharmacokinetic	PK
Phosphate-buffered saline	PBS
Pyrazinamide	PZA
Pyridoxal 5'-phosphate	PLP
Rat liver microsomes	RLM
Rifampicin	RIF
Simplified molecular-input line-entry system	SMILES
Standard operating procedures	SOPs
Streptomycin	STR
Structure-activity relationship	SARs
Structure-property relationship	SPRs
Thin-layer chromatography	TLC
Topological polar surface area	tPSA
Totally drug-resistant	TDR
Tuberculosis	TB
World Health Organization	WHO

List of Figures

List of Tables

List of Schemes

Chapter 1: Introduction and literature review

1.1 Chapter overview

This chapter provides an overview of tuberculosis (TB) and its current treatment, including its epidemiology, transmission, pathogenesis, challenges associated with current chemotherapy, as well as advances made in anti-TB drug discovery and development. In addition, D-cycloserine (DCS) and its structural derivative terizidone are discussed as these structural motifs form the basis of this work as potential scaffolds for anti-TB drug discovery. Lastly, a research program is presented, and the rationale, hypothesis, and specific aims are stated.

1.2 Epidemiology of TB

Tuberculosis (TB) is one of the oldest and deadliest infectious diseases plaguing mankind.[1,2] Its causative agent in humans is the airborne bacterium *Mycobacterium tuberculosis (Mtb)*. Among infectious diseases, TB remains a global pandemic as it is the leading cause of death from a single infectious agent worldwide, competing with human immunodeficiency virus (HIV).[3,4] According to the World Health Organization (WHO), one third of the world's population is infected with *Mtb* and 10 million people developed TB in 2018 with 1.4 million deaths globally (**Figure 1.1**).[4]

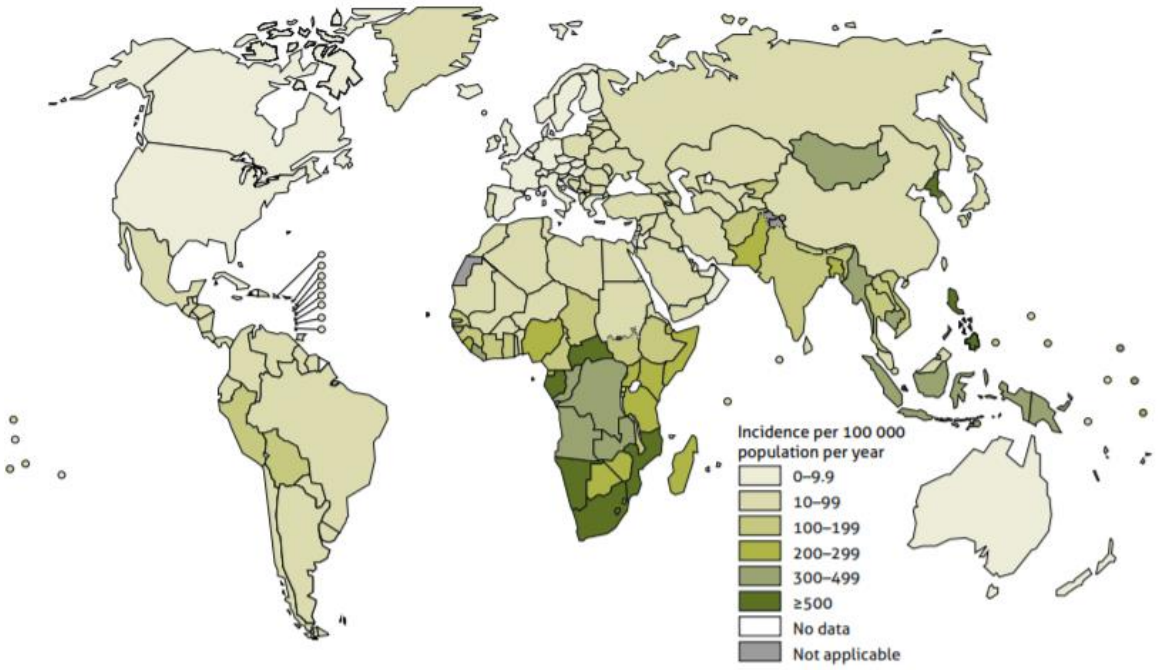

Figure 1.1: Estimated global tuberculosis (TB) incidence rates for 2018[4]

TB is the leading cause of death amongst TB/HIV co-infected patients worldwide, accounting for more than 0.4 million cases and 0.37 million deaths in 2018 (**Figure 1.2**).[3,4] Such cases of co-infection may occur in patients previously immune-compromised as a result of other epidemics such as HIV and diabetes, consequently increasing their risk of developing TB.[3,4] Although TB is a global concern, its geographical distribution is disproportionate as 87% of TB-related deaths were reported in developing countries, with countries in Asia (India, Indonesia, China, Philippines, and Pakistan) and Africa (Nigeria and South Africa) being the most affected.[4]

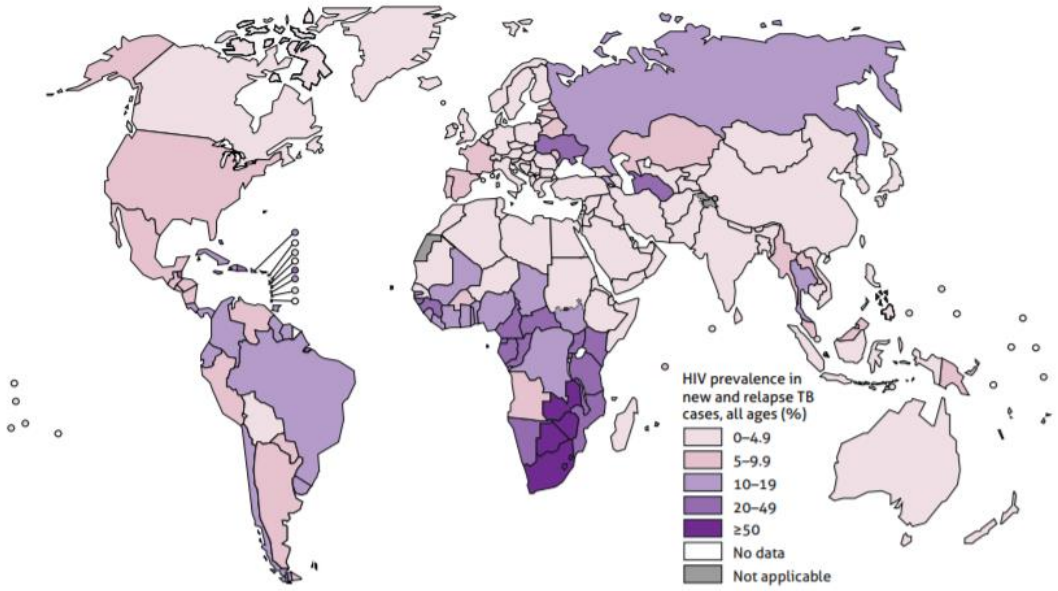

Figure 1.2: Estimated human immunodeficiency virus (HIV) prevalence in new and relapse tuberculosis (TB) cases in 2018[4]

1.3 Transmission and pathogenesis

TB is a communicable disease that is transmitted through coughing and sneezing by means of aerosols carrying infectious bacilli. Upon inhalation of these air droplets, the pathogen reaches the alveoli in the lungs, which is the primary site of infection (pulmonary TB).[4-6] It is from this point that bacteria may enter the bloodstream and infect other sites such as the lymphatic and genitourinary systems, bones and joints to cause extrapulmonary TB.[1] In the alveoli, *Mtb* bacilli are engulfed by the main phagocytic cells known as macrophages. These are prime defence cells against microbial intruders (**Figure 1.3**).[6] Infected macrophages induce a localized pro-inflammatory response to *Mtb,* and phagosome maturation takes place to eradicate the bacterial infection. However, *Mtb* has developed mechanisms to escape and survive within macrophages, thus differing from other mycobacterial infections.[1,6-7] Dendritic cells which are an important mediator between the innate and adaptive

immune response, also take up mycobacteria and mycobacterial fragments and can engulf mycobacterial antigens via receptor-mediated phagocytosis. Upon activation, dendritic cells migrate to the draining lymph nodes and prime naïve T cells (CD4+ & CD8+). This results in effector T-cells (CD+4, CD+8 and Regulatory T cells) migrating back to the site of infection in the lungs, and in combination with other leukocytes, stimulate the formation of granulomas.[1,6-7]

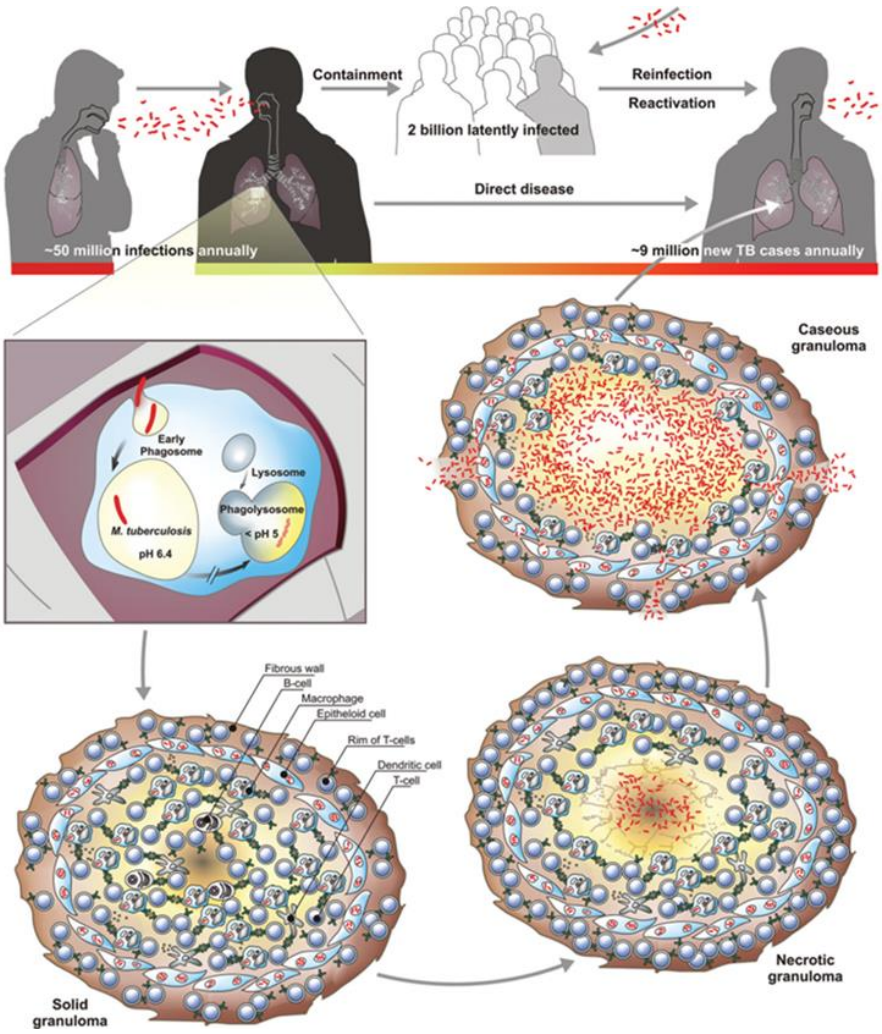

Figure 1.3: Transmission and pathology of tuberculosis (TB)[1]

Granulomas comprise concentric layers of infected macrophages in the core, surrounded by foamy macrophages (macrophage surrounded by the rim of lymphocytes and by a coat of fibroblast that encloses it) and foamy giant cells as well as activated T and B cells (**Figure 1.3**).[1,6] In 90% of cases, this interplay between the innate and adaptive immune responses serves to control the infection, but the patient will remain latently infected and thus at risk of reactivation.[6] However, in 10% of cases, the mycobacteria proliferate, resulting in the reduction and impaired function of CD4+ cells causing

macrophages to degrade and granulomas to become necrotic, thus resulting in the release of bacteria into the extracellular medium.[6,7]

In an immunocompetent individual, latent TB infection (LTBI) may persist for decades with no clinical symptoms of active TB.[1,6] However, during immunosuppression, *Mtb* may become metabolically active. There are approximately 2 billion people infected with LTBI who are therefore at risk of disease reactivation.[1,6] Children under the age of 5 years, the elderly, individuals recently exposed to active TB (recent contact of <2 years), those living in over-crowded places, who are being treated with immunosuppressants, or are HIV-positive are at a high risk of developing active TB. This includes individuals with silicosis, chronic renal failure, and those that are malnourished.[1,4,9] The symptoms of active TB include weight loss, poor appetite, night sweats, fever, productive or dry cough, and chest pain.[4]

1.4 Etiology of TB

TB is characterized as an aerobic, slow-growing, immobile, non-sporulating, weakly gram-positive, and acid-fast bacillus. As the Latin name suggests, the bacilli are slightly curved or straight rod-shaped organisms and are 1-4 µm in length and 0.3-0.6 µm in width (**Figure 1.4**).[1,8-9]

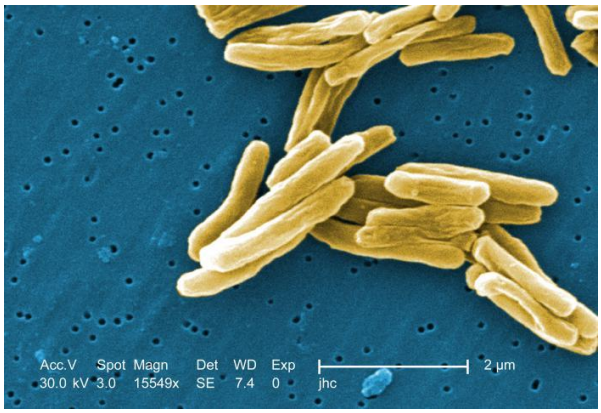

Figure 1.4: Scanning electron micrograph of *Mycobacterium tuberculosis*[10]

TB may also be caused in humans and animals by several other mycobacterial species, including *Mycobacterium bovis, Mycobacterium africanum, Mycobacterium microti,* and *Mycobacterium canetti*, which are collectively known as the mycobacterium complex.[11] Mycobacteria are thought to have originated from soil-dwelling ancestors and evolved as pathogens to both human and animal hosts during the domestication of animals 10 000 years ago.[1] *Mtb* is an extremely successful pathogen that has co-evolved with humans as specific hosts for thousands of years. This distinctive relationship

has uniquely shaped the mycobacterial genome to encode mechanisms that allow the bacilli to resist attack and elimination by the human immune system.[12] *Mtb*'s cell wall is unique in comparison to other prokaryotes as it comprises a G+C-rich genome, a distinctive structure composed of lipids, proteins, and carbohydrates, which are key for its survival. The cell wall is composed of peptidoglycans, arabinogalactans, and mycolic acids that are surrounded by a non-covalently linked outer capsule of proteins and polysaccharides (**Figure 1.5**).[13,14] This cell envelope is critical for the mycobacterium's physiology as numerous crucial processes occur in this compartment. These include the protection of bacterial cells from hostile environments, mechanical resistance of cells, transport of solutes or proteins, and adhesion to receptors.[15]

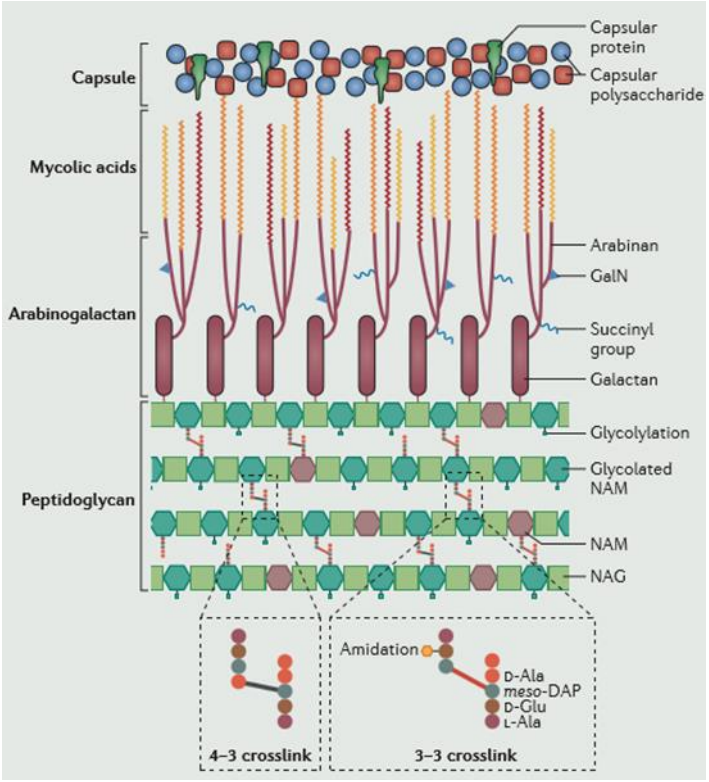

Figure 1.5: The mycobacterial cell wall, composed of three distinct macromolecules[12]
NAM, N-acetylmuramic acid; NAG, N-acetylglucosamine; DAP, diaminopimelic acid.

The hallmark of *Mtb* is its unusual abundance of lipids, which constitute 40% of the dry weight of the cell wall and include the exceptionally long-chain α-branched saturated fatty acids known as mycolic acids.[14] The mycolic acids are responsible for *Mtb*'s unusually thick waxy cell wall, whose unique characteristics such as acid-fastness against staining, hydrophobicity, resistance to drying, and resistance to varying acid/alkaline environments enable survival in its host.[4]

Lipids have been implicated in many of the biological properties of mycobacteria, as both structural and virulence factors that activate or supress the immune response.[11] For example, lipids may serve

as receptors for the invasion of macrophages and dendritic cells, prevent phagolysosome maturation enabling *Mtb* to survive within the macrophages, and mask pathogen-associated molecular patterns (PAMPS) on the cell to avoid toll-like receptor evading innate immunity. Lipids play a key role in enlisting proinflammatory cytokines that stimulate granuloma formation. Lastly, lipids enable *Mtb* to escape the adaptive immune response of the host by dendritic cell maturation and T-cell activation.[12]

Evidently, the remarkable success of *Mtb* as a human pathogen requires a sophisticated programme for control of host immune responses by the bacilli. In addition, and considering the evolutionary history of the *Mtb* genome, it is not surprising that immune evasion programmes expressed by this organism interfere with many of the known host innate and adaptive immune response pathways.[12] As *Mtb* remains a global public health concern, developing a more comprehensive understanding of immune evasion remains key in the quest for more effective vaccines and treatments for TB.

1.5 Anti-TB chemotherapy

Anti-TB chemotherapy development began in the 1940s with the discovery of streptomycin (STR) and *para*-aminosalicylic acid (PAS; **Figure 1.6**). Although it was effective in the short term, STR monotherapy was discontinued as many patients developed STR-resistant TB or experienced serious side effects such as loss of hearing.[3,5] Simultaneously, PAS was identified as a bacteriostatic agent against *Mtb,* including STR-resistant strains, and was able to prevent the development of STR resistance. PAS monotherapy was also shown to be effective against pulmonary TB.[8,11] Unfortunately, PAS resistance also developed, and the drug was poorly tolerated in patients leading to gastrointestinal side effects and occasional hepatitis. By the end of the 1940s, the standard treatment for TB was STR-PAS combined therapy, thus driving the shift from conventional monotherapies to novel combination therapy.[8,11]

When isoniazid (INH; **Figure 1.6**) was discovered in the 1950s, its anti-tubercular bactericidal activity was found to be more effective as part of combination treatment with STR and PAS than when administrated alone. This led to standardization of the first combination chemotherapy regimen. This triple drug therapy was shown to prevent the development of resistance to STR, INH, and PAS, and the entire course of treatment was extended to 18-24 months.[3,16] Several other antitubercular agents were discovered and developed in the 1950s, including pyrazinamide (PZA), cycloserine, ethionamide, prothionamide, and kanamycin (**Figure 1.6**). These drugs were originally only used in patients who did not respond to standard therapy, as these were thought to be inferior to the triple drug combination-based therapy.[3,17]

In the 1960s, the introduction of rifampicin (RIF; **Figure 1.6**) revolutionized anti-TB therapy as it shortened treatment from 18 to 9 months without increasing the relapse rate.[17] In addition, reintroducing PZA at a non-toxic, lower dosage than that previously used paved the way for the current, widely used regimen.[3,17]

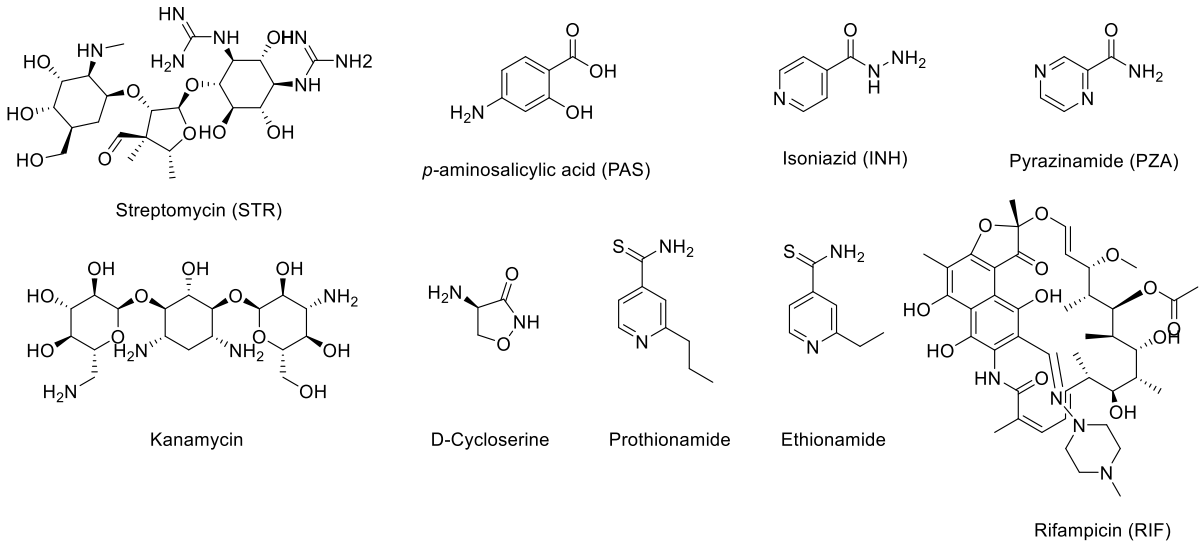

Figure 1.6: TB drugs introduced in 1940s, 1950s, and 1960s

1.5.1 Current anti-TB treatment

Current anti-TB treatment comprises drugs that can be classified according to their efficacy, potency, drug-class, and experience of use (**Table 1.1**). Anti-TB drugs are divided into first-line drugs (Group 1) and second-line drugs (Groups 2-5). First-line drugs are used to treat drug-susceptible TB (DS-TB), with the exception of STR which is classified as an injectable drug (Group 2), and second-line drugs are used for the treatment of drug-resistant TB. These are further divided into groups according to features such as cross-resistance.[18]

The paramount objectives for TB therapy are to: (*i*) shorten and simplify treatment for active, drug-sensitive TB, (*ii*) improve the efficacy, safety, and duration of treatment, (*iii*) improve the safety of combination therapy for patients co-infected with TB and other chronic diseases, and (iv) establish an effective therapy for LTBI.[3]

Table 1.1: First-line and second-line anti-TB drugs

Group	Drug type	Drugs

1	First-line oral agents	Isoniazid (INH), rifampicin (RIF), rifapentine, pyrazinamide (PZA), ethambutol (ETB), rifabutin
2	Injectable agents	Aminoglycosides: Kanamycin, amikacin, streptomycin (STR), Polypeptide: Capreomycin
3	Fluoroquinolones	Levofloxacin, moxifloxacin, ofloxacin, gatifloxacin
4	Oral bacteriostatic second-line agents	*p*-Aminosalicylic acid, cycloserine, terizidone, ethionamide, prothionamide
5	Drugs with limited efficacy or safety data	Bedaquiline, delamanid, clofazimine, linezolid, Amoxicillin/clavulanate, thioacetazone, meropenem, imipenem/cilastatin, clarithromycin

1.5.2 DS-TB therapy

Approximately 80-95% of patients diagnosed with pulmonary TB are infected with fully drug-susceptible *Mtb* strains.[4] To ensure optimal treatment of DS-TB and prevention of drug resistance, the WHO recommends application of the standardized chemotherapeutic treatment regime termed as the Directly Observed Treatment, Short-Course (DOTS; **Figure 1.7**). The regimen for new DS-TB cases under DOTS involves an intensive phase during which INH, RIF, PZA, and ETB are administrated daily for 2–4 months. During this phase, the bacilli are killed rapidly, and this is followed by a continuation phase to avoid relapse. The continuation phase comprises administration of INH and RIF in combination with some second-line drugs (**Figure 1.7**).[8,11,17]

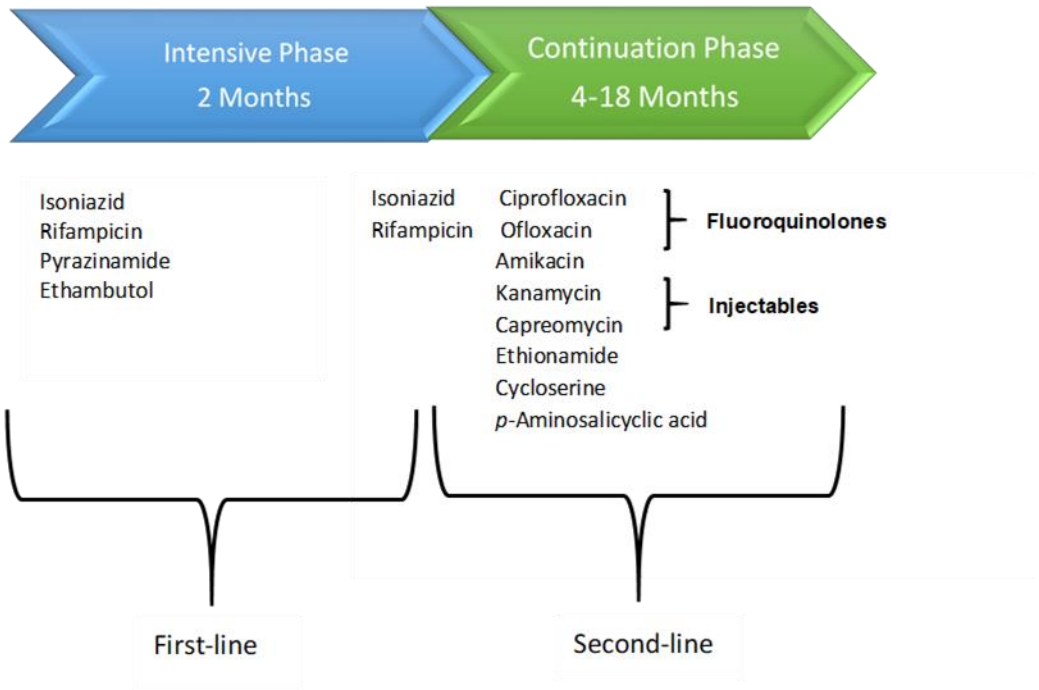

Figure 1.7: Summary of the current short anti-TB treatment regimen

There are three treatment plans available for HIV/TB co-infected patients. These include the administration of INH daily for 6 months, INH and RIF daily for 3 months, or INH and RIF twice weekly for 3 months.[5] However, drawbacks of this combination therapy include toxicity and intolerance,

which may lead to treatment interruption and regimen changes, drug-drug interactions with antiretrovirals in HIV co-infected patients, and consequent poor patient compliance, which has been associated with the development of drug resistance.[18]

1.5.3 Management of DS-TB

Although first-line drugs have been instrumental in the successful treatment and prevention of TB, drug resistance remains an issue. Drug-resistant TB may be classified as mono-resistant (resistance to a single first-line agent), multi-drug resistant (MDR-TB; resistance to INH and RIF), or extensively drug-resistant (XDR-TB, resistance to INH, RIF, any of the fluoroquinolones, and at least one of the three second-line injectable drugs). Strains that are resistant to all available first- and second-line drugs are termed totally drug-resistant (TDR-TB).[19]

The WHO recommends the use of five second-line drugs for the treatment of MDR-TB (**Figure 1.8**). The choice of drugs is based on susceptibility testing of *Mtb* against available drugs. In the absence of susceptibility results, the choice of the regimen is based on factors such as drug resistance patterns in the geographic area, previous drug exposure, presence of underlying medical conditions, and adverse effects associated with the drugs. Frequently used regimens include PZA (**Figure 1.6**), a fluoroquinolone, amikacin (**Figure 1.8**) or kanamycin (**Figure 1.6**), ethionamide/prothionamide (**Figure 1.6),** cycloserine (**Figure 1.6**), and PAS (**Figure 1.6**).[5,11,20]

Although an *M. bovis* Bacille Calmette-Guerin (BCG) vaccine is currently available, it is primarily used as a protective measure against paediatric TB, and is unfortunately not effective in preventing pulmonary TB in adults.[1]

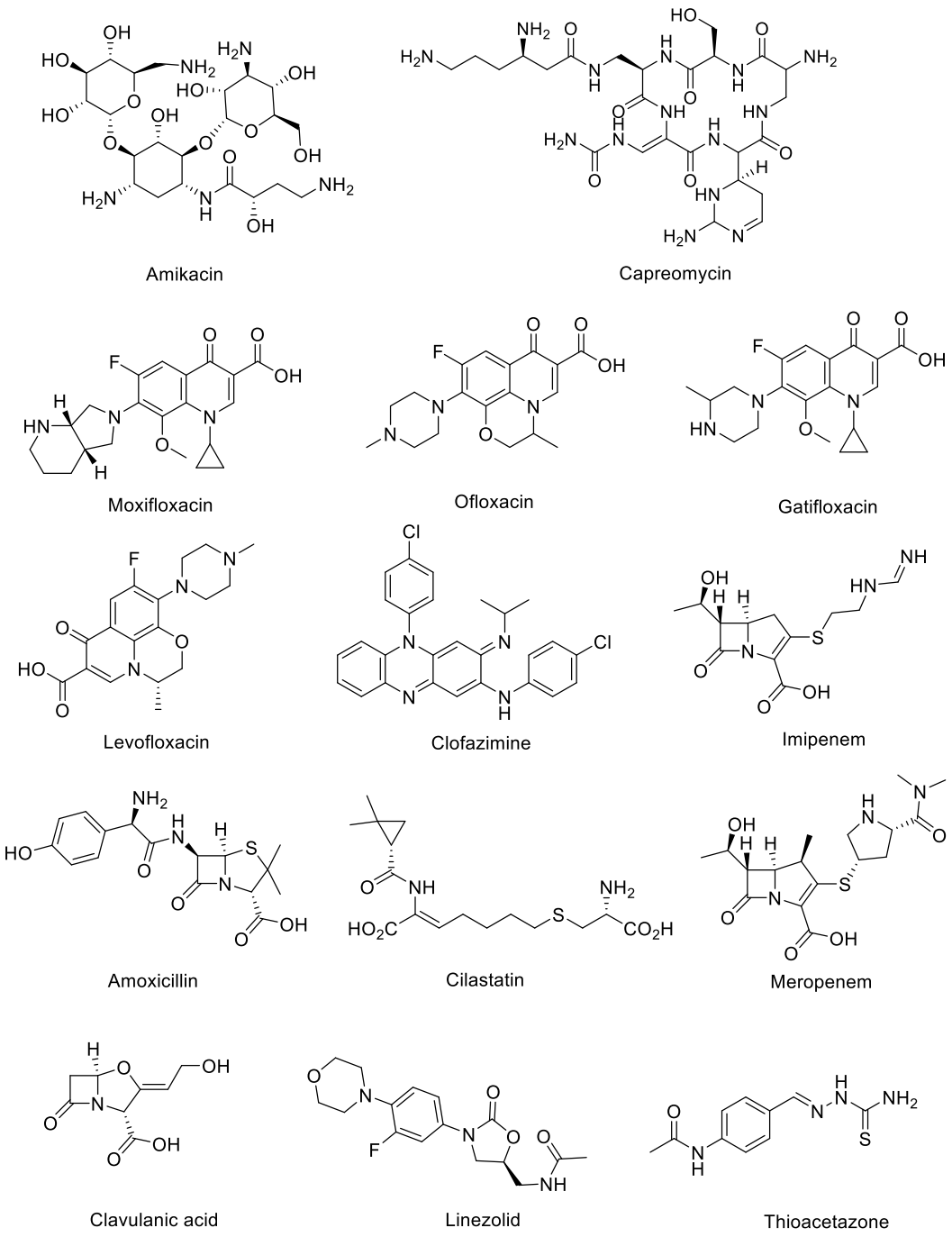

Figure 1.8: Second-Line anti-TB drugs

1.5.4 Present status and development of resistance globally

Extensive combination therapies were prescribed to limit the risk of developing resistance to every new agent, as seen through the history of clinical development of TB drugs. In the 1990s, the rate of relapse was high despite the introduction of both short-course chemotherapy and DOTS. This period was also marked by increasing numbers of mono- and multidrug-resistant TB cases.[8] There are two types of drug resistance: primary resistance occurs in a person who has been infected with a resistant

Mtb strain, and secondary resistance develops during therapy either through improper chemotherapy use or poor patient compliance relating to side effects from the cocktails of antibiotic therapies.[4,8] Outbreaks of drug-resistant strains (primary infected) occurred as early as the 1970s, and in the 1990s, there were numerous MDR-TB outbreaks in patients co-infected with HIV. This may be attributed to the fact that no viable treatment for HIV was available during this period, and HIV-positive patients were therefore more susceptible to TB infection. The development of MDR-TB in infected patients ultimately led to transmission of drug-resistant *Mtb*, first within institutions and hospitals and eventually the community.[8,20]

TB drug resistance may be ascribed to mutations that result in a loss of susceptibility to antibiotics. For example, INH's primary target is InhA, which encodes enoyl-ACP-reductase, a key enzyme for the production of mycolic acids. INH is a prodrug that requires bioactivation by *Mtb* catalase (KatG) to form an isonicotinic acyl radical.[20-22] INH resistance may therefore arise from a variety of mutations that can either affect INH activation by KatG, binding of INH to target InhA, or InhA expression. However, amino acid substitution at position 315 from serine to threonine (S315T) in KatG results in a high level of INH resistance, with full virulence.[22] Resistance to RIF may also be observed. This drug inhibits RNA polymerase at the level of the β-subunit encoded by the *rpoB* gene. Resistance to RIF is acquired because of a point mutation that is located predominantly in the 511-533 regions of the RpoB polypeptide. Approximately 95-98% of RIF resistance mutations are located in the 81-bp segment of *rpoB*.

Treatment of MDR-, XDR-, and TDR-TB requires the introduction of second-line drugs and use of repurposed agents such as fluoroquinolones. Unfortunately, these second-line drugs lack proven efficacy in untested combinations. In cases in which first- and second-line agents have failed because of extensive resistance, agents from the non-WHO-approved list of third-line agents may be used. However, there are minimal data to support the use of third-line agents apart from linezolid whose use is limited by toxicity and high cost.[8] Consequently, treatment of MDR-TB with poorly active second- and third-line drugs has led to the emergence of XDR-TB. Unfortunately, second- and third-line drugs for MDR- and XDR-TB are expensive, resulting in the failure of many low-resourced countries to afford treatment. This ultimately leads to non-compliance by patients, resulting in high transmission of MDR-TB strains in communities.[4,8]

1.5.5 Challenges associated with current TB chemotherapy

New anti-TB drugs are required because of the complexity, length, and toxicity of the current TB chemotherapy program. As previously mentioned, the incidence of MDR- and XDR-TB continues to

increase (**Figure 1.9**), and the next generation of anti-TB drugs should therefore inhibit new targets. Furthermore, there is growing awareness of the need for new anti-TB drugs to cure *Mtb* in different physiological states, including LTBI. It is estimated that one third of the world's population is infected with latent TB, which includes certain specific cases with paediatric TB (TB meningitis).[4,11,23]

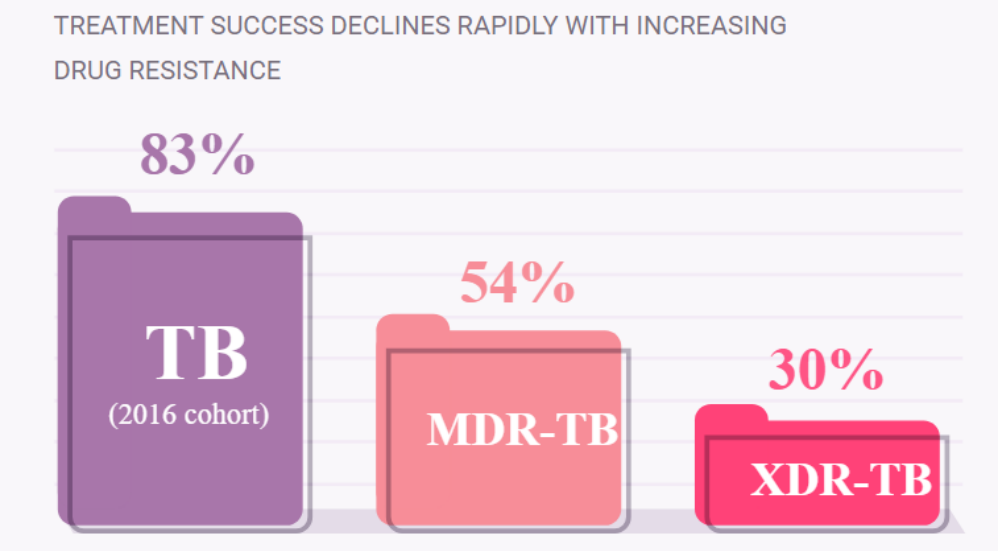

Figure 1.9 Proportion of MDR-TB and XDR-TB incidence in 2018[3,4]

Considering that the majority of highly TB-burdened countries are developing countries, there will always be a demand for inexpensive and easily accessible drugs. Therefore, new anti-TB drugs need to provide short, simpler, and affordable multi-drug regimens for DS-TB, and shorter, more effective, less toxic, and less expensive regimens for DR-TB.[17,20,23] Additionally, TB remains an opportunistic infection in an immunocompromised host. Therefore, patients who are co-infected with HIV or diabetes require new anti-TB drugs that cause fewer drug-drug interactions and are compatible with antiretroviral drugs (ARVs).[11,17,20] For example, RIF cannot be combined with the ARVs indicated in **Figure 1.10** because of unfavourable drug-drug interactions and additive toxicities. This is because RIF is a potent inducer of cytochrome P450 (CYP) enzymes, which are responsible for metabolizing ARVs to their inactive metabolites, thereby reducing effective serum concentration and exposure. Thus, co-infected patients are required to complete TB treatment first before initiating HIV treatment, which consequently fuels the dual epidemics.[8,21]

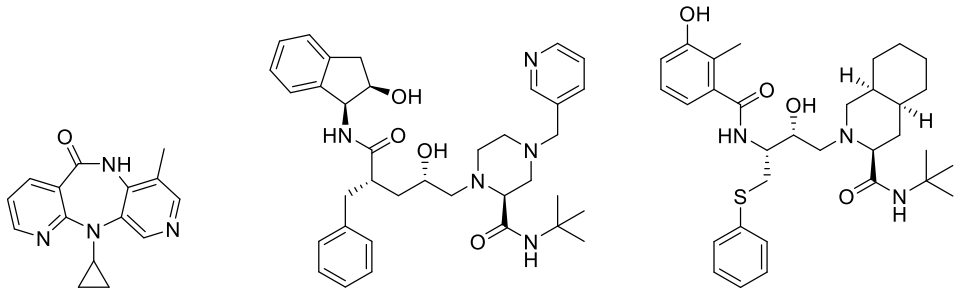

Figure 1.10: ARV drugs that show drug-drug interactions with RIF

1.5.6 Advances in the development of new anti-TB drugs

After half a century with no new anti-TB drugs developed, a promising pipeline has emerged during the last 5 years. The recent increase in TB drug portfolio is driven by the repurposing of old drugs, repositioning of existing anti-bacterial compounds, and discovery of new drug leads.[17] There are several candidates currently in preclinical and clinical development as potential anti-TB agents (**Figure 1.11**).[17]

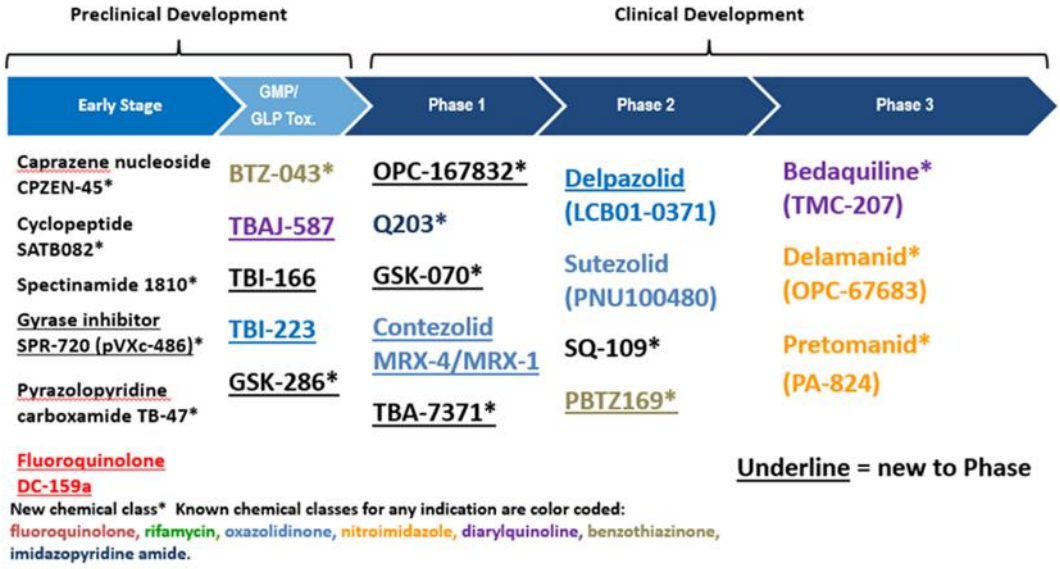

Figure 1.11 The global drug pipeline of new anti-TB drugs in preclinical and clinical development[23]

Bedaquiline (**Figure 1.12**), one of the most noteworthy compounds, is a bactericidal drug that belongs to the class of diarylquinolines.[21] Its mechanism of action (MoA) involves inhibition of mycobacterial

ATP synthase, an enzyme essential for energy generation. Although bedaquiline received accelerated approval from the United States Food & Drug Administration (FDA) in 2012, its development in clinical trials lasted 10–15 years.[22-23]

Bedaquiline was discovered through a whole-bacteria screening approach and early mouse studies suggested its treatment-shortening potential. This led to its progression to phase II studies, which showed that administration of bedaquiline in combination with drugs already used in the treatment of XDR-TB significantly reduced the sputum culture conversion time.[21-22] Bedaquiline was thus added to the existing drug treatment regimen for patients with extrapulmonary TB, pregnant women, HIV/TB co-infected patients, and adults with MDR-TB. Unfortunately, safety concerns were raised during phase IIb trials because of the unexplained higher mortality rate detected in the group treated with bedaquiline compared to that in the placebo group.[25-26]

Nitroimidazoles include two prodrugs: delamanid and pretomanid (**Figure 1.12**). These prodrugs are selectively active against both replicating and non-replicating *Mtb*. They are activated by deazaflavin-dependent nitroreductase enzyme and their MoA involves inhibition of *Mtb* cell wall synthesis and cell respiration. Delamanid has been approved for use by the FDA to treat MDR-TB in patients for whom no other effective tolerable treatment is available, and pretomanid is still currently in clinical trials.[27-28]

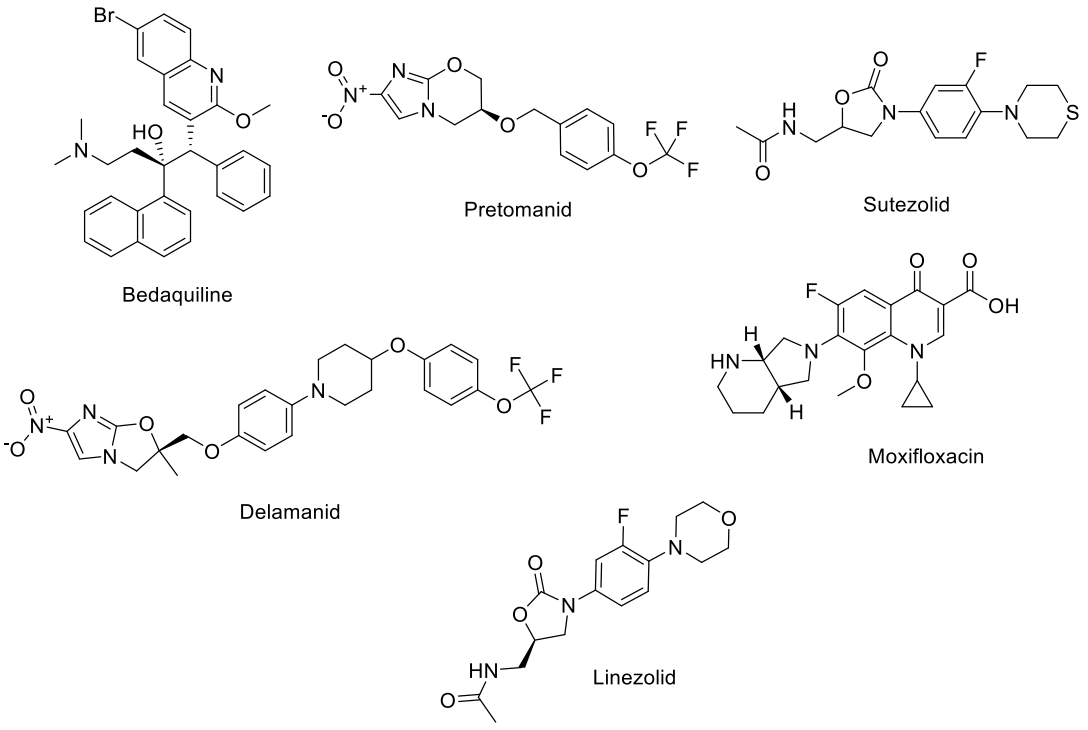

Figure 1.12 Chemical structures of new anti-TB drugs in clinical trials and those recently approved[22-28]

Oxazolidinones, such as linezolid and sutezolid, are repurposed agents. The MoA of these drugs is the inhibition of mycobacterial protein synthesis but also that of human mitochondria. However, the efficacy and toxicity of oxazolidinones are caused by similar mechanisms. Their usability in clinic therefore depends on differential effects on the bacteria in contrast to that in the human mitochondria.[29-30] Fortunately, linezolid has been used for the treatment of highly resistant TB for many years. In addition to this, a 2012 clinical trial clearly showed that linezolid activity improved when used in combination with other drugs for the treatment of MDR-TB.[31]

Other compounds that have been repurposed for the treatment of TB include fluoroquinolones, gatifloxacin, and moxifloxacin (**Figure 1.12**). These were originally developed for treatment of respiratory tract infections, and fluoroquinolones have been commonly used as second-line drugs for DR-TB as well as in patients who cannot tolerate first-line agents.

In summary, the past decade has seen some promising advances in the development of anti-TB drugs. However, there are some notable gaps in clinical development, as well as an insufficient number of drug candidates in the later stages of development. Therefore, there is an ongoing need to develop potent drugs that can combat the various limitations of the current regimens.

1.6 D-Cycloserine (DCS)

DCS (**Figure 1.6**) is an oral, bacteriostatic, second-line anti-tubercular drug that is primarily used for the treatment of MDR-TB.[1–3] In addition to this, DCS has been explored as a potential treatment agent for various neuropsychiatric conditions as it is a partial agonist of the glycine binding site of the *N*-methyl-D-aspartate (NMDA) receptor in the central nervous system (CNS).[5] DCS is a cyclic analogue of D-alanine, which is an essential amino acid for peptidoglycan synthesis.

DCS functions by competitively inhibiting two important enzymes in the alanine metabolic pathway: alanine racemase (Alr) and D-alanine:D-alanine ligase (Ddl). These two enzymes are essential for the biosynthesis of the peptidoglycan cell wall. Alr is key for the conversion of L-alanine to D-alanine, which combines with another D-alanine molecule to produce a dipeptide. This dipeptide is formed by Ddl and allows for further elongation to create the peptidoglycan cell wall (**Figure 1.13**).[33-35]

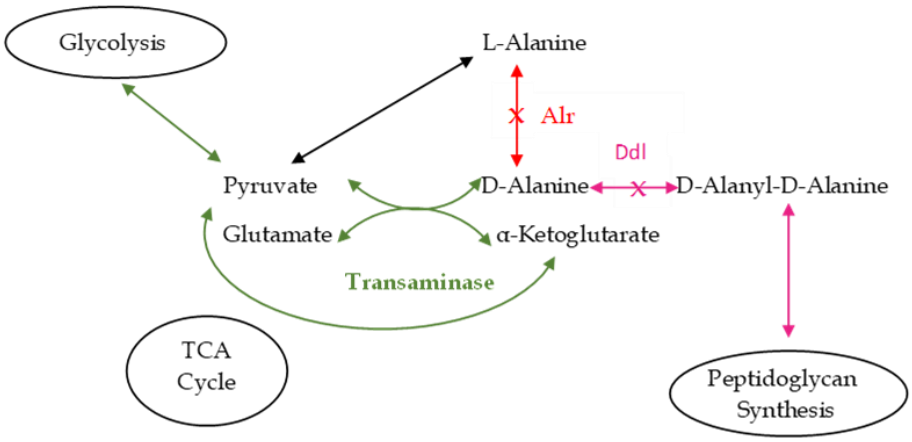

Figure 1.13: Schematic representation of pathways that synthesize D-alanine [33-35]

D-cycloserine (DCS) inhibits the primary pathway of D-alanine production (red) and inhibits D-alanine:D-alanine ligase (Ddl, pink) which ultimately inhibits peptidoglycan biosynthesis of the mycobacterial cell wall. Alr, alanine racemase; TCA cycle, tricarboxylic acid cycle.

As seen in **Figure 1.13**, *Mtb* encodes enzymes that synthesize branched-chain amino acids, thereby making these pathways attractive targets for the development of novel antibiotics. Specifically, the pyridoxal 5'-phosphate (PLP)-dependent transaminases perform the final biosynthetic step in the L-leucine, L-isoleucine, and L-valine pathways by producing chain amino acids from an α-keto acid precursor using chain amino acid transaminase. DCS has been shown to irreversibly inhibit bacterial D-amino acid transaminase and a recent study also showed that DCS inhibits *Mtb*'s branched-chain amino acid transaminase (MtIlvE).[35-36]

DCS is a noteworthy drug because, among its many advantages, it shows high gastric tolerability in comparison to other drugs within this group, as well as the absence of cross-resistance to other drugs in the treatment of DR-TB. However, just like other second-line anti-TB drugs, DCS displays significant toxicity. This ranges from relatively mild side effects such as dizziness, headaches, tremors, slurred speech, insomnia, anxiety, lethargy, and inability to concentrate, to more serious side effects including severe depression, psychosis, and seizures.[20,32,37] Nevertheless, DCS remains a cornerstone drug for the treatment of MDR- and XDR-TB, thus making this compound an attractive prototype for the development of novel antitubercular drugs.

Terizidone (**Figure 1.14**), a derivative of DCS, is a broad-spectrum antibiotic that shows great improvement of the disadvantages associated with DCS, such as an improved safety profile.[37] Terizidone acts as a pro-drug, which may be defined as a pharmacologically inactive form of a drug that is converted via hydrolysis or enzymatic action to the pharmacologically active form.

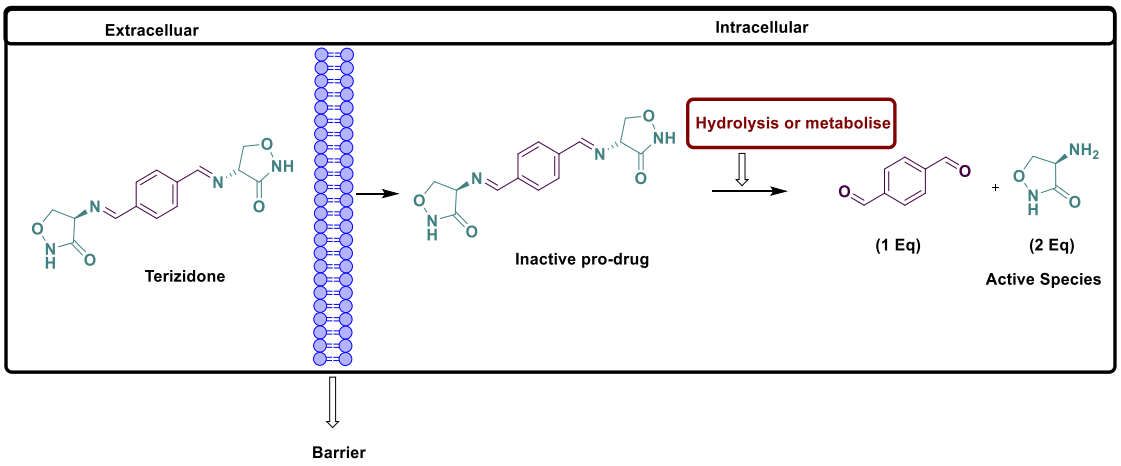

Figure 1.14: Hypothetical description of the probable pro-drug-based activity of terizidone[29]

1.7 Research program

1.7.1 Rationale

As shown in the literature review, there is an urgent need to develop novel anti-TB agents with enhanced potency, novel mechanisms of action, and improved safety and efficacy profiles against both DS and DR strains of *Mtb*. The literature review also highlighted the adequate space to study and investigate DCS analogues as potential anti-TB drug leads.

1.7.2 Hypothesis

To identify novel DCS-based anti-TB drug leads with favourable solubility, potency, and metabolic stability.

1.7.3 Objective

The overall objective of this work was to utilize DCS and its synthetic analogue terizidone as starting points for antimycobacterial structure-activity relationship (SAR) and structure-property relationship (SPR) studies for the target compounds.

1.7.4 Specific aims

Synthesize different sets of compounds: (i) DCS analogues and (ii) hybrid analogues combining DCS with other anti-TB drugs (**Chapter 2**).

Biologically evaluate the antimycobacterial potency, cytotoxicity, and in relevant cases microsomal stability of target compounds synthesized (**Chapter 3**).

Profile all final target compounds with respect to physicochemical properties and deduce SPRs (**Chapter 4**).

1.8 References

(1) Gengenbacher, M.; Kaufmann, S. H. E. Mycobacterium Tuberculosis: Success through Dormancy. *FEMS Microbiol. Rev.* **2012**, *36* (3), 514–532.

(2) Fogel, N. Tuberculosis: A Disease without Boundaries. *Tuberculosis* **2015**, *95* (5), 527–531.

(3) TB Alliance https://www.tballiance.org/ (accessed October 29, 2019).

(4) World Health Organization. *Global Tuberculosis Report 2018*.

(5) Stewart, G. R.; Robertson, B. D.; Young, D. B. Tuberculosis: A Problem with Persistence. *Nat. Rev. Microbiol.* **2003**, *1* (2), 97–105.

(6) Nunes-Alves, C.; Booty, M. G.; Carpenter, S. M.; Jayaraman, P.; Rothchild, A. C.; Behar, S. M. In Search of a New Paradigm for Protective Immunity to TB. *Nat. Rev. Microbiol.* **2014**, *12* (4), 289–299.

(7) Kinchen, J. M.; Ravichandran, K. S. Phagosome Maturation: Going through the Acid Test. *Nat. Rev. Mol. Cell Biol.* **2008**, *9* (10), 781–795.

(8) Marriner, G. A.; Nayyar, A.; Uh, E.; Wong, S. Y.; Mukherjee, T.; Via, L. E.; Carroll, M.; Edwards, R. L.; Gruber, T. D.; Choi, I.; et al. The Medicinal Chemistry of Tuberculosis Chemotherapy. In *BC Medical Journal*; 2011; Vol. 53, pp 47–124.

(9) Sakamoto, K. The Pathology of Mycobacterium Tuberculosis Infection. *Vet. Pathol.* **2012**, *49* (3), 423–439.

(10) Scanning electron micrograph of *Mycobacterium tuberculosis* https://phil.cdc.gov/phil/details.asp?pid=9997 (accessed Oct 28, 2019)

(11) Zumla, A.; Nahid, P.; Cole, S. T. Advances in the Development of New Tuberculosis Drugs and Treatment Regimens. *Nat. Rev. Drug Discov.* **2013**, *12* (5), 388–404.

(12) *Tuberculosis and the Tubercle Bacillus, Second Edition*; Jacobs, Jr., W. R., McShane, H., Mizrahi, V., Orme, I. M., Eds.; American Society of Microbiology, 2017.

(13) Kieser, K. J.; Rubin, E. J. How Sisters Grow Apart: Mycobacterial Growth and Division. *Nat. Rev. Microbiol.* **2014**, *12* (8), 550–562.

(14) Todar, K, Mycobacterium tuberculosis and Tuberculosis http://textbookofbacteriology.net/tuberculosis.html (accessed Oct 29, 2019).

(15) Chiaradia, L.; Lefebvre, C.; Parra, J.; Marcoux, J.; Burlet-Schiltz, O.; Etienne, G.; Tropis, M.; Daffé, M. Dissecting the Mycobacterial Cell Envelope and Defining the Composition of the Native Mycomembrane. *Sci. Rep.* **2017**, *7* (1), 1–12.

(16) Saltini, C. Chemotherapy and Diagnosis of Tuberculosis. *Respir. Med.* **2006**, *100* (12), 2085–2097.

(17) Zumla, A. I.; Gillespie, S. H.; Hoelscher, M.; Philips, P. P. J.; Cole, S. T.; Abubakar, I.; McHugh, T.

D.; Schito, M.; Maeurer, M.; Nunn, A. J. New Antituberculosis Drugs, Regimens, and Adjunct Therapies: Needs, Advances, and Future Prospects. *Lancet Infect. Dis.* **2014**, *14* (4), 327–340.

(18) Zumla, A.; Nahid, P.; Cole, S. T. *Nat. Rev. Drug Discov.* **2013**, *12* (5), 388–404.

(19) Zhang, Y.; Scorpio, A.; Nikaido, H.; Sun, Z. *J. Bacteriol.* **1999**, *181* (7), 2044–2049.

(20) Yuan, T.; Sampson, N. S. Hit Generation in TB Drug Discovery: From Genome to Granuloma. *Chem. Rev.* **2018**, acs.chemrev.7b00602.

(21) Sacchettini, J. C.; Rubin, E. J.; Freundlich, J. S. Drugs versus Bugs: In Pursuit of the Persistent Predator Mycobacterium Tuberculosis. *Nat. Rev. Microbiol.* **2008**, *6* (1), 41–52.

(22) Brossier, F.; Veziris, N.; Truffot-Pernot, C.; Jarlier, V.; Sougakoff, W. Performance of the Genotype MTBDR Line Probe Assay for Detection of Resistance to Rifampin and Isoniazid in Strains of Mycobacterium Tuberculosis with Low- and High-Level Resistance. *J. Clin. Microbiol.* **2006**, *44* (10), 3659–3664.

(23) TBFACTS.Org https://www.tbfacts.org/new-tb-drugs/ (accessed Oct 29, 2019).

(24) Working on New TB drugs https://www.newtbdrugs.org/pipeline/discovery (accessed Oct 27, 2019).

(25) Gualano, G.; Capone, S.; Matteelli, A.; Palmieri, F. New Antituberculosis Drugs: From Clinical Trial to Programmatic Use. *Infect. Dis. Rep.* **2016**, *8* (2), 43–49.

(26) Kakkar, A. K.; Dahiya, N. Bedaquiline for the Treatment of Resistant Tuberculosis: Promises and Pitfalls. *Tuberculosis* **2014**, *94* (4), 357–362.

(27) Manjunatha, U.; Boshoff, H. I. M.; Barry, C. E. The Mechanism of Action of PA-824. *Commun. Integr. Biol.* **2009**, *2* (3), 215–218.

(28) Lechartier, B.; Rybniker, J.; Zumla, A.; Cole, S. T. Tuberculosis Drug Discovery in the Post- Post-Genomic Era. *EMBO Mol. Med.* **2014**, *6* (2), 1–11.

(29) Islam, M. M.; Hameed, H. M. A.; Mugweru, J.; Chhotaray, C.; Wang, C.; Tan, Y.; Liu, J.; Li, X.; Tan, S.; Ojima, I.; et al. Drug Resistance Mechanisms and Novel Drug Targets for Tuberculosis Therapy. *J. Genet. Genomics* **2017**, *44* (1), 21–37.

(30) Villemagne, B.; Crauste, C.; Flipo, M.; Baulard, A. R.; Déprez, B.; Willand, N. Tuberculosis: The Drug Development Pipeline at a Glance. *Eur. J. Med. Chem.* **2012**, *51*, 1–16.

(31) Lee, M.; Lee, J.; Carroll, M. W.; Choi, H.; Min, S.; Song, T.; Via, L. E.; Goldfeder, L. C.; Kang, E.; Jin, B.; et al. Linezolid for Treatment of Chronic Extensively Drug-Resistant Tuberculosis. *N. Engl. J. Med.* **2012**, *367* (16), 1508–1518.

(32) Halouska, S.; Fenton, R. J.; Zinniel, D. K.; Marshall, D. D.; Barletta, R. G.; Powers, R. Metabolomics Analysis Identifies D-Alanine-D-Alanine Ligase as the Primary Lethal Target of D-

Cycloserine in Mycobacteria. *J. Proteome Res.* **2014**, *13* (2), 1065–1076.

(33) Desjardins, C. A.; Cohen, K. A.; Munsamy, V.; Abeel, T.; Maharaj, K.; Walker, B. J.; Shea, T. P.; Almeida, D. V; Manson, A. L.; Salazar, A.; et al. Genomic and Functional Analyses of Mycobacterium Tuberculosis Strains Implicate Ald in D-Cycloserine Resistance. *Nat. Genet.* **2016**, *48* (5), 544–551.

(34) David, S. Synergic Activity of D-Cycloserine and Beta-Chloro-D-Alanine against Mycobacterium Tuberculosis. *J. Antimicrob. Chemother.* **2001**, *47* (2), 203–206.

(35) Amorim Franco, T. M.; Favrot, L.; Vergnolle, O.; Blanchard, J. S. Mechanism-Based Inhibition of the Mycobacterium Tuberculosis Branched-Chain Aminotransferase by D - And L -Cycloserine. *ACS Chem. Biol.* **2017**, *12* (5), 1235–1244.

(36) Tremblay, L. W.; Blanchard, J. S. The 1.9 Å Structure of the Branched-Chain Amino-Acid Transaminase (IlvE) from Mycobacterium Tuberculosis. *Acta Crystallogr. Sect. F Struct. Biol. Cryst. Commun.* **2009**, *65* (11), 1071–1077.

(37) Hwang, T. J.; Wares, D. F.; Jafarov, A.; Jakubowiak, W.; Nunn, P.; Keshavjee, S. Safety of Cycloserine and Terizidone for the Treatment of Drug-Resistant Tuberculosis: A Meta-Analysis. *Int. J. Tuberc. Lung Dis.* **2013**, *17* (10), 1257–1266.

Chapter 2: Design and synthesis of derivatives

2.1 Chapter overview

In this chapter, the concept of hybrid molecules and prodrugs is briefly outlined and the design, synthesis, and spectroscopic characterization of D-cycloserine (DCS) derivatives are presented.

2.2 Introduction

DCS (**Figure 2.1A**) is a natural product derived from *Streptomyces orchidaceous* and *Streptomyces garyphalus* that was first isolated in the 1950s.[1–3] DCS is a cyclic analogue of the amino acid D-alanine (**Figure 2.1B**), which is an essential metabolite for peptidoglycan synthesis. DCS is a broad-spectrum agent that is active against both gram-positive and -negative bacteria and is primarily used to treat MDR-TB.[4] DCS interferes with bacterial cell wall synthesis by competitively inhibiting the enzymes L-alanine racemase and D-alanine:D-alanine ligase (Ddl), thereby inhibiting peptidoglycan formation in the cell wall of *Mtb*.[1,2,5]

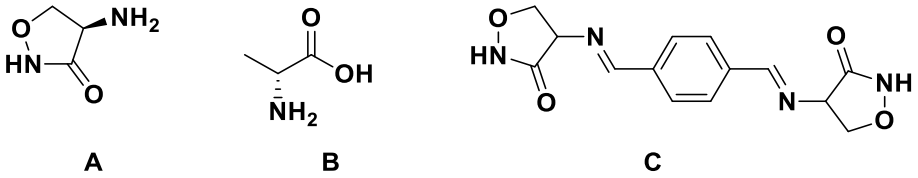

Figure 2.1: Chemical structures of D-cycloserine (**A**), D-alanine (**B**), and terizidone (**C**)[1-3,8]

Like other second-line anti-TB drugs, DCS displays significant toxicity. This ranges from relatively mild side effects such as dizziness, headaches, tremors, insomnia, and anxiety to severe depression and psychosis. Thus, the propensity of DCS to cause profound neuropsychiatric side effects and the limited data available showing its efficacy against *Mtb* mean that it is often used as a last-line treatment option. However, despite these drawbacks, the emergence of MDR-TB and extensively drug-resistant TB (XDR-TB) has rendered its use in TB treatment necessary.[3,7,8] Conversely, terizidone (**Figure 2.1C**), a derivative of DCS, is a broad-spectrum antibiotic with a greatly improved safety profile compared to that of DCS.[8] Nevertheless, DCS remains a cornerstone drug for the treatment of MDR-TB and XDR-TB, thus making this compound an attractive prototype for the development of novel antitubercular drugs.

2.3 Design of DCS derivatives

2.3.1 Prodrugs

Prodrugs are inactive, bio-reversible derivatives of drug molecules designed to undergo *in vivo* enzymatic and/or chemical transformation to release the active parent drug, which then exerts the desired pharmacological effect at efficacious levels.[9-12] Prodrugs represent a widely used strategy for enhancing the pharmacokinetic, physicochemical, and biopharmaceutical properties of pharmacological agents in drug discovery and development.[14-15] The prodrug approach has been successfully applied to a wide variety of drugs and it is estimated that 10% of drugs currently marketed worldwide can be classified as prodrugs.12 Some of the undesirable properties that have been successfully addressed by using a prodrug approach include low bioavailability, formulation challenges, and poor drug delivery such as low aqueous solubility, poor oral absorption, rapid metabolism, and toxicity.[8,12,16-17]

2.3.2 Classification of prodrugs

Generally, prodrugs only require one or two chemical and/or enzymatic biotransformation processes to yield the pharmacologically active compound (**Figure 2.2**).[17]

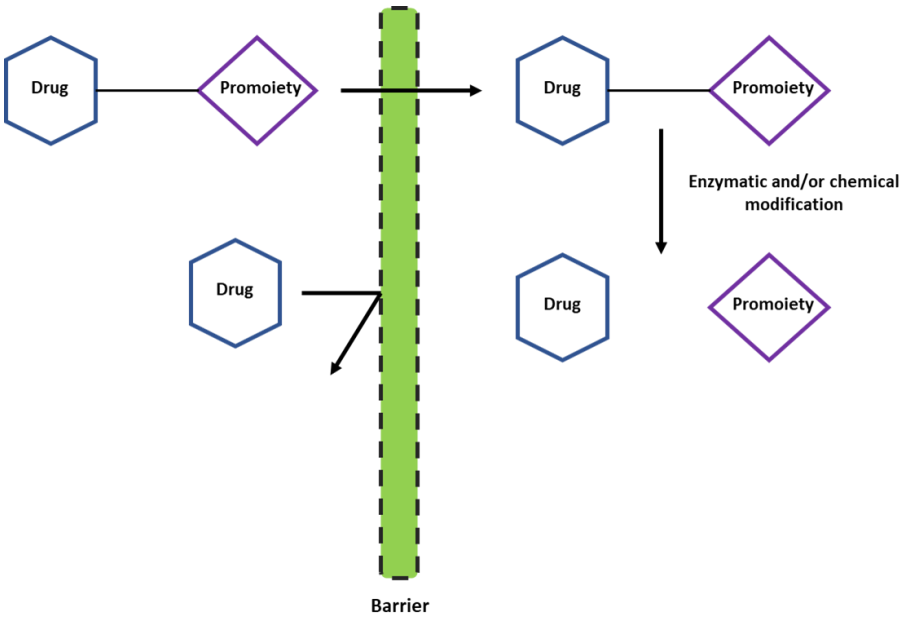

Figure 2.2: Illustration of the prodrug concept (adapted from Rautio *et al.* 2008)[17]

Prodrugs are classified according to derivatization and the type of carrier attached to the drug. Therefore, prodrugs can be classified into two categories: carrier-linked prodrugs and bioprecursors. In carrier-linked prodrugs, the promoiety is covalently linked to the active drug but can easily be cleaved enzymatically or non-enzymatically to furnish the parent drug.[18] Bioprecursor drugs result

from modification of the active drug itself, yielding a novel compound that is subsequently chemically or enzymatically converted to the active metabolite.[17] An important factor to be considered in prodrug design is the presence of functional groups in the molecule that are predisposed to chemical prodrug derivatization. Generally, the most commonly used functional groups are hydroxyl, carboxylic acid, amine, and phosphonate groups.[17] The modification of these groups produces esters, amides, carbonates, and phosphate group prodrugs among others.[17]

The use of amides as prodrugs is less common, owing to their relatively high enzymatic stability *in vivo*. However, amides are often used to enhance oral absorption and in the synthesis of specific intestinal uptake transporter substrates.[10,17] Once administrated, the amide bond is hydrolysed by ubiquitous carboxylesterases, peptidases, or proteases.[19] An example of a clinically used amide prodrug is the anti-TB agent pyrazinamide (PZA). PZA undergoes enzymatic hydrolysis as it is a substrate of mycobacterial and host amidase, which hydrolyses it to pyrazinoic acid (POA), the pharmacologically active moiety.[20]

In contrast, esters are the most common prodrugs and are estimated to make up 49% of all marketed prodrugs.[14] Ester prodrugs are often used to enhance the lipophilicity and thus membrane permeability of hydrophilic drugs by masking charged groups such as carboxylic acids and phosphates.[17,21] Once administered, the ester bond is hydrolysed by ubiquitous carboxylesterases, acetylcholinesterases, or arylesterases to the respective alcohol and carboxylic acid. An example of a clinically used ester prodrug is the enzyme (ACE) inhibitor enalapril, which exhibits improved bioavailability.[17] Examples of ester and amide prodrugs are listed in **Table 2.1**.

Table 2.1: Examples of prodrugs[14,17,20]

Prodrug name	Functional group	Structure	Pharmacologically active metabolite/moiety
Pyrazinamide	Amide of pyrazinamide	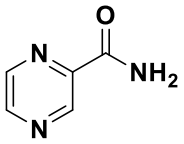	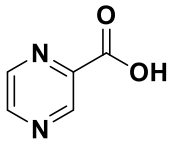
Enalapril (angiotensin-converting enzyme inhibitor)	Monoethyl ester of enalapril	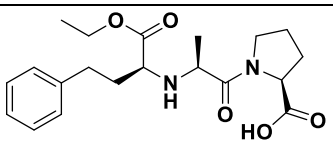	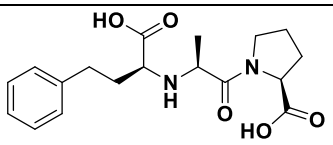

2.3.3 Hybrid drugs

A hybrid compound is a compound that has been chemically modified by combining two or more pharmacophoric units of different known bioactive molecules, either directly or via a linker, to form a single chemical entity.[22] Hybrid molecules offer several advantages over combination therapy and single molecules. Drug hybrids have the potential to reduce the emergence and spread of resistance to treatment by combining two pharmacophores that exert dual or multiple drug action into a single chemical entity with different modes of action.[23-25] These combinations may lead to synergistic effects, resulting in an increased potency. Physicochemical properties (e.g., solubility and permeability) can be improved by incorporating moieties with the desired properties.[23-25] Drug interactions leading to synergy may result from a simple uptake effect, as the increased permeability of one drug may cause accumulation of the other, thus improving treatment efficacy. This uptake effect has been shown in interactions between aminoglycosides and β-lactam antibiotics.[26] In addition, it is possible to impart selectivity for a drug target such as a receptor. For example, the anti-cancer hybrid drug estramustine was designed to selectively deliver toxic mustard to cancer cells by binding to steroid receptors on prostate tumours.[27] Lastly, hybrid molecules are able to overcome the additive toxic effects of individual drugs with the added convenience of a single formulation, thus improving overall patient adherence at a potentially lower cost.[23,28]

2.3.4 Classification of hybrid drugs

Hybrid molecules may be classified into three distinct groups: (i) cleavable, (ii) non-cleavable, and (iii) merged or overlapping hybrids (**Figure 2.3**). Cleavable hybrids are covalently linked directly or indirectly through a spacer devised to be hydrolysed, usually enzymatically. These linkers are generally esters, amides, or carbamates. Upon hydrolysis, the two bioactive motifs are expected to elicit their pharmacological effects individually.[27] Non-cleavable hybrid molecules are covalently linked but differ from cleavable hybrids as they are designed to retain their biological activities in their single hybrid forms. In contrast, merged or overlapping hybrids are designed by overlapping the common structural motifs of two or more pharmacophores and elicit a pharmacological effect that is distinct from that of the original molecules.[27]

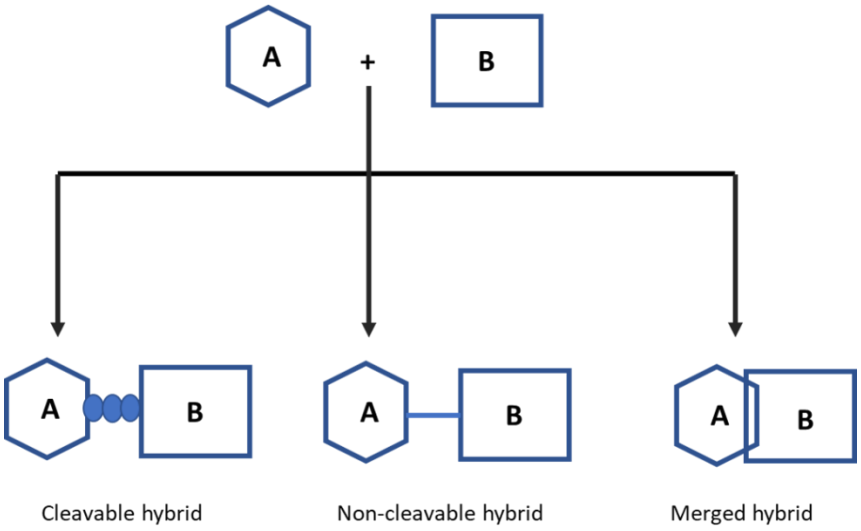

Figure 2.3: Classification of hybirds[27]

2.4 Design and rationale of DCS derivatives

The efficacy of a drug is determined by its various physiochemical properties including absorption, distribution, mechanism of interaction between the drug and its cellular target, metabolism, excretion, and toxicity. Lipophilicity and solubility are two key factors that affect both the extent and rate of drug absorption.[28] TB treatment is further challenged by the existence of a barrier called the caesium, a necrotic and hydrophobic ring that consists chiefly of immune cells such as macrophages and neutrophils encasing the bacilli.[29-30] This presents the added challenge of drug penetration into the necrotic lesions where persistent bacilli reside, requiring a hydrophobic/hydrophilic balance to achieve an effective concentration for antimycobacterial activity.[29,31]

As discussed, DCS's main liability is it toxicity. However, its structural analogue terizidone has shown improved potency and reduced toxicity. Although the discovery of terizidone was serendipitous, it functions and behaves similarly to a prodrug. Therefore, it was hypothesized that introducing a lipophilic carrier to DCS may produce a new entity with the same metabolic fate as terizidone. This was hypothesized to consequently potentially reduce toxicity while maintaining and/or enhancing the potency of DCS. In order to explore this class of compounds, structural changes around DCS were proposed. A variety of analogues were selected based on this, resulting in two points of diversity, **SAR 1** and **SAR 2**, whilst the DCS core scaffold remains fixed (**Figure 2.4**).

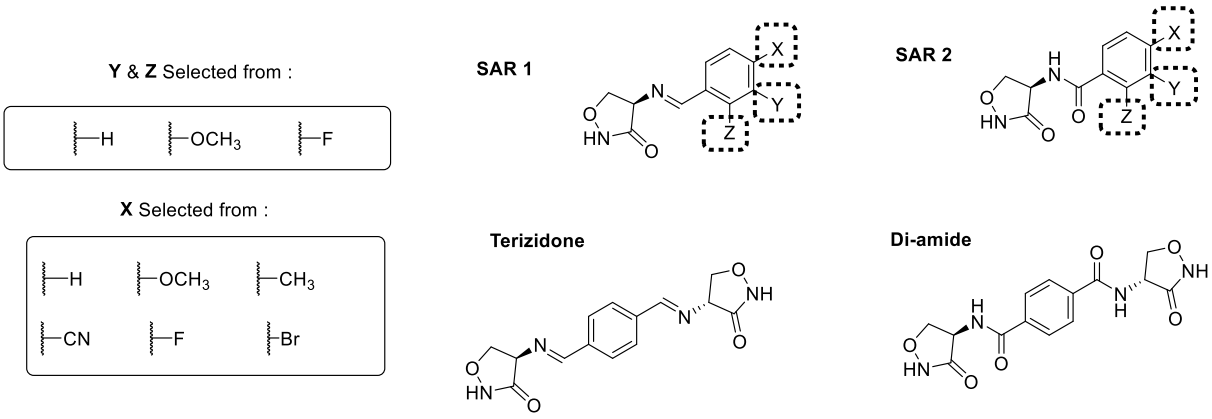

Figure 2.4: Chemistry plan for the synthesis of D-cycloserine analogues

Inspired by the structure of terizidone, a prodrug approach was employed to synthesize DCS-mono- and di-amide derivatives as well as DCS-imine derivatives. This involved the introduction of one or two units of DCS covalently linked by an inert carrier group with the hypothesis that they would be metabolized to DCS through *in vivo* hydrolysis by *Mtb* enzymes and/or host enzymes.

Desired chemical and biological properties may be obtained by manipulating the compounds' physicochemical properties using a Craig plot (**Figure 2.5**). A Craig plot predicts the correlation between the physicochemical properties of a drug and its biological activity through a graph of the hydrophobic character (π) of a substituent and its electronic effects (Hammett substitution, σ).[32] Therefore, to create structural diversity, different X, Y, and Z substituents from the four quadrants of the Craig plot were used in both **SAR 1** and **SAR 2**.

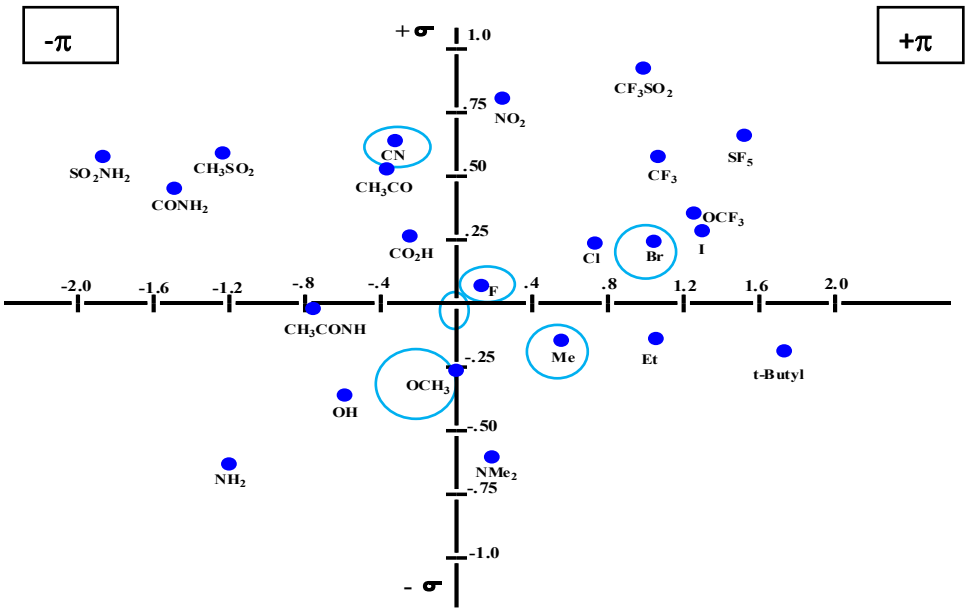

Figure 2.5: Craig plot capturing substituents **X**, **Y**, and **Z**

Additionally, amide derivatives including the prodrug PZA and the DCS moiety were also designed. Similarly, the compound **NITD S5** (**Figure 2.6**) was covalently coupled to the DCS moiety to generate amide prodrug-like derivatives. The prodrug PZA (**Table 2.1**) and **NITD S5** (**Figure 2.6**) were chosen because of their high potency against *Mtb*. As discussed, the active metabolite of PZA is POA, which is secreted by a weak efflux pump and is converted to the protonated conjugate acid. This protonated conjugate acid may re-enter the cell and accumulate as a result of inefficiency of the efflux pump in removing the drug, thus causing non-specific damage to the bacillus.

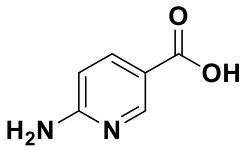

NITD S5

in vitro antimycobacterial activity
(MIC_{99}) = 2.5 µM

Figure 2.6: Chemical structure and biological activity of the hit compound **NITD S5.**
MIC_{99}: minimum inhibitory concentration causing 99% inhibition.

It is for this reason that hybrid approaches were considered to combine both PZA and **NITD S5** with DCS, based on the hypothesis that once administered, these would release DCS, POA, and **NITD S5** as active metabolites *in vivo.*

2.5 Synthesis and characterization of D-CS derivatives

2.5.1 Synthesis of SAR 1 target compounds

The novel (with an exception of compound **1.1**) isoxazolidine-3-one-imines were synthesized using the procedure described by Ernst Felder *et al.,*[33] with modifications. The target compounds were furnished by a Schiff base-type condensation between the commercially available relevant aldehyde and an excess of DCS (Scheme 2.1). The reactions were carried out under reflux in methanol, affording the desired products (**1.1-1.11**) in low to high yields (4-88%) without the use of column chromatography for purification (**Table 2.2**). Compounds were characterized via nuclear magnetic resonance (NMR) and mass spectrometry, and their melting points determined.

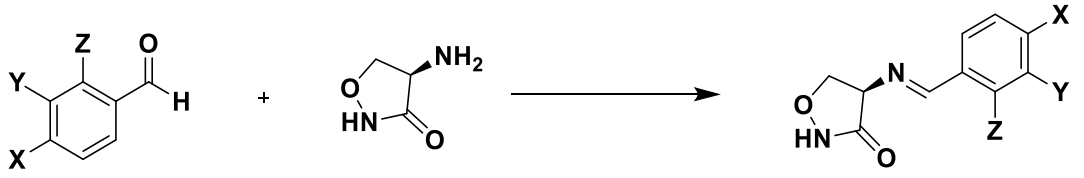

Scheme 2.1: General synthetic protocol of isoxazolidin-3-one-imines

Reagents and conditions: methanol, 65 °C, 10 min, 4-88 %

Table 2.2: Isolated yields of isoxazolidine imines

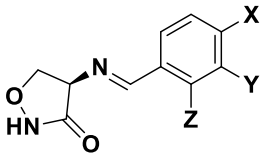

Compound Code	X	Y	Z	% Yield
1.1	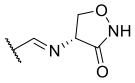	H	H	88
1.2	H	H	H	20
1.3	CH_3	H	H	35
1.4	CN	H	H	10
1.5	OCH_3	H	H	59
1.6	H	OCH_3	H	4
1.7	H	H	OCH_3	47
1.8	H	F	H	44
1.9	F	H	H	41
1.10	H	H	F	49
1.11	Br	H	H	28

2.5.2 Mechanistic details and spectroscopic analyses of SAR 1 target compounds

For mechanistic purposes, compound **1.5** will be used as an illustrative example. The formation of target compound **1.5** (**Figure 2.7**) is initiated by nucleophilic attack of DCS's amino nitrogen onto the electron-deficient carbonyl carbon of *p*-anisaldehyde. This is followed by a proton transfer step between the amine and the negatively charged oxygen. Subsequently, abstraction of an acidic methanolic proton occurs, resulting in the protonation of the hydroxyl group, thus making it a stronger leaving group. Intramolecular elimination of a water molecule results in the formation of an iminium ion intermediate. Lastly, a deprotonation step of the iminium yields final targets **1.1-1.11** maintaining the original chirality of the analogues.

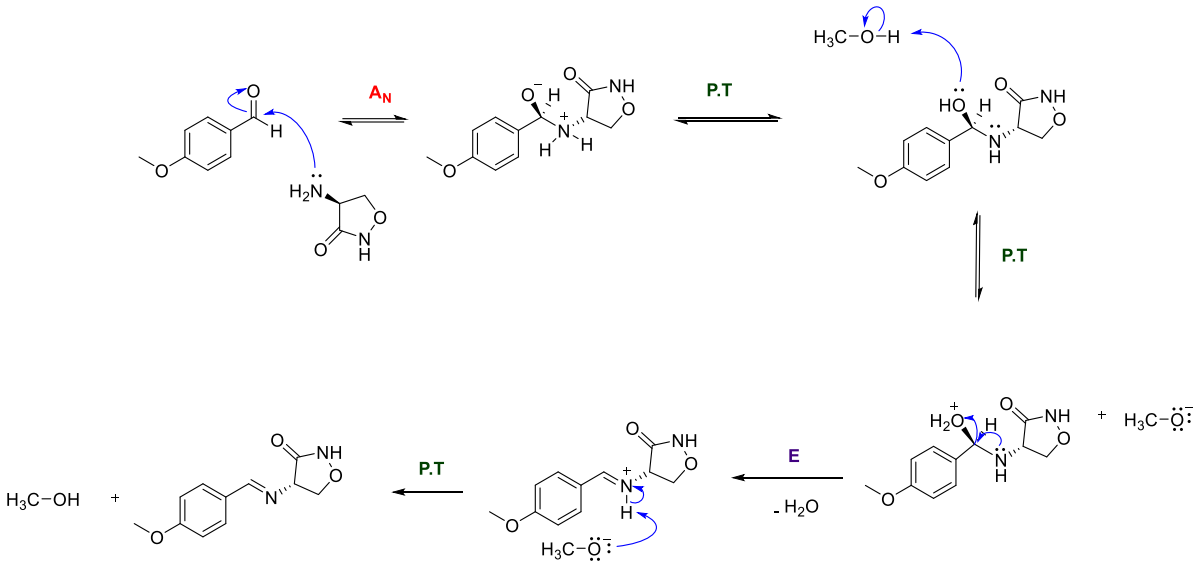

Figure 2.7: Proposed reaction mechanism for the formation of final target **1.5**

A_N: nucleophilic addition, P.T: proton transfer, E: elimination

NMR assignments for final target compounds (**1.1-1.11**) were assisted by both one-dimensional (1D) proton and carbon (^{1}H and ^{13}C) as well as two-dimensional (2D) heteronuclear single quantum correlation (HSQC) and correlation spectroscopy (COSY) NMR experiments. For characterization purposes, compounds **1.5-1.10** will be used as illustrative examples to highlight the NMR spectral differences between *ortho-*, *meta-*, and *para*-substituted analogues. All *p*-isoxazolidine Schiff base analogues (**1.3**, **1.4**, **1.9**, and **1.11**) exhibited similar ^{1}H-NMR spectra as that of **1.5** (**Figure 2.8**).

The successful incorporation of DCS into the molecule was confirmed by the appearance of distinctive multiplicity signals in the aliphatic region. A multiplet at δ_H = 4.32 ppm integrating for two protons (2H), was attributed to protons H2a and H2b, while another multiplet at δ_H = 4.14 ppm integrating for one proton (1H), was assigned to H3. The signals of the phenyl ring hydrogens were observed in the aromatic region of the ^{1}H-NMR spectrum resonating as a pair of doublets at δ_H = 7.54 and 6.96 ppm with similar coupling constants of J = 8.85 and 8.78 Hz, respectively. These were unambiguously assigned to protons H5 and H6, respectively. Meanwhile, the olefinic proton H4 of the imine was observed as a singlet at δ_H = 8.18 ppm. Furthermore, the NH proton of the D-CS moiety resonated as a singlet at the most downfield chemical shift (δ_H = 8.31 ppm). The methoxy protons (H7) appeared at δ_H = 3.78 ppm as a singlet integrating for three protons.

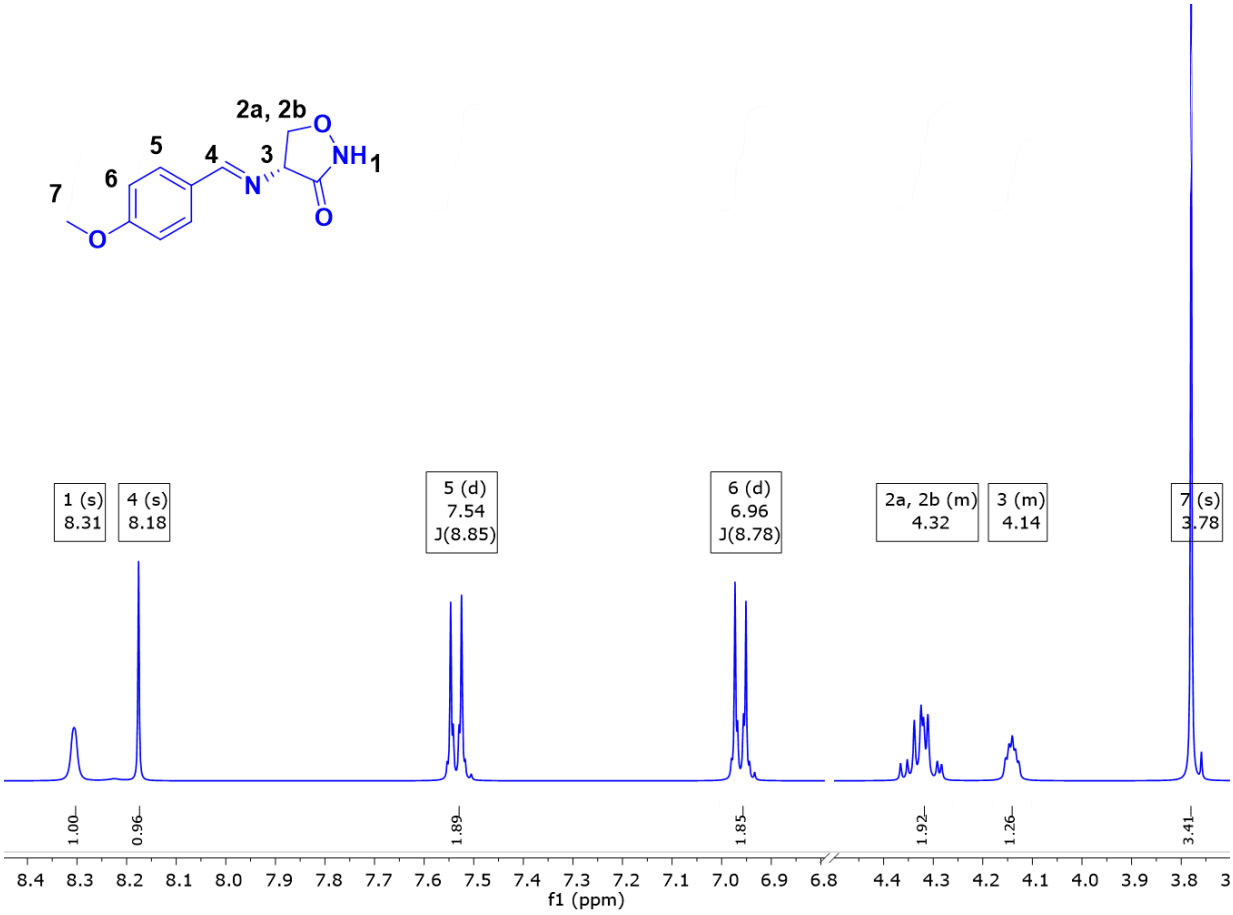

Figure 2.8: Assigned ^{1}H-NMR spectrum confirming the successful synthesis of target compound **1.5**

The ^{1}H-NMR spectra acquired for the *ortho*-substituted isoxazolidine Schiff base analogues (**1.7** and **1.10**) are exemplified by the ^{1}H-NMR spectrum of compound **1.7** (**Figure 2.9**). Each aromatic proton of the phenyl ring exhibited a unique chemical shift, and this was attributed to the fact that the methoxy group was in the *ortho* position. The distinctive multiplicity pattern in the aromatic region includes a doublet of doublet of doublets (*ddd*) at δ_H = 7.40 ppm, which was assigned to proton H7. This proton experiences a close range (J^3) coupling to protons H6 and H8, as confirmed by the large coupling constants (J = 8.79 and 7.52 Hz, respectively), and long-range coupling to proton H5, as confirmed by the small coupling constant (J = 1.81 Hz). Proton H5 splits as a doublet of doublets at δ_H = 7.63 ppm. This proton experiences long-range coupling to proton H7, as seen by the small coupling constant observed (J = 1.72 Hz). In addition, H5 also experiences vicinal coupling to proton H6, as confirmed by the comparatively large coupling constant (J = 7.66 Hz). Proton H8 resonates as a doublet at δ_H = 7.06 ppm and shows short-range coupling with H7, as confirmed by the large coupling constant J = 8.35 Hz. In addition to this, what appears to be a triplet at δ_H = 6.95 ppm is in fact a coalesced doublet of doublets corresponding to proton H6. This proton experiences vicinal (J^3) coupling to protons H7 and H5, as confirmed by the large coupling constants (J = 8.78 and 7.66 Hz). Finally, the

proton signals of DCS and the methyl group of the methoxy were not significantly influenced by the change in position of the methoxy group on the phenyl ring, and their chemical shift values are therefore very similar to those of **1.5** (**Figure 2.8**).

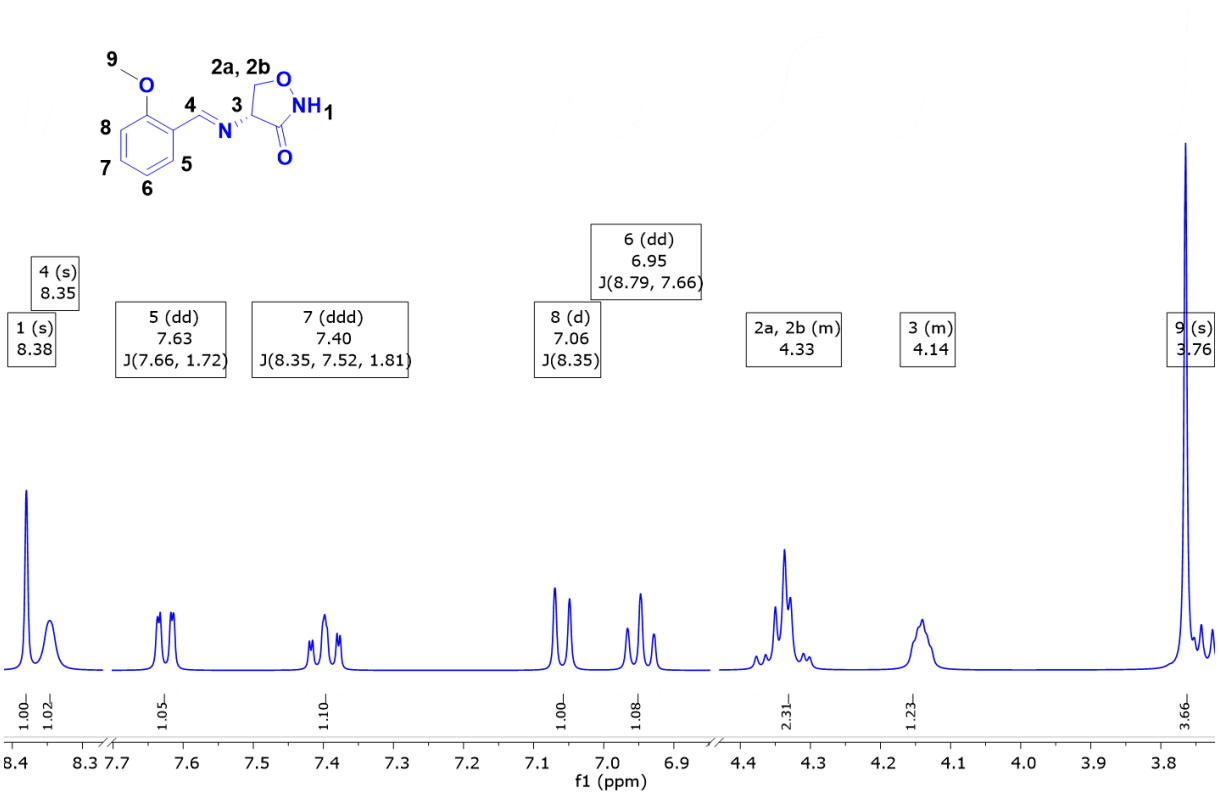

Figure 2.9: Assigned ^{1}H-NMR spectrum confirming the successful synthesis of target compound **1.7**

The ^{1}H-NMR spectra acquired for the *meta*-substituted isoxazolidine Schiff base analogues (**1.6** and **1.8**) are exemplified by the ^{1}H-NMR spectrum of compound **1.6** (**Figure 2.10**). The distinctive multiplicity patterns observed in the aromatic region include a *ddd* at δ_H = 6.98 ppm, which was unambiguously attributed to proton H8. This proton experiences long-range (J^4) coupling with protons H6 and H5, as confirmed by the small coupling constants of J = 2.60 and 1.07 Hz, respectively, and close-range vicinal coupling to H7 with a correspondingly larger coupling constant of J = 8.26 Hz. In addition to this, the two unusual multiplets at δ_H = 7.32 and 7.16 ppm correspond to protons H7 and H5,6. Finally, the proton signals of DCS and the methyl group of the methoxy were not significantly influenced by the change in position of the methoxy group on the phenyl ring, and their chemical shifts are therefore very similar to those of **1.5** (**Figure 2.8**).

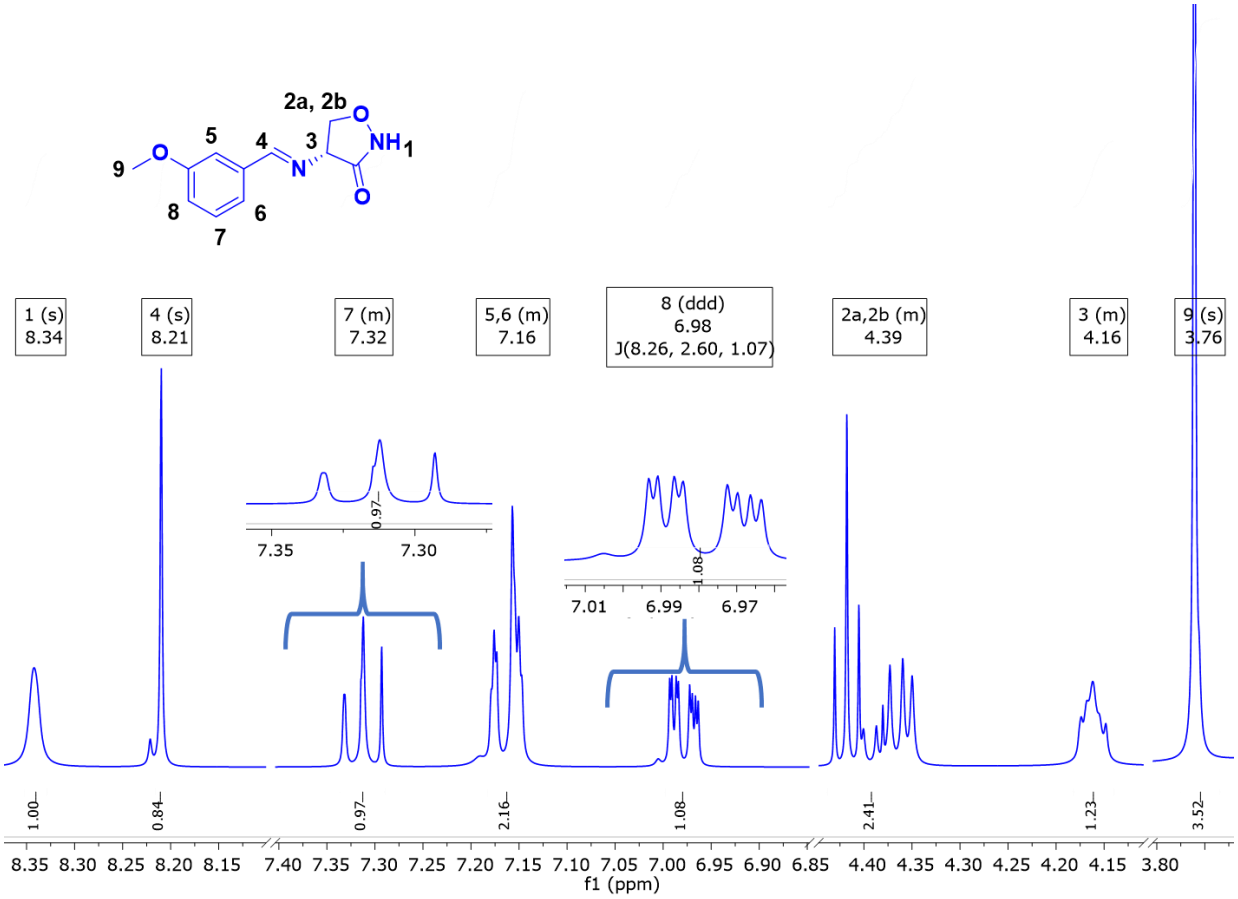

Figure 2.10: Assigned ^{1}H-NMR spectrum confirming the successful synthesis of target compound **1.6**

2.5.3 Synthesis of SAR 2 target compounds

The 3-isoxazolidin-4-yl amides were synthesized according to Scheme 2.2. The commercially available relevant carboxylic acid underwent chlorination by heating under reflux in thionyl chloride ($SOCl_2$) or at room temperature (20-24 °C) in oxalyl chloride to yield the relevant acyl chloride intermediates. DCS was then coupled to these acyl chloride intermediates to yield the desired products **3.1-3.5** in very low to low yields (5-21%; **Table 2.3**).

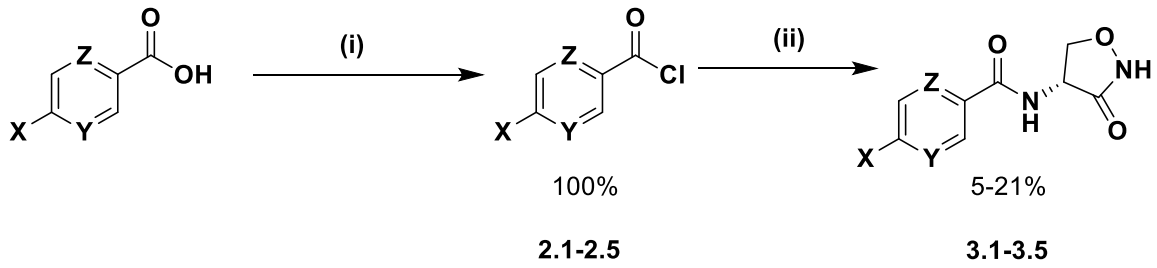

Scheme 2.2: Synthetic protocol for target compounds **3.1-3.5**

Reagents and conditions: (i) $SOCl_2$, toluene (**3.4**), neat (**3.2**, **3.3**), reflux (75 °C), 12-15 h/oxalyl chloride, dichloromethane (DCM), catalytic dimethylformamide (DMF) (**3.1, 3.5**), 20-24 °C; (ii) D-CS, triethylamine (TEA), DMF/*N*-methyl-2-pyrrolidone (NMP), RT (20-24 °C), 3-4 h

Table 2.3: Yields of 3-isoxazolidin-4-yl amides

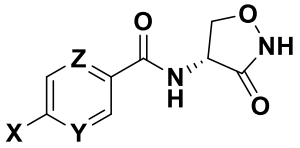

Compound code	X	Y	Z	% Yield
3.1	H	CH	CH	19
3.2	OCH_3	CH	CH	20
3.3	Br	CH	CH	5
3.4	H	N	CH	21
3.5	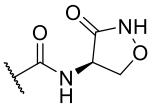	CH	CH	3

The reaction for step (i) is initiated by nucleophilic attack of the hydroxyl oxygen of the carboxylic acid on the electron-deficient thionyl chloride sulphur (**Figure 2.11**), resulting in the formation of an unstable tetrahedral intermediate. The intermediate collapses as the chloride ion is expelled, thus deprotonating the resulting intermediate to form a chlorosulfide anhydride and hydrochloric acid as a by-product. In the final step, the chlorosulfide intermediate undergoes nucleophilic substitution as the chloride attacks the carbonyl carbon, subsequently resulting in the formation of the carbonyl chloride with sulphur dioxide and hydrogen chloride gas as by-products.

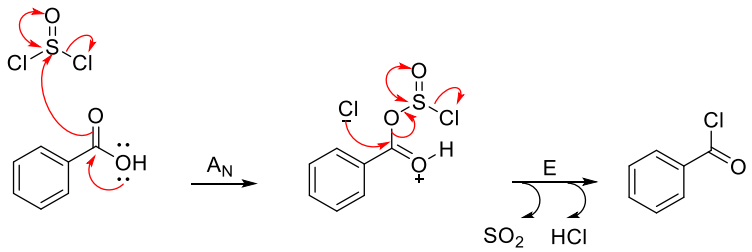

Figure 2.11: Proposed reaction mechanism for the formation of the acyl chloride intermediate

All acyl chloride intermediates (**2.1-2.5**) were used without purification or characterization. The next step was the introduction of D-CS into the molecule via nucleophilic substitution of the chloro group by DCS in the presence of triethylamine (TEA).

The appearance of new proton signals corresponding to DCS in the ^{1}H-NMR spectrum (**Figure 2.13**) confirmed that a successful nucleophilic substitution reaction had occurred. These characteristic signals include the broad NH singlet at δ_H = 11.51 ppm and the amide doublet at δ_H = 8.93 ppm. These were assigned to H1 and H4, respectively. In addition to this, distinctive multiplicity patterns in the aliphatic region, including a doublet of doublets at δ_H = 4.12 ppm, were observed and attributed to proton H2a. This proton experiences vicinal coupling with proton H3, as confirmed by the relatively small coupling constant (*J* = 8.32 Hz), and germinal coupling with H2b, as indicated by the large coupling constant (*J* = 10.38 Hz). The unusual quartet at δ_H = 5.05 ppm was attributed to proton H3. A pair of doublet of doublets at δ_H = 7.88 and 7.49 ppm were unambiguously assigned to protons H5 and H6, respectively. The triplet of triplets resonating at δ_H = 7.56 ppm was assigned to proton H7.

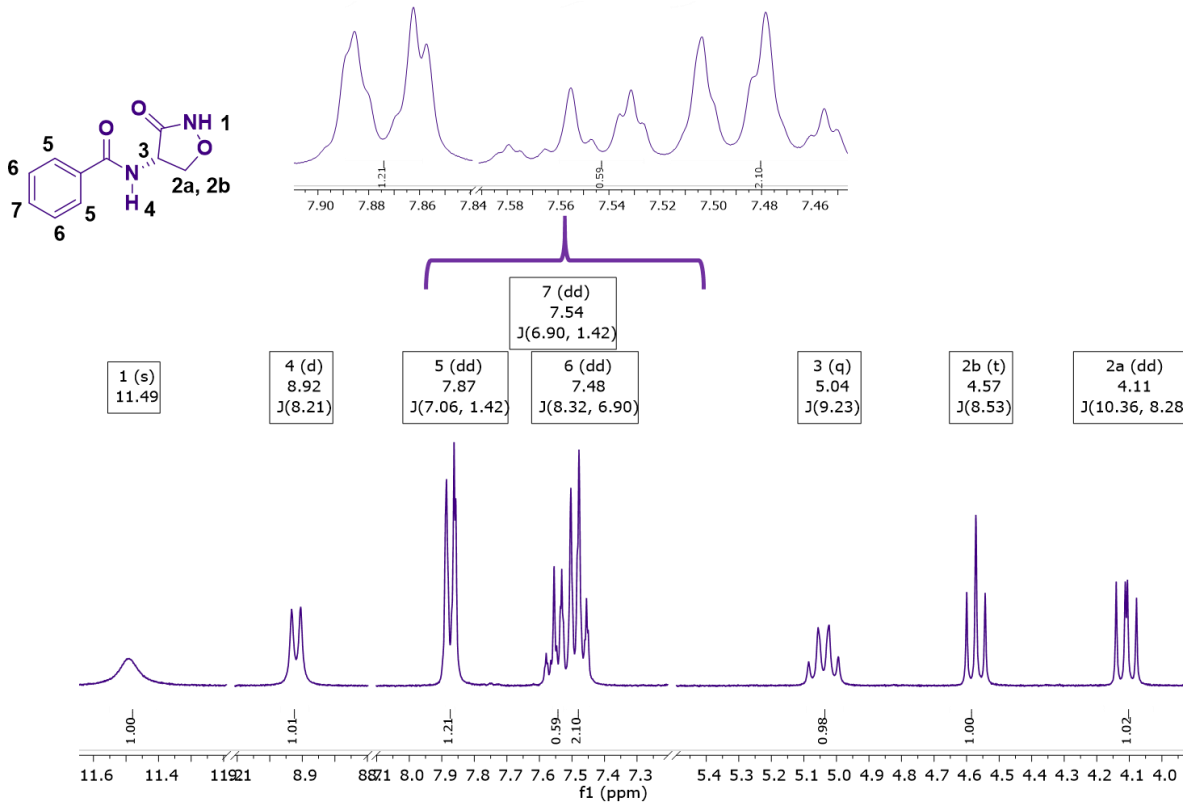

Figure 2.12: ^{1}H-NMR spectrum of compound **3.1**

The successful incorporation of two units of D-CS into the molecule was confirmed by the distinctive multiplicity pattern in the aliphatic region (**Figure 2.14**). A two-proton doublet of doublets signal at δ_H = 4.12 ppm was attributed to protons H2a and a triplet at δ_H = 4.58 ppm corresponding to two protons was assigned to H2b, as confirmed by the coupling constants. The quartet observed at δ_H = 5.05 ppm was attributed to proton H3, accounting for two protons. The aromatic signals of the phenyl ring were observed at δ_H = 7.97 ppm corresponding to four H5 protons. Furthermore, the NH protons of the

amide resonated as a doublet at δ_H = 9.08 ppm while the NH protons of the DCS ring resonated as a broad singlet at the most downfield chemical shift (δ_H = 11.51 ppm). Furthermore, data obtained from LC-MS provided more information on the structural characteristics of compound **2.14.** The LC chromatogram provided the purity as > 99%, based on the percentage peak area; the mass spectrum exhibited a pseudo-molecular ion [$(M+H)^+$] of 334.09 as the base peak (100%), corresponding to the calculated one for $C_{14}H_{14}N_4O_6$. The UV-VIS spectrum displayed one peaks depicting the λ_{max} as 240nm.

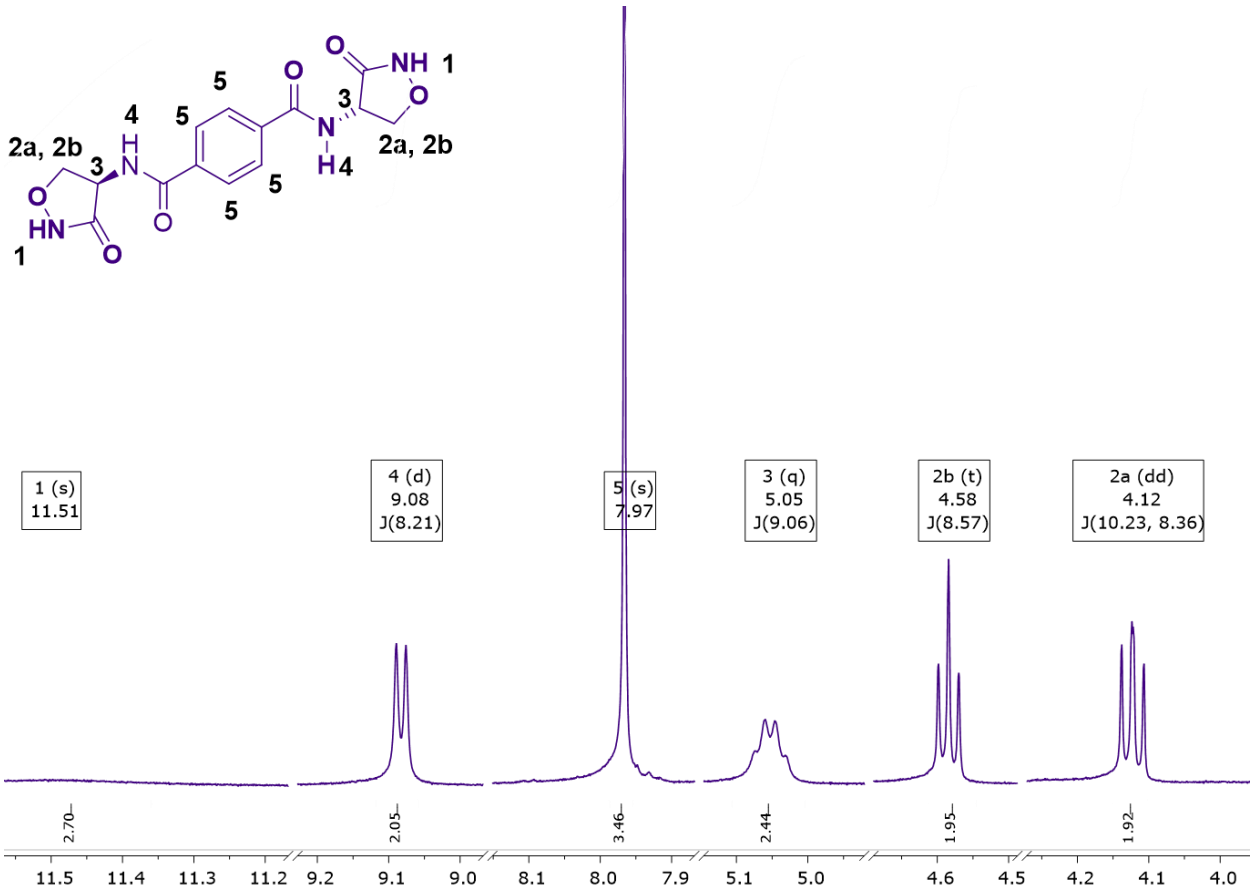

Figure 2.14: ^{1}H-NMR spectrum of compound **3.5**

The successful incorporation of DCS into the pyrazine motif was confirmed by distinctive multiplicity in the aliphatic region (see spectrum for compound **3.4** in **Figure 2.15** and **Figure 2.16**). These characteristic signals include the broad NH singlet at δ_H = 11.55 ppm and the amide doublet at δ_H = 9.32 ppm. These were assigned to H1 and H4, respectively. In addition to this, another distinctive multiplicity pattern including a doublet of doublets at δ_H = 4.25 ppm was observed and attributed to proton H2a. This proton experiences vicinal coupling with proton H3, as confirmed by the coupling

constant (J = 8.17 Hz), and germinal coupling with H2b, as indicated by the larger coupling constant (J = 11.06 Hz). The doublet of triplets at δ_H = 5.06 ppm was attributed to proton H3, which experiences unequal coupling to protons H2 and H4.

Lastly, pyrazinyl hydrogens were accurately assigned using 2D COSY and HSQC (**Figure 2.16**). The doublets at δ_H = 9.20 and 8.90 ppm were unambiguously assigned to protons H5 and H6, respectively. H5 resonates as a simple doublet as the small coupling constant (J = 1.46 Hz) corresponding to proton H5 suggests that this proton experiences only long-range coupling to H6. The doublet of doublets resonating at δ_H = 8.77 ppm was assigned to proton H7.

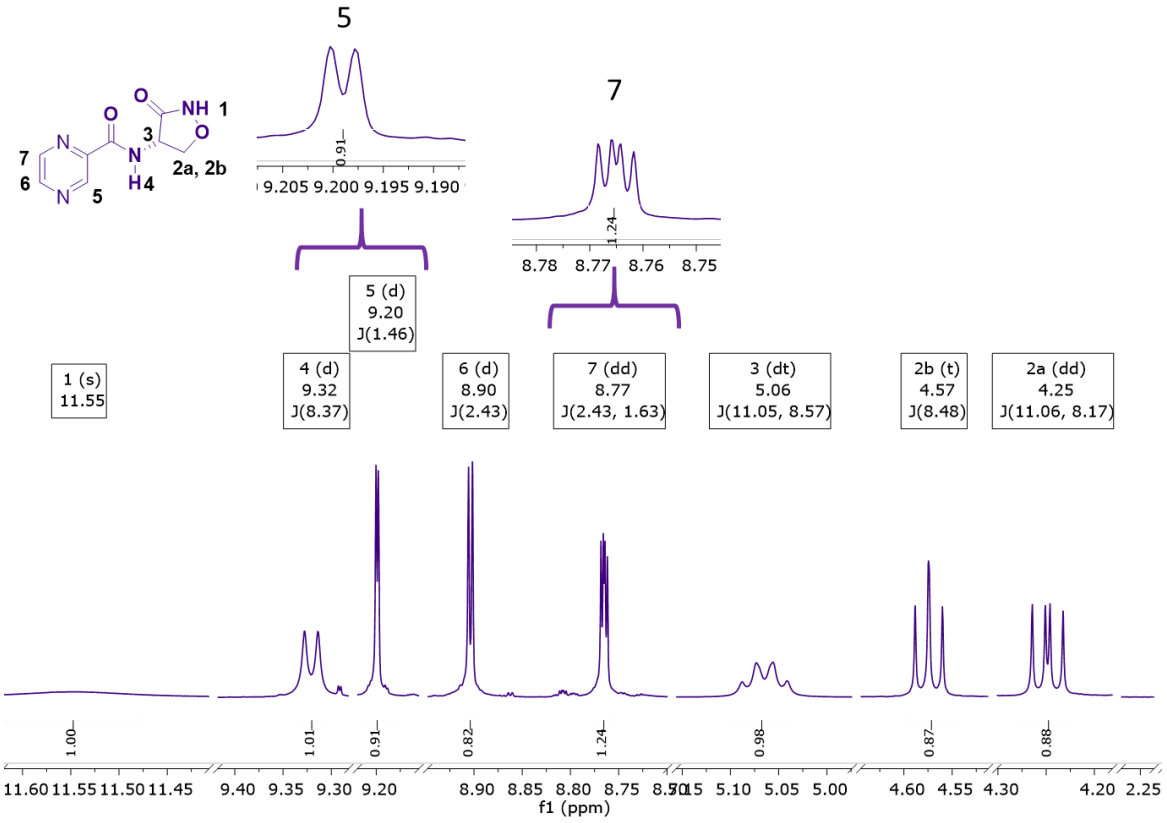

Figure 2.15: ^{1}H NMR spectrum of compound **3.4**

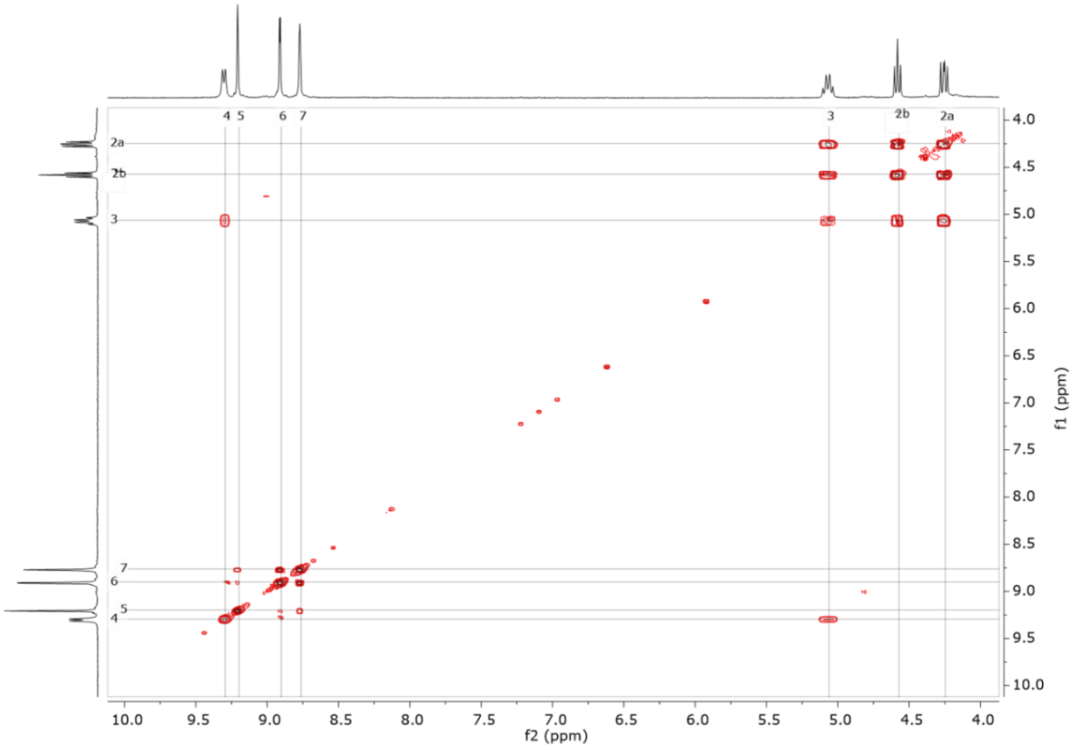

Figure 2.16: Key correlation spectroscopy (COSY) for target compound **3.4**

2.6 References

(1) Prosser, G. A.; De Carvalho, L. P. S. Reinterpreting the Mechanism of Inhibition of Mycobacterium Tuberculosis D -Alanine: D -Alanine Ligase by D -Cycloserine. *Biochemistry* **2013**, *52* (40), 7145–7149.

(2) Hong, W.; Chen, L.; Xie, J. Molecular Basis Underlying Mycobacterium Tuberculosis D-Cycloserine Resistance. Is There a Role for Ubiquinone and Menaquinone Metabolic Pathways? *Expert Opin. Ther. Targets* **2014**, *18* (6), 691–701.

(3) Halouska, S.; Fenton, R. J.; Zinniel, D. K.; Marshall, D. D.; Barletta, R. G.; Powers, R. Metabolomics Analysis Identifies D-Alanine-d-Alanine Ligase as the Primary Lethal Target of d-Cycloserine in Mycobacteria. *J. Proteome Res.* **2014**, *13* (2), 1065–1076.

(4) Ma, Z.; Ginsberg, A. M.; Spigelman, M.; Alliance, G.; Development, D.; York, N. 7.24 Antimycobacterium Agents. **2007**, 699–730.

(5) *Tuberculosis and the Tubercle Bacillus, Second Edition*; Jacobs, Jr., W. R., McShane, H., Mizrahi, V., Orme, I. M., Eds.; American Society of Microbiology, 2017.

(6) Schade, S.; Paulus, W. D-Cycloserine in Neuropsychiatric Diseases : A Systematic Review. **2016**, *19*, 1–7.

(7) Yuan, T.; Sampson, N. S. Hit Generation in TB Drug Discovery: From Genome to Granuloma. *Chem. Rev.* **2018**, acs.chemrev.7b00602.

(8) Hwang, T. J.; Wares, D. F.; Jafarov, A.; Jakubowiak, W.; Nunn, P.; Keshavjee, S. Safety of Cycloserine and Terizidone for the Treatment of Drug-Resistant Tuberculosis: A Meta-Analysis. *Int. J. Tuberc. Lung Dis.* **2013**, *17* (10), 1257–1266.

9) Jum, S.; Karaman, R. Prodrugs Overview. **2014**, No. July, 1-23.

(10) Rautio, J.; Meanwell, N. A.; Di, L.; Hageman, M. J. The Expanding Role of Prodrugs and Development, J.*Nat. Rev.* Drug Discov., **2008**, 7 (3), 255-270

(11) Huttunen, K. M.; Raunio, H.; Rautio, J. Prodrugs — from Serendipity to Rational Design. **2011**, *63* (3), 750–771.

(12) Mori, G. et al New Prodrugs against Tuberculosis. *Drug Discov. Today* **2016**, 1-7

(13) Testa, B. Prodrug Research: Futile or Fertile? Biochemical pharmacology, **2004**, *68*, 2097–2106.

(14) Ettmayer, P.; Amidon, G. L.; Clement, B.; Testa, B. Lessons Learned from Marketed and Investigational Prodrugs. *J.Med Chem*, **2004**, *47* (10), 2393-2403

(15) Stella, V. J. Prodrugs as Therapeutics, *Expert Opin. Ther. Pat.* **2004**, 2002–2005.

(16) Jornada, D. H.; Felipe, G.; Chiba, D. E.; Regina, T.; Melo, F. De; Leandro, J.; Chung, M. C. The Prodrug Approach: A Successful Tool for Improving Drug Solubility. **2016**, 1-31.

(17) Rautio, J.; Kumpulainen, H.; Heimbach, T.; Oliyai, R. Prodrugs: Design and Clinical Applications, *Nat. Rev. Drug Discov.* **2008**, *7* (march), 255–270.

(18) Hamad, M. O.; Kiptoo, P. K.; Stinchcomb, A. L.; Crooks, P. A. Synthesis and Hydrolytic Behavior of Two Novel Tripartate Codrugs of Naltrexone and 6 b-Naltrexol with Hydroxybupropion as Potential Alcohol Abuse and Smoking Cessation Agents, *Bioorg. Med. Chem*.. **2006**, *14*, 7051–7061.

(19) Shirke, S.; Shewale, S.; Satpute, M. Available Online at Www.Ijpcbs.Com PRODRUG DESIGN : AN OVERVIEW. **2015**, *5* (1), 232–241.

(20) Via, L. E.; Savic, R.; Weiner, D. M.; Zimmerman, M. D.; Prideaux, B.; Irwin, S. M.; Lyon, E.; Brien, P. O.; Gopal, P.; Eum, S.; et al. Host-Mediated Bioactivation of Pyrazinamide: Implications for Efficacy, Resistance, and Therapeutic Alternatives, *ACS Infect. Dis.* **2015**, 1, 5, 203-2014

(21) Beaumont, K.; Webster, R.; Gardner, I.; Dack, K. Design of Ester Prodrugs to Enhance Oral Absorption of Poorly Permeable Compounds: Challenges to the Discovery Scientist, Current drug metabolism, **2003**, No. 01304, 461–485.

(22) Njogu, P. M.; Chibale, K. Recent Developments in Rationally Designed Multitarget Antiprotozoan Agents. **2013**.

(23) Agarwal, D.; Gupta, R. D.; Awasthi, S. K. Antimalarial Hybrid Molecules : A Close Reality or a Distant Dream? Downloaded from Http://Aac.Asm.Org/ on November 24, 2018 by Guest. **2017**, No. March, 1–29.

(24) Meunier, B. Hybrid Molecules with a Dual Mode of Action : Dream or Reality ? **2008**, *41* (1), 69–77.

(25) Musonda, C. C.; Whitlock, G. A.; Witty, M. J.; Brun, R.; Kaiser, M. Chloroquine-Astemizole Hybrids with Potent in Vitro and in Vivo Antiplasmodial Activity. *Bioorganic Med. Chem. Lett.* **2009**, *19*, 481–484.

(26) Walsh, J. J.; Bell, A. Hybrid Drugs for Malaria. **2009**, 2970–2985.

(27) Srivastava, V.; Lee, H. Chloroquine-Based Hybrid Molecules as Promising Novel Chemotherapeutic Agents. *Eur. J. Pharmacol.* **2015**, 1–15.

(28) Lin, J. H.; Lu, A. Y. H. *Pharmacol. Rev.* **1997**, *49* (4), 403–449.

(29) Tan, S.; Russell, D. G.; Russell, D. G. Trans-Species Communication in the Mycobacterium Tuberculosis-Infected Macrophage*, Immunol.Rev.* **2015**, No. 5, 233–248.

(30) Russell, D. G.; Russell, D. G. Mycobacterium Tuberculosis and the Intimate Discourse of a Chronic Infection. *Immunol. Rev.* **2011**, *240*, 252–268.

(31) Dartois, V.; Barry, C. E. Bioorganic & Medicinal Chemistry Letters BMCL Digest A Medicinal Chemists ' Guide to the Unique Difficulties of Lead Optimization for Tuberculosis. *Bioorg. Med. Chem. Lett.* **2013**, *23* (17), 4741–4750.

(32) Craig, P. Interdependence between Physical Parameters and Selection of Substituen. *J. Med. Chem.* **1971**, *14* (12), 680–684.

(33) D-CS Patent, *US Patent 3,117,122 Jan 7,1964*

3.1 Chapter overview

This chapter describes the biological studies that were conducted to evaluate the antimycobacterial potency, cytotoxicity, and (in one case) microsomal stability of the synthesized target molecules. These studies followed a well-defined screening cascade (**Figure 3.1**).

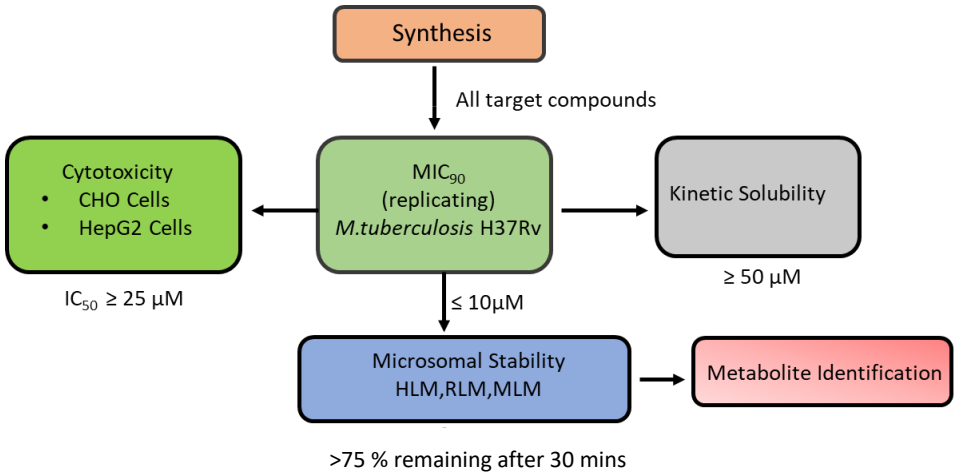

Figure 3.1: Screening cascade used for the biological evaluation of target compounds
CHO, Chinese hamster ovarian cells; HepG2, Human hepatic cells; MIC_{90}, 90% minimum inhibitory concentration; HLM, human liver microsomes; RLM, rat liver microsomes; MLM, mouse liver microsomes; DCS, D-cycloserine

Compounds were submitted for evaluation of antimycobacterial activity against *M. smegmatis* (Mc^2 155, *M. smeg*) and *M. tuberculosis* H37Rv strains, cytotoxicity in Chinese hamster ovarian (CHO) and human hepatic (HepG2) cells, and solubility studies using turbidimetric and HPLC-based kinetic solubility assays. The microsomal metabolic stability of any compound with minimum inhibitory concentration (MIC_{90}) ≤10 µM was assessed in human liver microsomes (HLM), rat liver microsomes (RLM), and mouse liver microsomes (MLM).

In metabolic stability assays, any analogue for which >75% of the parent compound remained present after 30 min incubation was deemed metabolically stable. Any compound that fulfilled these criteria would under normally be subjected to further *in vivo* tests to investigate pharmacokinetic (PK) properties such as bioavailability, exposure, and clearance for efficacy studies in a mouse model. However, these assays were not carried out here as this was beyond the scope of the project.

3.2 Evaluation of *in vitro* antimycobacterial activity against *M. smegmatis* and *M. tuberculosis*

3.2.1 *In vitro* antimycobacterial activity

The *in vitro* antimycobacterial activities of all compounds were evaluated against *M. smegmatis* (Mc^2 155, *M. smeg*) and *M. tuberculosis* H37Rv under replicating conditions. All assays were conducted according to laboratory standard operating procedures (SOPs). Assays evaluating activity against *M. smeg* were performed in Luria Broth (LB) medium using RIF as the reference drug. Assays evaluating activity against the H37Rv strain of *Mtb* were conducted by the TB Biology group at the Drug Discovery and Development Centre (H3D), based at the Institute of Infectious Diseases and Molecular Medicine (IDM), University of Cape Town, South Africa. These assays were performed in three different types of growth media; Middlebrook 7H9 GLU ADC TW (7H9 medium enriched with albumin-dextrose-catalase (ADC) and supplemented with 0.4% glucose and 0.05% Tween 80), Middlebrook 7H9 ADC TW (7H9 medium enriched with ADC and supplemented with 0.05% Tween 80), and Middlebrook 7H9 GLU ADC (7H9 medium enriched with ADC and supplemented with 0.4% glucose).

M. smeg has been used extensively as a non-pathogenic surrogate to study highly pathogenic *Mtb* physiology because of its ease of manipulation in a biosafety level 1 facility, close resemblance to *Mtb* with regard to both structural and genetic features, and its significantly shorter doubling time in comparison to that of *Mtb*.[1] In addition to studying mycobacterial physiology, numerous reports in the literature have indicated its usefulness in antimycobacterial compound screens. For instance, bedaquiline, the first novel anti-tuberculous agent to be approved for clinical use after over four decades, was initially discovered after a screening campaign in *M. smeg*. [2] However, considering the phenotypic and genotypic differences between *M. smeg* and *Mtb*, there are limitations to the applicability of results obtained in *M. smeg* in drug discovery.

Test compounds were stratified into four categories for the purpose of this SAR analysis. All compounds with $MIC_{90} \leq 10$ µM were regarded as active, those with MIC_{90} 10 to 20 µM as moderately active, MIC_{90} values between 20 and 125 µM denoted as having poor activity, and compounds with $MIC_{90} > 125$ µM were categorized as inactive. As shown in **Tables 3.1** and **3.2**, compounds showed little or no glycerol-dependent activity and no differences in activity against *Mtb* were observed in media with and without Tween-80. Furthermore, structural changes in SAR 1 and SAR 2 generally yielded inactive compounds. For instance, all isoxazolidine-3-one imines analogues were inactive, with the exception of compound **1.1**, which displayed high activity (7.81 µM). Similarly, in SAR 2, all 3-isoxazolidin-4-yl amide analogues were inactive with the exception of **3.3** (2.90 µM), which was active

across all three media types. Notably, the replacement of bromo (**3.3**) with methoxy (**3.2**) or a proton (**3.1**) abolished activity.

Overall, antimycobacterial activity appeared generally to be independent of electronic properties and hydrophobicity imparted by various substituents

Table 3.1: *In vitro* antimycobacterial activities of SAR 1 target compounds against *Mycobacterium smegmatis* and *Mycobacterium tuberculosis (Mtb)*

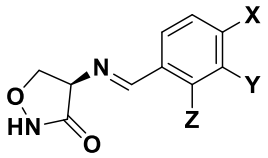

Compound code	X	Y	Z	*In vitro* antimycobacterial activity MIC_{90} (µM)			
				M. smegmatis mc²155	*Mtb* H37*Rv*		
				LB	7H9/ADC with glycerol	7H9/ADC with Tween 80 and glycerol	7H9/ADC with Tween 80
1.1	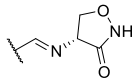	H	H	>1654.04	7.8	7.8	7.8
1.2	H	H	H	1854.20	>125	>125	>125
1.3	CH_3	H	H	1224.11	>125	>125	>125
1.4	CN	H	H	1161.65	>125	>125	>125
1.5	OCH_3	H	H	2270.35	>125	>125	>125
1.6	H	OCH_3	H	1135.17	>125	>125	>125
1.7	H	H	OCH_3	>2270.35	>125	>125	>125
1.8	H	F	H	>2401.65	>125	>125	>125
1.9	F	H	H	>2401.65	>125	>125	>125
1.10	H	H	F	>2401.65	>125	>125	>125
1.11	Br	H	H	>1858.05	>125	>125	>125
Controls		D-Cycloserine		607.38	15.63-31.25	15.63 -31.25	15.63-31.25
		Rifampicin		97.21	N/A	N/A	N/A

MIC_{90}, 90% minimum inhibitory concentration; H37Rv, drug-susceptible *Mtb* strain; LB, Luria broth; ADC, albumin-dextrose-catalase

Table 3.2: *In vitro* antimycobacterial activities of SAR 2 target compounds against *Mycobacterium smegmatis* and *Mycobacterium tuberculosis (Mtb)*

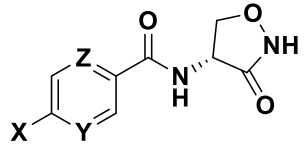

				***In vitro* antimycobacterial activity MIC_{90}(μM)**			
Compound code	**X**	**Y**	**Z**	***M. smegmatis mc²155***	***Mtb* H37*Rv***		
				LB Broth	**7H9/ADC with glycerol**	**7H9/ADC with Tween 80 and glycerol**	**7H9/ADC with Tween 80**
3.1	H	CH	CH	>2424.830	>125	>125	>125
3.2	OCH_3	CH	CH	>2116.58	>125	>125	>125
3.3	Br	CH	CH	>2580.62	2.9	2.9	2.9
3.4	H	N	CH	>2401.76	> 125	>125	>125
3.5	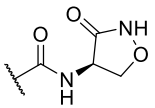	CH	CH	>1495.70	>125	>125	>125
3.6	NH_2	N	CH	ND	ND	ND	ND
Controls		D-Cycloserine		607.38	15.63-31.25	15.63 -31.25	15.63-31.25
		Rifampicin		97.21	N/A	N/A	N/A

MIC_{90}, 90% minimum inhibitory concentration; H37Rv, drug-susceptible *Mtb* strain; LB, Luria broth; ADC, albumin-dextrose-catalase

From the data in **Tables 3.1** and **3.2** above, a general trend was observed with relatively higher MIC_{90} values in *M. smeg* than in *Mtb.* To promote visualization, MIC_{90} values were converted to $pMIC_{90}$ (**Figure 3.2**). The discrepancies observed may be attributed to the genotypic, physiological, and metabolic differences between *M. smeg* and *Mtb*. Moreover, despite being analogues of DCS, target compounds are novel compounds that may have distinct or additional molecular targets besides the known target of DCS, and this may result in a different phenotypic profile to that of DCS.

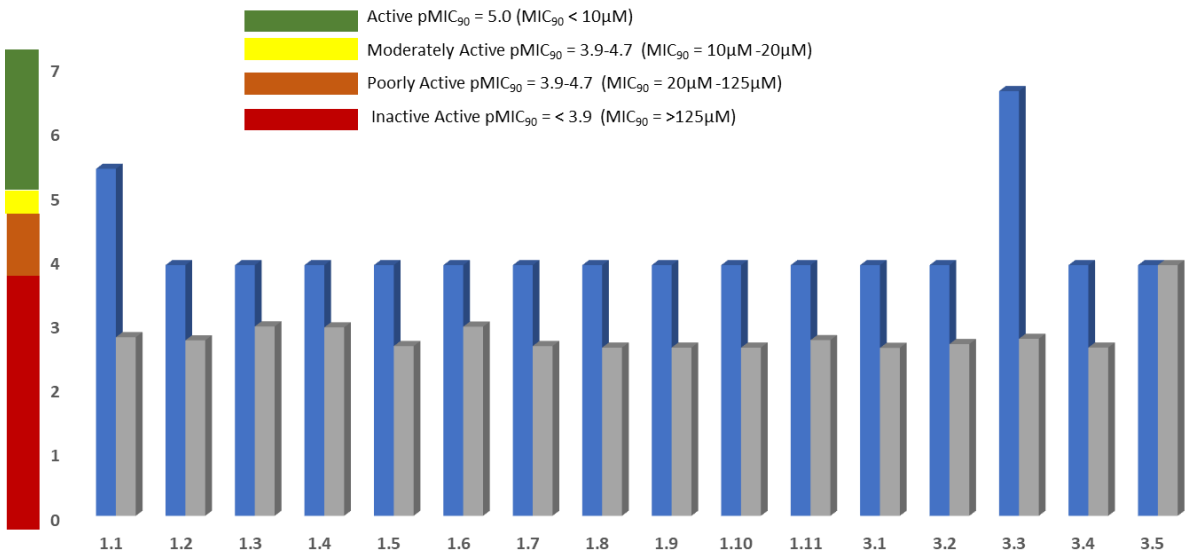

Figure 3.2: Graphical representation of MIC_{90} values in *Mycobacterium smegmatis* (grey) and in *Mycobacterium tuberculosis* (blue)
MIC_{90}, 90% minimum inhibitory concentration.

3.2.2 *In vitro* antibacterial activity against selected gram-positive and -negative pathogens

There is an urgent need for novel chemotherapeutic agents to control the growing crisis of antimicrobial resistance, especially since the end of the "Golden era" of antibiotics, which led to a decrease in the discovery of antimicrobials. The target compounds were screened against the top priority pathogens responsible for the worldwide spread of antimicrobial resistance identified by the WHO.[3] These include *Staphylococcus aureus, Klebsiella pneumoniae, Acinetobacter baumannii,* and *Enterobacteria* species (ESKAPE pathogens). In this experiment, we screened the 16 compounds synthesized in SAR 1 and 2 against these pathogens. None of the compounds showed activity comparable to that of D-cycloserine, thus confirming selectivity for *Mtb* (**Tables 3.3** and **3.4**).

Table 3.3: *In vitro* anti-bacterial activity of SAR 1 target compounds against ESKAPE pathogens

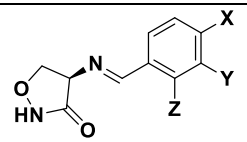

Compound code	X	Y	Z	MIC$_{90}$ (µM)			
				Staphylococcus aureus ATCC 25923	***Klebsiella pneumoniae ATCC BAA-1705***	***Acinetobacter baumannii ATCC 19606***	***Escherichia coli ATCC 25922***
1.1	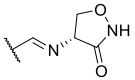	H	H	1654.04	>1654.04	827.02	413.51
1.2	H	H	H	>2851.42	>2851.42	>2851.42	>2851.42
1.3	CH_3	H	H	>2448.22	>2448.22	>2448.22	>2448.22
1.4	CN	H	H	>2323.31	2323.31	>2323.31	>2323.31
1.5	OCH_3	H	H	>2270.35	>2270.35	>2270.35	>2270.35
1.6	H	OCH_3	H	>2270.35	>2270.35	2270.35	>2270.35
1.7	H	H	OCH_3	>2270.35	>2270.35	>2270.35	>2270.35
1.8	H	F	H	>2401.65	>2401.65	>2401.65	>2401.65
1.9	F	H	H	>2401.65	>2401.65	>2401.65	>2401.65
1.10	H	H	F	>2401.65	>2401.65	>2401.65	>2401.65
1.11	Br	H	H	>1858.05	>1858.05	>1858.05	>1858.05
Controls			**D-cycloserine**	607.38	607.38	1214.77	303.69
			Gentamycin	1.308	0.00374	0.130	0.654
			Streptomycin	4.298	0.00749	1.719	8.597

MIC90, 90% minimum inhibitory concentration

Studies were performed in Muller-Hinton Broth and reported as MIC$_{90}$ values at day 8.

Table 3.4: *In vitro* anti-bacterial activity of SAR 2 target compounds against ESKAPE pathogens

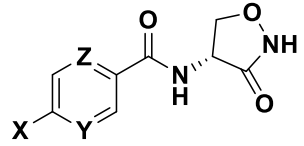

Compound code	X	Y	Z	MIC$_{90}$ (µM)			
				Staphylococcus aureus ATCC 25923	***Klebsiella pneumoniae ATCC BAA-1705***	***Acinetobacter baumannii ATCC 19606***	***Escherichia coli ATCC 25922***
3.1	H	CH	CH	>2424.830	>2424.830	2424.830	>2424.830
3.2	OCH_3	CH	CH	>2116.58	2116.58	>2116.58	2116.58
3.3	Br	CH	CH	>1753.77	>1753.77	>1753.77	>1753.77
3.4	H	N	CH	2401.76	>2401.76	2401.76	>2401.76
3.5	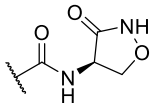	CH	CH	1654.04	>1654.04	827.02	413.51
Controls		D-Cycloserine		607.38	607.38	1214.77	303.69
		Gentamycin		1.308	0.00374	0.130	0.654
		Streptomycin		4.298	0.00749	1.719	8.597

Studies were performed in Muller-Hinton Broth and reported as MIC$_{90}$ values at day 8.

3.3 Cytotoxicity

To determine the safety profiles of the compounds and their selectivity versus *Mtb*, *in vitro* cytotoxicity studies were performed in two mammalian cells line (CHO and HepG2 cells) at the Division of Clinical Pharmacology, University of Cape Town. Cytotoxicity was measured using the well-established 3-(4,5-dimethylthiazil-2-yl)-2,5-diphenyltetrazolium bromide (MTT) assay, a colorimetric assay that measures cell viability as a function of metabolism/reduction of MTT (yellow colour) to formazan (purple colour) by cytosolic NAD(P)H-dependent oxidoreductase enzymes. Emetine was used as the positive control and DMSO as the negative control. Cytotoxicity results from these two assays (**Tables 3.5** and **3.6**) were expressed as the concentrations required to inhibit growth by 50% (IC_{50}), which were obtained by analyzing dose-response curves. In contrast, *in vitro* antimycobacterial activities were expressed as MIC_{90}, and it would therefore be inaccurate to calculate selectivity indices based on these two inhibitory concentrations. The acceptable level of cytotoxicity was thus set as a cut-off value of IC_{50} > 25µM and all compounds exhibited low cytotoxicity (IC_{50} > 25 µM) against the two cell lines. At this juncture, only active compounds **1.1** and **3.3** were advanced to downstream biological studies in the screening cascade.

Table 3.5*: In vitro* cytotoxicity assay results for SAR 1 target compounds

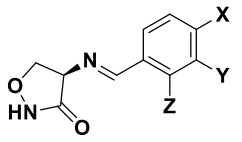

				IC₅₀ (µM)	
Compound code	**X**	**Y**	**Z**	**CHO**	**HepG2**
1.1	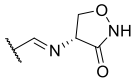	H	H	>50	>50
1.2	H	H	H	>50	>50
1.3	CH_3	H	H	>50	>50
1.4	CN	H	H	>50	>50
1.5	OCH_3	H	H	>50	>50
1.6	H	OCH_3	H	>50	>50
1.7	H	H	OCH_3	>50	>50
1.8	H	F	H	>50	>50
1.9	F	H	H	>50	>50
1.10	H	H	F	>50	>50
1.11	Br	H	H	>50	>50
Controls		Emetine		0.0139	0.023

IC_{50}, 50% inhibitory concentration; CHO, Chinese hamster ovarian cells; HepG2, human hepatic cell line.

Table 3.6: *In vitro* cytotoxicity assay results for SAR 2 target compounds

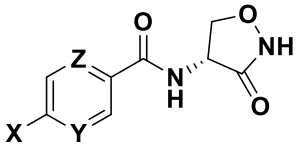

				IC_{50} (µM)	
Compound code code	**X**	**Y**	**Z**	**CHO**	**HepG2**
3.1	H	CH	CH	>50	>50
3.2	OCH_3	CH	CH	>50	>50
3.3	Br	CH	CH	>50	>50
3.4	H	N	CH	>50	>50
3.5	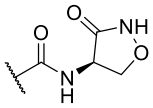	CH	CH	>50	>50
3.6	NH_2	N	CH	>50	>50
Controls		Emetine		0.0139	0.023

IC50, 50% inhibitory concentration; CHO, Chinese hamster ovarian cells; HepG2, human hepatic cell line.

3.4 Microsomal stability

Drug metabolism has implications for drug efficacy and safety as a consequence of one or more of the following: (1) enzymatic inactivation (detoxification), (2) biotransformation into active metabolites, and (3) enzymatic modification into reactive metabolites that cause toxicity.[4-5] Generally, hepatic metabolism involves a variety of chemical modifications carried out by an array of enzymes. In addition, hepatic metabolism is the primary route of elimination for most xenobiotics, which in turn influences their bioavailability, clearance, and half-life. Furthermore, although the liver is the main organ at play in drug metabolism, the skin, lungs, blood cells, and plasma also contribute to the biotransformation of certain drugs.[4-6]

The most commonly used *in vitro* models are hepatic, as the liver plays a central role as the major drug-metabolizing organ. Some of these systems, in decreasing order of biological complexity, include whole perfused liver, liver slice, hepatocytes, S9 fractions, and microsomes. Microsomes are the most commonly used model as the majority of systems comprise cytochrome P (CYP)450 enzymes, and are thus applicable to the metabolism of clinically used drugs. In contrast to the S9 sub-cellular liver fractions that most complete sub-cellular fraction at enzymatic liver as the system mostly comprises phase I and II enzymes.

Therefore, it is important to screen compounds in *in vitro* assays that employ liver microsomes. Three types of liver microsomes (HLMs, RLMs, and MLMs), composed of several membrane-bound enzymes such as CYP450 (phase 1 metabolism), are employed to determine any interspecies differences.[3] Rodent models are the most relevant as these are typical animal models for *in vivo* PK and efficacy studies.

The most potent ($MIC_{90} \leq 10$ µM) and least cytotoxic ($IC_{50} > 25$ µM) analogues were selected and their *in vitro* metabolic stability was evaluated. These experiments were conducted by Dr. Mathew Njoroge at the Division of Clinical Pharmacology, University of Cape Town. The *in vitro* metabolic stability of compound **3.3** was determined in HLMs, RLMs, and MLMs. Samples were incubated for 30 min and analyzed via high-performance liquid chromatography-mass spectrometry (HPLC-MS/MS) to determine the percentage remaining.

Table 3.7: Microsomal metabolic stability results of selected compounds, reported as a percentage remaining

		Metabolic stability (% remaining)		
Compound Code	**Structure**	**HLM**	**RLM**	**MLM**
3.3	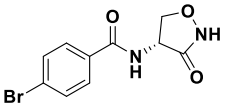	**>99**	**96.76**	**88.59**

HLM, human liver microsomes; RLM; rat liver microsomes; MLM; mice liver microsomes

A percentage remining >75% after 30 min was considered to be within acceptable limits according to the screening cascade in **Figure 3.1**. Therefore, results obtained in **Table 3.7** suggest high metabolic stability for compound **3.3** in the liver microsomes of all three species. Based on these results, compound **3.3** could in future be evaluated further in *in vivo* PK and efficacy studies in a mouse model of tuberculosis as it is expected to show high exposure because of its high metabolic stability in MLMs.

3.5 Conclusion

In this chapter, various assays were used as part of the biological evaluation of the final target compounds synthesized in SAR 1 and 2. The antimycobacterial activities of all compounds synthesized were evaluated against *Mtb.* All compounds were inactive with the exception of compounds **3.3** and **1.1**, which exhibited MIC_{90} values of 2.9 and 7.8 µM, respectively. None of the 16 compounds whose

in vitro antibacterial activities were evaluated against ESKAPE pathogens showed any activity, suggesting that these compounds are selective for *Mtb* in contrast to *M. smeg* or ESKAPE pathogens. All compounds displayed a favourable cytotoxicity profile in both CHO and HepG2 cell lines. Finally, the microsomal metabolic stability of the most potent antimycobacterial compound ($MIC_{90} \leq 10$ μM) with low cytotoxicity ($IC_{50} > 25$ μM) was evaluated. Compound **3.3** displayed high metabolic stability in human, mouse, and rat liver microsomes. The aqueous solubility of all compounds synthesized was evaluated, and this was analyzed in correlation with selected physicochemical factors in an attempt to deduce SPRs. These studies are discussed further in **Chapter 4**.

3.6 References

(1) Baloni, P.; Padiadpu, J.; Singh, A.; Gupta, K. R.; Chandra, N. Identifying Feasible Metabolic Routes in Mycobacterium Smegmatis and Possible Alterations under Diverse Nutrient Conditions. **2014**, 1–15.

(2) Andries, K.; Verhasselt, P.; Guillemont, J.; Göhlmann, H. W. H.; Neefs, J. M.; Winkler, H.; Van Gestel, J.; Timmerman, P.; Zhu, M.; Lee, E.; et al. A Diarylquinoline Drug Active on the ATP Synthase of Mycobacterium Tuberculosis. *Science (80-.).* **2005**, *307* (5707), 223–227.

(3) Masimirembwa, C. M.; Bredberg, U.; Andersson, T. B. Metabolic Stability for Drug Discovery and Development Pharmacokinetic and Biochemical Challenges,*Clin Pharmacokinet,* **2003**, *42* (6), 515–528.

(4) Jakoby, W. B.; Ziegler, D. M. *J. Biol. Chem.* **1990**, *265* (34), 20715–20718.

(5) Glue, P.; Clement, R. P. *Cell. Mol. Neurobiol.* **1999**, *19* (3), 309–323.

(6) Meyer, U. A. *Drug Metab. Rev.* **2007**, *39* (2–3), 639–646.

Chapter 4: Physicochemical profiling

4.1 Chapter overview

In this chapter, a discussion of the physicochemical properties (solubility, cLogP, melting point, total polar surface area, and the presence of hydrogen bond donors and acceptors) of the compounds synthesized is provided. Within the context of structure-property relationship (SPR) studies. The chapter begins with an outline and discussion of the correlation between the *in silico* predicted and experimentally determined physicochemical properties of the final synthesized target compounds. Statistical analyses were performed to establish the disruption profiles of each property across compound datasets. Additionally, various compound datasets were statistically evaluated and compared, including conventional anti-TB drugs and other drug candidates in clinical development in an attempt to establish the chemical space occupied by each cluster of compounds prepared in this study. Subsequently, the correlation between measured and predicted parameters was reviewed to elucidate the various factors that may contribute to and explain the aqueous solubility observed.

4.2 General introduction

Physiochemical properties play an integral role in the drug design process as they relate to the *in vitro* potency and *in vivo* efficacy exhibited by compounds. The impact of physicochemical properties on drug action was first rationalized by the early work of Hansch.[1–4] However, a more holistic approach to the drug design process considers absorption, distribution, metabolism and excretion (ADME) characteristics and safety profiles in parallel with target affinity. Ideally, drug candidates should possess favourable physicochemical and molecular properties that will increase their chances of eventually reaching the market.[5] Literature has extensively shown that unfavourable ADME profiles and formulation challenges are often attributed to poor physicochemical properties, particularly aqueous solubility.[6]

Several studies have shown a relationship between physicochemical properties and drug-likeness.[6-7] This led to the determination of a set of guidelines for acceptable cut-off values for calculated surrogate molecule descriptors, which are key in predicting optimal physicochemical properties for an oral drug-like space. For example, Lipinski's rule of five (RO5) predicts that a compound is more likely to display high oral absorption and permeation when cLogP (the calculated 1-octanol/water partition coefficient) is <5, molecular weight (MW) ≤500 Da, number of hydrogen-bond donors (HBD) ≤5, and

the number of hydrogen-bond acceptors (HBA) ≤10.[7,8] Furthermore, additional guidelines were suggested by Veber et al., postulating that compounds with ≤10 rotatable bonds (measure of molecular flexibility) and topological polar surface area (tPSA) ≤140 $Å^2$ (or HBD + HBA ≤12) have a greater chance of achieving high oral bioavailability.[9]

4.3 Evaluation of physicochemical properties

The oral bioavailability of a drug is influenced by its aqueous solubility, permeability, and metabolic stability.[9] Of these three factors, this study focused mainly on strategies to improve aqueous solubility. The molecular descriptors (MW, cLogP, tPSA, HBD, and HBA) relating to the isoxazolidin-3-one-imines (ISI) and 3-isoxazolidin-4-yl amides (ISA) synthesized were predicted using StarDrop©6.4 Software to establish whether these compounds fall within the chemical space prescribed by the Lipinski's RO5 and parameters outlined by Veber et al., which would potentially translate to high oral bioavailability during hit-to-led optimization.

Moreover, because selected compounds displayed antimycobacterial activity, their predicted physicochemical properties were compared to those of conventional anti-TB drugs and drug candidates currently in clinical development, as mentioned in chapter 1. This was done to establish the significance of any similarities or differences between the pairs, which would in turn partially explain the activity observed as well as inform the design of analogues with drug-like properties similar to those of anti-TB drugs.

Therefore, for each compound, a Simplified Molecular-Input Line-Entry System (SMILES) was generated using ChemBioDraw Ultra and used as the primary format of data entry into StarDrop©6.4 for property predication. All statistical analyses were performed using Microsoft® office Excel 2018.

4.3.1 Kinetic solubility

The apparent solubility of all compounds synthesized was determined using a turbidimetric kinetic solubility assay. Hydrocortisone and reserpine were used as the respective positive and negative controls. The turbidimetric solubility of the target molecules was assessed in 96-well microtiter plates. Target molecules were dissolved in dimethyl sulfoxide (DMSO) to obtain 10-mM stock solutions from which serial dilutions were prepared in a pre-dilution plate with DMSO to obtain final concentrations of 0–10 μM in triplicate. Secondary dilutions were prepared in both DMSO and phosphate-buffered

saline (PBS, pH 7.4) to achieve final concentrations of 0–200 µM and incubated at room temperature (24–25 °C) for 2 h.

As their concentration in PBS increases, compounds are expected to precipitate and thus increase turbidity, as most organic compounds are not freely soluble in aqueous media. Turbidity was detected by measuring the absorbance at 620 nm and the approximate solubility was determined by plotting concentration against absorbance. The limit of solubility was determined as the concentration at which absorbance of the PBS solution rises above that of the DMSO solution for each compound (**Chapter 6**, **Figures 6.3** and **6.4**).[8,10]

The general classification of turbidimetric solubility for organic compounds using the turbidimetric solubility assay is as follows:[10]

High: >100 µM
Moderate: 20–100 µM
Low: <20 µM
However, determination of solubility via the turbidimetric method is far less accurate than that using high performance liquid chromatography (HPLC). This can be attributed to the non-specificity of the assay as the observed values depend on turbidity and solubility may only be determined as part of the ranges listed above rather than specific values. Nevertheless, the turbidimetric method is simple as well as cost- and time-effective when handling large sample sizes.

The recorded kinetic solubility values were statistically correlated with experimental factors such as melting point, HPLC retention time, and thin liquid chromatography (TLC) retardation factor (R_f). Each of these factors was used to measure a particular inherent compound characteristic that subsequently influences solubility. For instance, the melting point was used a measure of crystal packing energy, R_t, R_f, and tPSA as measures of polarity, and cLogP was indicative of lipophilicity.

4.3.2 HPLC-based solubility

Additionally, an alternative and more accurate method, which incorporates elements of kinetic and thermodynamic solubility in a hybrid method, was used to determine aqueous solubility. In this DMSO dry-down method adapted from Zhou et al.,[11] high and medium calibration standards (220 and 100 µM, respectively) in duplicate, as well as samples (200 µM) in triplicate, were added to a 96-well plate from a 10-mM stock solution in DMSO. DMSO was then evaporated from the samples for 2 h. Standards were dissolved in DMSO again and after vortexing the plate, the high standard was used to

prepare a low (11 µM) calibration standard in DMSO. PBS (pH 7.4) was added to the sample wells and the plate was incubated for 32 h at 25 °C with shaking. The plate was then centrifuged at 2500 × *g* for 30 min and the supernatants were transferred to another plate for analysis. Aqueous solubility was calculated using the ratio of the samples' UV peak areas to that of the standards with best-fit calibration curves.[12]

The general classification of solubility ranges obtained using the HPLC-based solubility method is defined as follows:

High: >150 µM
Moderate: 50–150 µM
Low: 11–50 µM
Very low: <11 µM

4.3.3 Results and discussion

The calculated and experimentally determined physicochemical properties of the 3-isoxazolidin-4-yl amide and isoxazolidine-3-one-imines series are listed in **Tables 4.1** and **4.2** below.

Table 4.1: Physicochemical properties of **SAR 2** 3-Isoxazolidin-4-yl amides (**IZAs**)

	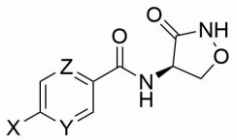			Calculated physicochemical properties[ǂ]					Experimental physicochemical properties			
Sample code	X	Y	Z	MW (g/mol)	cLogP	tPSA (A^{o2})	HBD	HBA	R_f[a]	t_R[b] (min)	m.p[c] (°C)	Turbidimetric Solubility at pH 7.4 (µM)
3.1	H	CH	CH	206.20	0.0552	67.43	2	5	0.13	0.45	187.3-186.6	200
3.2	OCH_3	CH	CH	236.23	0.0460	76.66	2	6	0.12	0.57	315.2-317.8	160
3.3	Br	CH	CH	269.10	0.8116	67.43	2	5	0.14	0.75	317.4-318.8	200
3.4	H	N	N	208.18	-0.5127	93.21	2	7	0.11	0.17	313.5-318.2	200
3.5	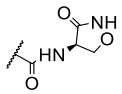	CH	CH	334.29	-0.3416	134.90	4	10	0.08	0.29	366.1-368.2	200
3.6	NH_2	N	CH	220.20	-1.241	106.30	3	7	0.83	0.84	323.2-325.1	200

Abbreviations: MW = molecular weight; cLogP = calculated logarithm of n-octanol/water partition co-efficient; tPSA = topological polar surface area; HBD = hydrogen bond donor; HBA = hydrogen bond acceptors; R_f = retardation factor (thin layer chromatography, TLC), t_R= retention time (high-performance liquid chromatography, HPLC); m.p = melting point. [ǂ]calculated using StarDrop©6; [a]analytical (TLC) with 80% ethyl acetate in hexane, except **3.5** and **3.6:** 5% methanol in dichloromethane; [b]HPLC-based method described in chapter 6; [c]average of the melting point range; [d]turbidimetric solubility.

Table 4.2: Physicochemical properties of **SAR 1** Isoxazolidine-3-one imines (**IZIs**)

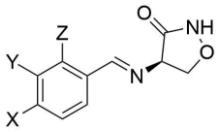				Calculated physicochemical properties[ǂ]					Experimental physicochemical properties		
Sample code	X	Y	Z	MW (g/mol)	cLogP	tPSA(Å^2)	HBD	HBA	R_f	m.p (°C)	Turbidimetric solubility(µM)
1.1	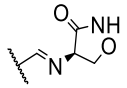	H	H	302.29	1.006	101.4	2	8	ND	264.20-265.10	200
1.2	H	H	H	190.20	1.083	50.69	1	4	ND	209.10-210.10	40
1.3	CH_3	H	H	204.23	1.464	50.69	1	4	ND	262.20-264.80	40
1.4	CN	H	H	215.21	1.066	74.48	1	5	ND	221.90-226.80	80
1.5	OCH_3	H	H	220.23	1.092	59.92	1	5	ND	303.0-305.70	80
1.6	H	OCH_3	H	220.23	1.092	59.92	1	5	ND	303.10-305.70	200
1.7	H	H	OCH_3	220.23	1.092	59.92	1	5	ND	339.70-340.20	20
1.8	H	F	H	208.19	1.209	50.69	1	4	ND	263.40-266.0	20
1.9	F	H	H	208.19	1.209	50.69	1	4	ND	240.20-242.40	20
1.10	H	H	F	208.19	1.209	50.69	1	4	ND	235.20-237.10	20
1.11	Br	H	H	269.10	1.851	50.69	1	4	ND	282.20-283.40	40

Abbreviations: MW = molecular weight; cLogP = calculated logarithm of n-octanol/water partition co-efficient; tPSA = topological polar surface area; HBD = hydrogen bond donor; HBA = hydrogen bond acceptors; R_f = retardation factor (thin layer chromatography, TLC), t_R= retention time (high-performance liquid chromatography, HPLC); m.p = melting point; ND, not determined. [ǂ]Calculated using StarDrop©6; [a]analytical TLC with 80% ethyl acetate in hexane, except **3.5** and **3.6:** 5% methanol in dichloromethane; [b]HPLC-based method described in chapter 6; [c]average of the melting point range; [d]turbidimetric solubility.

Overall, most of the predicted properties of compounds in the IZI and IZA series exhibited normal distribution profiles and this can be attributed to close similarities among analogues in each class. In contrast, the physicochemical properties of conventional anti-TB drugs and drug candidates were non-normally distributed, because of the diverse classes making up each category. For effective statistical comparison, all physicochemical properties were considered to be non-normally distributed. Therefore, the calculated median values rather than the means were used as the basis of comparison and analysis. The use of the calculated median as a more robust variable was also supported by the small number of compounds in each class (n < 45). The calculated median values and ranges of each property across the various datasets are listed in **Table 4.3**.

Table 4.3: Calculated median values for the predicted physicochemical parameters

Property	Calculated median values (range)			
	IZIs (*n* = 15)	**IZAs** (*n* = 6)	**TB.Ds** (*n* = 30)	**DCs** (*n* = 10)
MW	215.21	236.23	363.4	456.5
	(190.20-302.29)	(206.20-334.29)	(102.1–877.0)	(330.6-1196.0)
cLogP	1.092	-0.148	0.392	2.685
	(1.006 – 1.851)	(0.8116- -1.241)	(-3.23–7.59)	(-0.803-6.33)
tPSA	50.69	84.94	85.44	91.33
	(50.69-101.4)	(67.43-134.9)	(38.91-358.2)	(24.06-255.80)
HBD	1	2	3	1
	(1-2)	(2-4)	(0-13)	(0-7)
HBA	4	7	7	8
	(4-8)	(5-10)	(2-21)	(2-22)

Abbreviations: IZIs = isoxazolidine-3-one-imines; IZAs = isoxazolidin-4-yl amides; TB.Ds = conventional anti-TB drugs; DCs = anti-TB drug candidates; MW = molecular weight; cLogP = calculated logarithm of n-octanol/water partition coefficient; tPSA = topological polar surface area; HBD = hydrogen bond donors; HBA = hydrogen bond acceptors.

Calculated median values indicate that most of the compounds studied obeyed Lipinski's RO5. However, the ranges reveal some degree of deviation, particularly with regard to properties

associated with TB.Ds and DCs, further highlighting the structural diversity of compounds in these classes.

The non-parametric Mann-Whitney-Wilcoxon statistical comparison test was used as all compound sets were considered to have non-normal property distributions.[13,14] This comparison was performed to establish whether or not there were any statistically significant differences between the predicted properties of IZIs and IZAs and those of TB.Ds and DCs. The test was performed by comparing all the predicted properties of a pair of independent compound sets and determining the p-value at a 95% confidence level. The null hypothesis (Ho) for the Mann-Whitney-Wilcoxon comparison was that there was no significant statistical difference in the distribution and the mean values of the compared datasets, when the significant value was 0.05. Therefore, the null hypothesis was rejected in all cases of $p < 0.05$ and accepted when $p \geq 0.05$. Thus, there was no statistically significant difference between the parameters compared (**Table 4.4**).

Table 4.4: Mann-Whitney-Wilcoxon test results (p-value) comparing differences between the predicted physicochemical properties of IZIs and IZAs versus those of TB.Ds and DCs

	p-values				
	MW	**cLogP**	**tPSA**	**HBD**	**HBA**
IZIs vs TB.Ds	0.040	0.387	0.101	0.201	0.067
IZIs vs DCs	0.012	0.169	0.037	0.202	0.018
IZAs vs TB.Ds	0.015	0.474	0.080	0.168	0.051
IZAs vs DCs	0.014	0.824	0.014	0.145	0.004

Abbreviations: IZIs = isoxazolidine-3-one-imines; IZAs = isoxazolidin-4-yl amides; TB.Ds = conventional anti-TB drugs; DCs = anti-TB drug candidates; MW = molecular weight; cLogP = calculated logarithm of n-octanol/water partition coefficient; tPSA = topological polar surface area; HBD = hydrogen bond donors; HBA = hydrogen bond acceptors. Values in red ($p < 0.05$) indicate the null hypothesis was rejected at the significance level (that is, there is a difference in the compared datasets).

Consequently, significant differences between IZIs and TB.Ds with respect to MW were revealed. However, IZIs and DCs showed similar properties except with regard to MW and tPSA. IZAs differed from TB.DS in terms of MW, and with regard to MW, tPSA, and HBA when compared to DCs. Frequency distribution histograms were plotted (**Figures 4.1 and 4.2**). As depicted in **Figure 4.1A**, 82% of IZIs had MWs between 150 and 350 Da, while 80% of IZAs had MWs <300 Da. In contrast, 54% of TB.Ds and

30% of DCs had MWs <400 Da. However, considering the RO5, 22% of TB.Ds and 28% of DCs had MWs >500 Da, whereas all IZIs and IZAs had MWs <500 Da.

Significant differences in cLogP were observed between compound sets (**Figure 4.1B** and **Table 4.4**). Although 46%, 30%, and 49% of TB.Ds, DCs, and IZA, respectively, had cLogP < 1.0, none of the IZI analogues had cLogP values in this range (**Figure 4.1B**). Therefore, TB.Ds displayed uniquely lower cLogP values compared to the other clusters. cLogP values for all IZIs lay between 1.01 and 2.00, whereas only 20% of TB.Ds and 13% of DCs exhibited cLogP values in this range. In addition, 50% of IZAs had cLogP values in the range of 0.01 to 1.00. Lipinski's RO5 was violated (cLogP > 5) by 6% and 20% of TB.Ds and DCs, respectively (**Figure 4.1B**).

To visualize the various chemical spaces (with respect to MW and cLogP) occupied by the four compound sets, cLogP values were plotted against MW (**Figure 4.1C**). The plot revealed that TB.Ds, IZIs, and IZAs all occupied similar chemical spaces. In this case, 60% of TB.Ds showed cLogP < 2 and MW < 400 Da. TB.Ds outside this space belonged mainly to two classes of compounds: rifamycins and aminoglycosides. All IZIs showed cLogP < 2 and MW < 350 Da, and 67% of IZAs displayed cLogP < 0 and MW < 300 Da. Conversely, DCs occupied a unique chemical space that is distinct from that occupied by TB.Ds, IZAs, and IZIs. In this regard, 44% of DCs had MWs ranging from 300 to 450 Da and cLogP between 1.0 and 3.0. Notably, the most recently approved anti-TB drugs, bedaquiline and delamanid, occupy a chemical space similar to that of compound libraries produced via similar approaches in the discovery of small molecule anti-TB drugs during the last few decades.

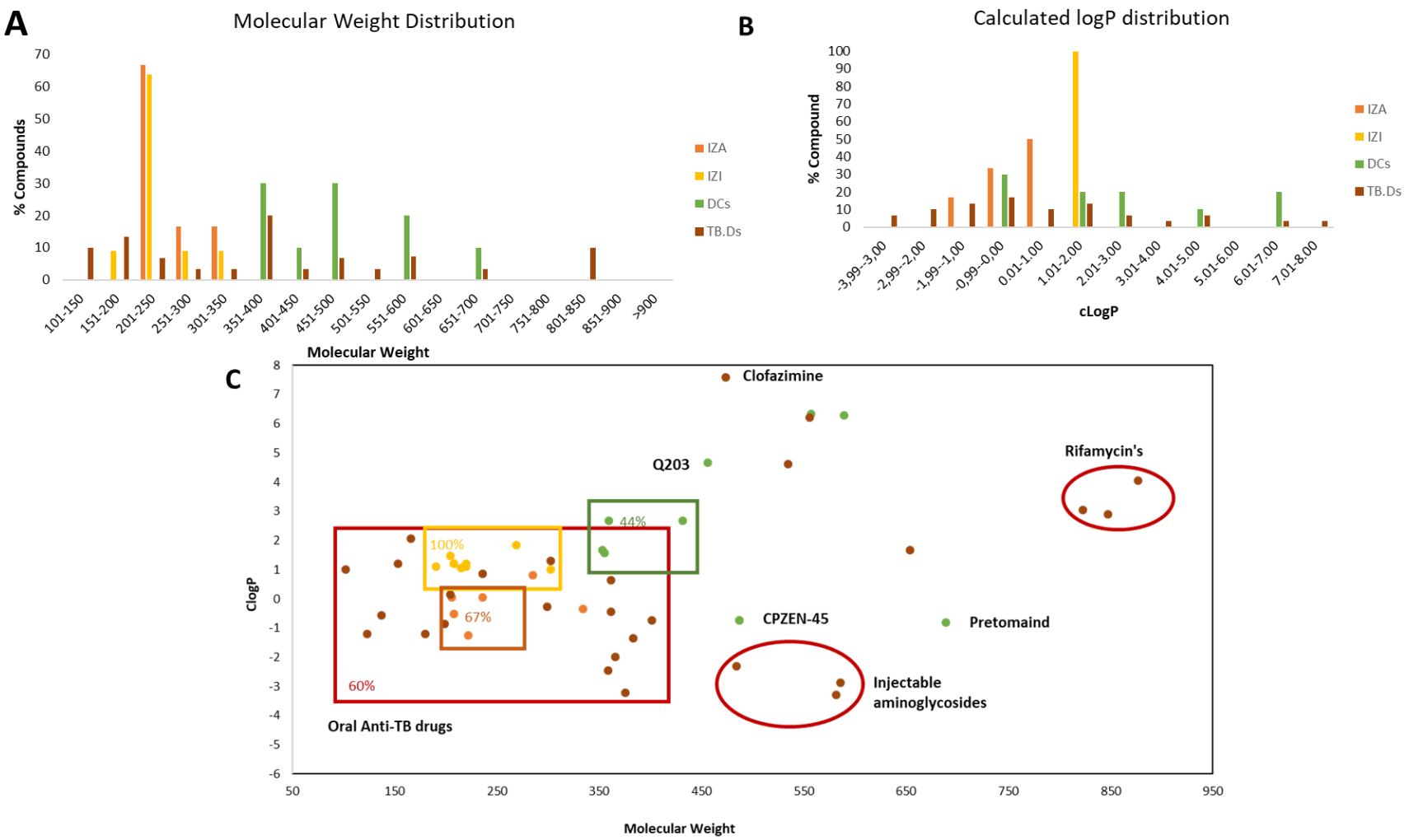

Figure 4.1: Frequency distribution histograms for **A.** molecular weight and **B.** calculated logarithm of n-octanol/water partition coefficient (cLogP). **C.** Scatter Plot showing the chemical space occupied by the compound sets studied with respect to molecular weight and cLogP. Abbreviations: IZI = isoxazolidine-3-one-imines; IZA = isoxazolidin-4-yl amides; TB.Ds = conventional anti-TB drugs; DCs = anti-TB drug candidates.

Incorporation of hydrogen bonding moieties is a strategy commonly employed to improve aqueous solubility and facilitate drug-target binding interactions at the sub-cellular active sites. However, a high number of HBDs and HBAs may limit the permeation of compounds across lipid-rich cell membranes. Lipinski's RO5 suggests that there should be ≤5 HBDs and ≤10 HBAs in an oral drug-like compound. The total number of HBAs and HBDs significantly affects the tPSA of a compound, which in turn influences its solubility and permeability. According to Veber et al., the combined number of HBDs and HBAs in a drug-like compound should be ≤12, and the tPSA should be ≤140 $Å^2$.[9]

In this study, most compounds exhibited tPSA values between 50 and 130 $Å^2$ (**Figure 4.2A**), thus in agreement with Veber's rule. Notably, injectable aminoglycosides as well as the orally administrated rifamycins exhibited relatively high tPSA values. It was also noted that all HBD distributions were skewed to the left (**Figure 4.2B**)**.** For example, 90% of IZIs comprised one HBD while 66% of IZAs contained two. In contrast, 20% of TB.Ds and 10% of DCs had >5 HBDs and were thus in violation of the RO5. All compound sets exhibited normal distributions of HBAs, with values ranging from 0 to 8 (**Figure 4.2C**). Approximately 20% of TB.Ds (primarily rifamycins and aminoglycosides) had >14 HBAs.

Overall, most compounds in this study occupied a similar chemical space with regards to tPSA (<140 $Å^2$) and the total number of HBDs and HBAs (<15; **Figure 4.3)**. This plot also highlighted a strong linear correlation between tPSA and the total number of HBDs and HBAs across all four compounds sets, resulting in linear regression factors (R^2) ranging from 0.9722 to 0.9891.

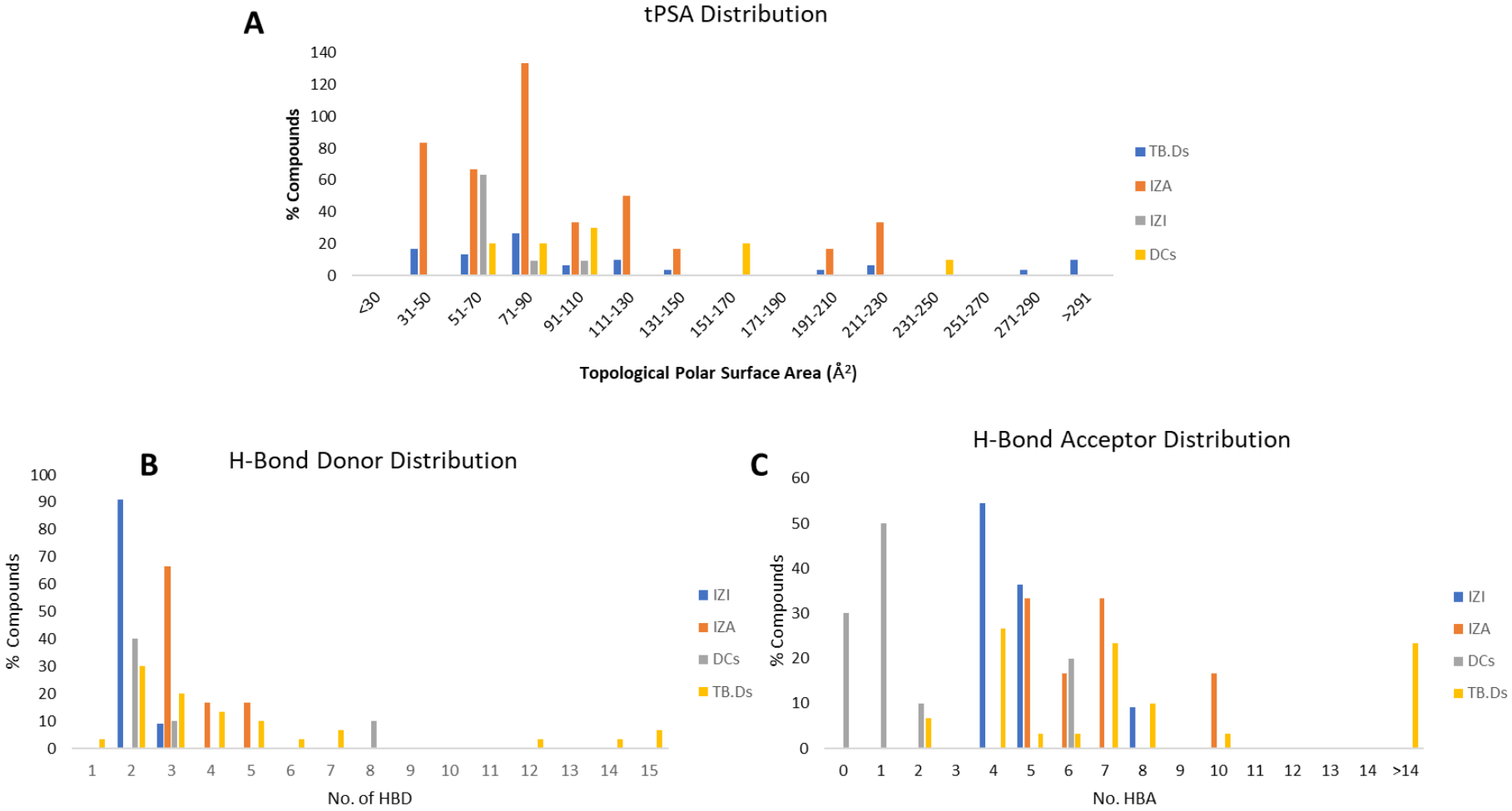

Figure 4.2: Frequency distribution histograms of **A.** topological surface area (tPSA), **B.** distribution of hydrogen bond donor (HBDs), and **C.** hydrogen bond acceptors (HBAs). Abbreviations: IZIs = isoxazolidine-3-one-imines; IZAs = isoxazolidin-4-yl amides; TB.Ds = conventional anti-TB drugs; DCs = anti-TB drug candidates

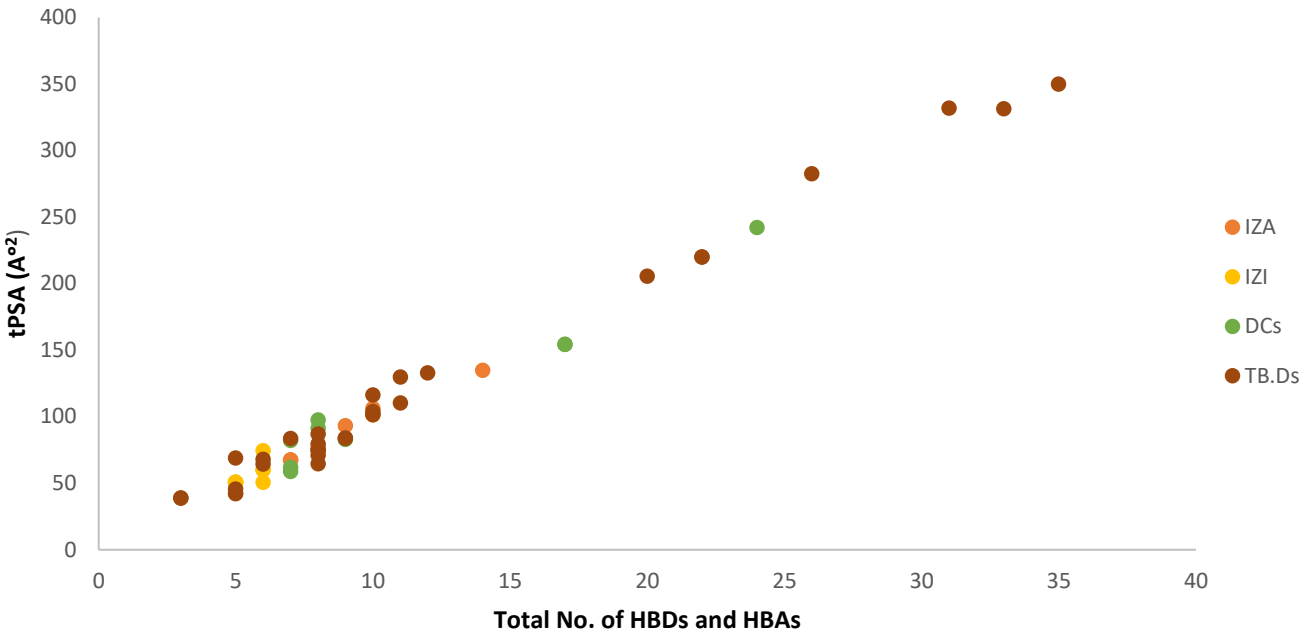

Figure 4.3: Plot showing the chemical space occupied by the compound sets studied with respects to tPSA and the total number of hydrogen bond donors (HBDs) and hydrogen bond acceptors (HBAs)

4.4 HPLC-based solubility versus kinetic solubility

There are differences in the results obtained using the turbidimetric and HPLC-based methods across the IZI and IZA series (**Figure 4.4**), and it is evident that the turbidimetric assay unsurprisingly yields higher solubility values than HPLC-based method.

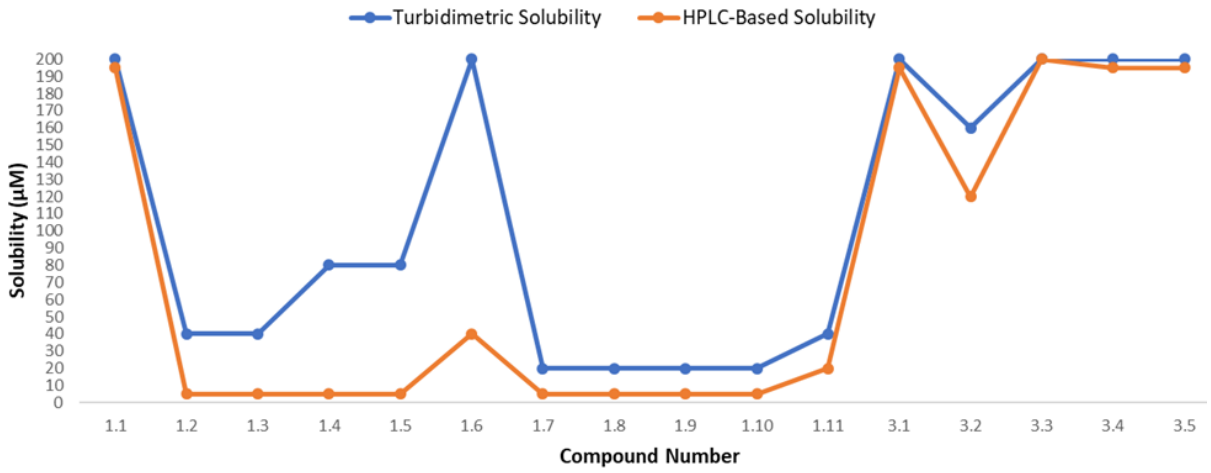

Figure 4.4: Line graph comparing solubility results using the turbidimetric assay and the high-performance liquid chromatography (HPLC)-based assay (pH 7.4) across all compounds in **SAR 1** and **SAR 2**

The turbidimetric assay yielded higher values than the HPLC-based method for 14 of the 16 compounds tested. This discrepancy may in part be attributed to the shorter incubation period in the turbidimetric method, with the measurements thus obtained in a saturated solution rather than a solution that has reached equilibrium.[14,15] In addition, the turbidimetric and HPLC assay differ with regard to the precipitate formed at equilibrium (amorphous or crystalline), as solubility is influenced by the solid-state form of a compound. Additionally, solubility values obtained may only be estimated in contrast to determination of the exact compound concentration in solution.

Generally, the turbidimetric method favors the formation of an amorphous precipitate due to the presence of DMSO whereas in the HPLC-based method, the form that is more energetically efficient is favored due to the long incubation time and absence of DMSO. If an amorphous solid precipitates in the HPLC-based assay, the results are likely to be closer to those of the turbidimetric method than if a crystalline precipitate is formed.[16]

Considering that the HPLC-based method is more rigorous, SPR analysis of the IZI and 3-IZA series was performed using the HPLC-based solubility results.

4.5 Structure-property relationships (SPRs)

Solubility plays a key role in drug discovery as it provides information for diverse research activities such as biological activity assessments, structure optimization, pharmacokinetic (PK) screening, and animal dosage form selection for efficacy, PK, and toxicity screening.[17] Therefore, it is essential to establish the solubility of potential drug candidates in the early stages of the drug discovery process[15,18] as this indicates how a drug molecule is likely to perform in subsequent *in vitro* assays, and may suggest possible problems with regard to ADME.[11] Poorly soluble compounds may precipitate out of solution during biological tests, thus leading to poorly reproducible and unreliable *in vitro* and *in vivo* study results.[19] Although solubility is a measurable parameter, the values obtained vary as they are dependent on solvent factors (pH, temperature, and co-solvent effects) and experimental conditions (time, detection method, and assay materials) at the time of measurement.[12,15]

Although the majority of compounds in the IZI series exhibited very low solubility (<11 μM) and those in the IZA series exhibited high (>150 μM) aqueous solubility, the aim was to decipher the factors affecting solubility. Factors responsible for improved solubility were deduced by measuring properties that are inherent and dependent on a compound's structural features. Accordingly, melting points were measured to provide information about crystal packing energies, tPSA was used as a relative estimate of polarity, while cLogP values were generated *in silico* and used as a measure of lipophilicity. To investigate the relationship between these factors and aqueous solubility across a particular class

of compounds, correlation graphs of aqueous solubility were plotted against the appropriate factor for each class of compounds and the correlation strength (R_2) was determined using Evans' guidelines as follows:[20]

0.0-0.19: Very weak
0.2-0.39: Weak
0.4-0.59: Moderate
0.6-0.79: Strong
0.8-1.00: Very strong

These plots revealed a very strong correlation between solubility and melting point in the IZA series (R^2 = 0.9318; **Figure 4.5C**), suggesting that the crystal packing efficiency of the compounds in crystal lattices was more dominant than changes in lipophilicity or polarity. In contrast, the IZI series showed moderate correlations between solubility and tPSA (**Figure 4.5B**). This may suggest that increasing the polarity of compounds in the IZI series led to improved aqueous solubility. There was no correlation between solubility and cLogP (lipophilicity) in either class of compounds (R^2 = 0.085 for IZIs and R^2= 0.0004 for IZAs).

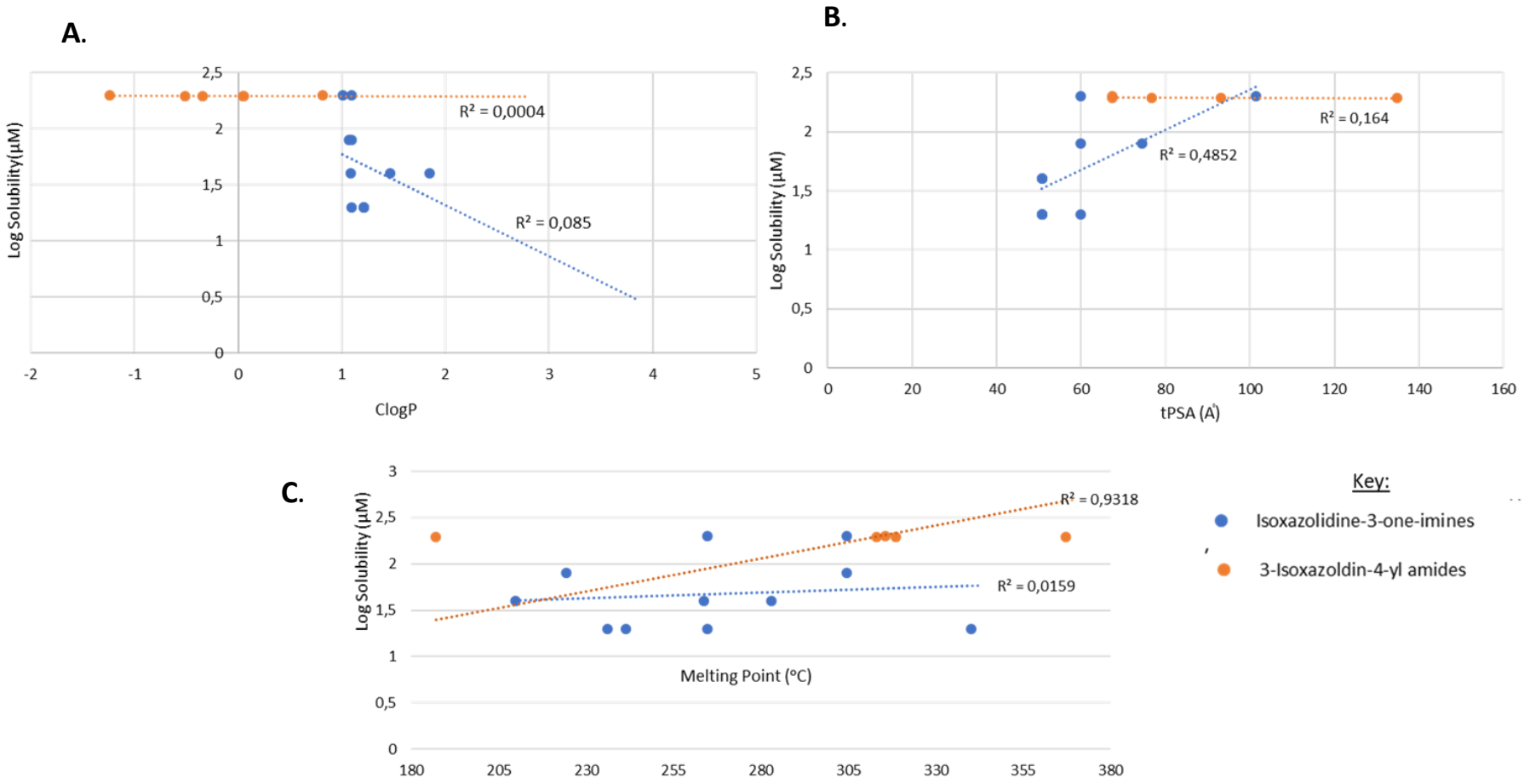

Figure 4.5: Correlation plots of Log solubility (determined using the HPLC-based method) against **A.** cLogP, **B.** tPSA, and **C.** melting point

4.6 Conclusions

This chapter described the studies conducted with respect to physicochemical profiling. This revealed that IZA, IZI and TB.Ds(with the exception of injectable aminoglycosides, Rifamycins and clofazimine) occupy very similar chemical spaces[Mwt and cLogP], which are distinct from that occupied by a majority of the anti-TB drugs candidates. There were minor violations of the Lipinski's RO5 was observed. In addition to this, SPR studies showed that solubility was strongly correlated to melting point in the IZA series (R^2 = 0.9318) and moderately correlated to tPSA for IZI(R^2 = 0.164, whereas there was no correlation between solubility and cLogP (lipophilicity) in either class of compounds (R^2 = 0.085 for IZIs and R^2= 0.0004 for IZAs).

4.7 References

(1) Gleeson, P.; Bravi, G.; Modi, S.; Lowe, D. Bioorganic & Medicinal Chemistry ADMET Rules of Thumb II: A Comparison of the Effects of Common Substituents on a Range of ADMET Parameters. *Bioorg. Med. Chem.* **2009**, *17* (16), 5906–5919.

(2) Waring, M. J.; Waring, M. J. Expert Opinion on Drug Discovery Lipophilicity in Drug Discovery Lipophilicity in Drug Discovery. *Expert Opin. Drug Discov.* **2010**, *5*, 235–248.

(3) Schuster, D.; Laggner, C.; Langer, T. Why Drugs Fail – A Study on Side Effects in New Chemical Entities. *Curr. Pharm. Des.* **2005**, *11*, 3545–3559.

(4) Hughes, J. D.; Blagg, J.; Price, D. A.; Bailey, S.; Decrescenzo, G. A.; Devraj, R. V; Ellsworth, E.; Fobian, Y. M.; Gibbs, M. E.; Gilles, R. W.; et al. Bioorganic & Medicinal Chemistry Letters Physiochemical Drug Properties Associated with in Vivo Toxicological Outcomes. *Biorgan. Med. Chem. Lett.* **2008**, *18*, 4872–4875.

(5) Meanwell, N. A. Improving Drug Design: An Update on Recent Applications Of. *Chem. Res. Toxicol.* **2016**, *29*, 564–616.

(6) Williams, H. D.; Trevaskis, N. L.; Charman, S. A.; Shanker, R. M.; Charman, W. N.; Pouton, C. W.; Porter, C. J. H. Strategies to Address Low Drug Solubility in Discovery and Development. *Pharmacol. Rev.* **2013**, *65* (1), 315–499.

(7) Oncology, H.; Hospital, C. Chemical Beauty Contest. *Nature* **1912**, *481* (January), 5–6.

(8) Franc, I.; Lipinski, A.; Feeney, P. J. Experimental and Computational Approaches to Estimate Solubility and Permeability in Drug Discovery and Development Settings. *Adv. Drug Deliv. Rev.* **1997**, *23*, 3–25.

(9) Veber, D. F.; Johnson, S. R.; Cheng, H.; Smith, B. R.; Ward, K. W.; Kopple, K. D. Molecular Properties That Influence the Oral Bioavailability of Drug Candidates. *J. Med* **2002**, *45*, 2615–2623.

(10) Bevan, C. D.; Lloyd, R. S. A High-Throughput Screening Method for the Determination of Aqueous Drug Solubility Using Laser Nephelometry in Microtiter Plates. *Anal. Chem.* **2000**, *72* (8), 1781–1787.

(11) Zhou, L.; Yang, L.; Tilton, S.; Wang, J. Development of a High Throughput Equilibrium Solubility Assay Using Miniaturized Shake-Flask Method in Early Drug Discovery. *J. Pharm. Sci.* **2007**, *96* (11), 3052–3071.

(12) Alsenz, J.; Kansy, M. High-Throughput Solubility Measurement in Drug Discovery and Development. *Adv. Drug Deliv. Rev.* **2007**, *59* (7), 546–567.

(13) Fay, M. P.; Proschan, M. A. NIH Public Access. *Stat. Surv.* **2010**, *4*, 1–37.

(14) Qu, Y.; Zhao, Y. D.; Rahardja, D. Wilcoxon – Mann – Whitney Test: Stratify or Not ? *J. Biopharm. Stat.* **2008**, *18*, 1103–1111.

(15) Kerns, E. H.; Di, L.; Carter, G. T. In Vitro Solubility Assays in Drug Discovery. *Curr. Drug Metab.* **2008**, *9* (9), 879–885.

(16) Saal, C.; Petereit, A. C. Optimizing Solubility: Kinetic versus Thermodynamic Solubility Temptations and Risks. *Eur. J. Pharm. Sci.* **2012**, *47* (3), 589–595.

(17) Li Di, E. H. K. *Drug-Like Properties (Second Edition) Concepts, Structure Design and Methods*

from ADME to Toxicity Optimization; 2016.

(18) Williams, H. D.; Trevaskis, N. L.; Charman, S. A.; Shanker, R. M.; Charman, W. N.; Pouton, C. W.; Porter, C. J. H. Strategies to Address Low Drug Solubility in Discovery and Development. *Pharmacol. Rev.* **2013**, *65* (1), 315–499.

(19) Savjani, K. T.; Gajjar, A. K.; Savjani, J. K. Drug Solubility: Importance and Enhancement Techniques. *ISRN Pharm.* **2012**, *2012* (100 mL), 1–10.

(20) Evans, J. D. *Straightforward Statistics for the Behavioral Sciences;* Brooks/Cole Pub Co., 1995.

Chapter 5: Conclusions and recommendations for future work

5.1 Summary and conclusions

The overall objective of this study was to conduct structure-activity relationships towards identifying new analogues of DCS with improved selective antimycobacterial activity. This was based on the hypothesis that the relatively safer DCS analogue Terizidone displayed enhanced antimycobacterial activity.

The first aim of the study was to design, synthesize and characterize new isoxazolidine-3-one-imines and 3-isoxazolidin-4-yl amides. All compounds were fully characterized using spectroscopic techniques (NMR spectroscopy); chromatographic methods (TLC and HPLC-MS) and physicochemical attributes (melting point, and aqueous solubility).

The second aim of the study was to pharmacologically evaluate the synthesized compounds for their *in vitro* antimycobacterial activity, cytotoxicity and microsomal metabolic stability. Two compounds (**1.1** and **3.3**) out of the 16 novel compounds displayed antimycobacterial potency against the drug-susceptible *Mtb* H37Rv strain cultured in 7H9/ADC media. Furthermore all 17 compounds exhibited low cytotoxicity against the CHO and HepG2 cell lines. The most potent compound, **3.3**, exhibited high microsomal metabolic stability across all species.

The third aim of the study was to profile all final target compounds with respect to physicochemical properties, including aqueous solubility. The HPLC-based solubility data obtained was correlated with the experimentally determined melting points, HPLC retention times (tR), TLC retardation factors (*R*f) as well as the virtually predicted physicochemical properties such as cLogP, in order to establish structure-property relationships. It was observed that, solubility was strongly correlated to melting point in the IZA series (R^2 = 0.9318) and moderately correlated to tPSA for IZI (R^2 = 0.164), whereas there was no correlation between solubility and cLogP (lipophilicity) in either class of compounds (R^2 = 0.085 for IZIs and R^2= 0.0004 for IZAs).

5.2 Recommendations for future work

I. Study the mechanism of action and resistance of selected active compounds using tool mycobacterial strains and/or metabolic rescue or biochemical assays.

II. Since compound **3.3** (as shown below) displayed good activity, low cytotoxicity, high metabolic stability, this compound should be progressed to in vivo pharmacokinetics and for efficacy studies in a mouse model of TB.

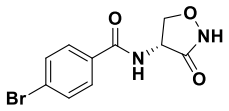

Compound 3.3

III. Study the metabolism of selected active compounds in *Mtb.*

Chapter 6: Experimental results

6.1 Chapter overview

The results related in Chapter 5 supplement those discussed in Chapters 2-4 by describing the experimental protocols involved, particularly those that are not outlined in the main text. In addition, the characterization data of all the synthesized compounds are provided in this chapter.

6.2 Methods: Chemistry

6.2.1 Reagents and solvents

All commercially available chemicals were purchased from Sigma-Aldrich or Combi-Blocks with the exception of 5-((tert-butoxycarbonyl)amino)picolinic acid, which was purchased from FluroChem, UK. All commercially available reagents were of analytical grade (AR) and were thus used without purification. N,N-Dimethylformamide (DMF) and methanol were purchased as anhydrous solvents whereas all other commonly used solvents were purchased from Science World. The high-performance liquid chromatography (HPLC)-grade solvents ammonium acetate and MeOH were obtained from Sigma-Aldrich for use in chromatography and mass spectrometry (MS).

6.2.2 Spectroscopic and physical characterization

NMR: ^{1}H-NMR spectra were recorded on Varian Mercury (300 MHz), Brucker Ultrashield-Plus Varian Mercury (400 MHz), or Bruker (600 MHz) instruments with tetramethylsilane (TMS) as the internal reference. ^{13}C-NMR spectra were recorded on the same instruments at 101 MHz or 151 MHz with TMS as the internal standard. ^{13}C chemical shift values are listed without specific assignment to carbon atoms. NMR samples were dissolved in deuterated dimethylsulfoxide (DMSO-d_6). Chemical shifts (δ) are reported in parts per million (ppm) to two decimal places and coupling constants (*J*) are reported in Hertz (Hz) to two decimal places. Abbreviations used in assigning in ^{1}H-NMR signals are: d (doublet), dd (doublets of doublets), ddd (doublets of doublets of doublets), m (multiplet), q (quartet), s (singlet), t (triplet), or td (triplets of doublets). Where assignment of ^{1}H-NMR and ^{13}C-NMR signals was ambiguous, two-dimensional NMR spectra from correlation spectroscopy (COSY) and heteronuclear single quantum coherence (HSQC) spectroscopy were acquired to facilitate accurate assignments.

Melting points: Melting points were measured using the Stuart automatic melting point apparatus SMP40 and are reported as uncorrected values. The recorded melting points were measured in duplicate and represent the average of the clear point, which is the temperature at which all solid materials in the melting tubes turns to liquid.

6.2.3 Chromatography

The peak purity, retention time, and molecular ions of the target compounds were determined using an Agilent HPLC-MS instrument with Agilent 1260® Infinity binary pump, Agilent 1260® Infinity diode array detector, Agilent 1290® Infinity column compartment, Agilent 1260® Infinity autosampler, Agilent 6120® quadrupole LC/MS, and Peak Scientific® Genius 1050 nitrogen generator. An X-bridge® (C18, 2.5 µm, 3.0 mm (ID) x 50 mm length) column maintained at 35 °C was used. The composition and gradient conditions of the mobile phase used at a flow rate of 0.9 mL/min with 2 µL injection volume are listed in **Table 5.1**. The mass spectra were acquired using electrospray ionization (ESI) or atmospheric pressure chemical ionization (APCI) in positive and negative ionization modes. All final compounds with the exception of compounds 1.1-1.11 were subjected to purity check experiments using LC-MS to ensure purity was ≥95%.

Table 6.1: Gradient used to investigate the purity and mass of compounds using HPLC-MS

Time (min)	% A	% B
0.00-1.00	90	10
1.00-3.00	5	95
3.00-5.00	5	95
5.00-6.50	90	10
6.50-7.00	90	10

Mobile phase A, 10 mM NH_4OAc in buffer (0.4% acetic acid); mobile phase B, 10 mM NH_4OAc (0.4% acetic acid) in 90% HPLC-grade CH_3OH in H_2O. HPLC-MS, high-performance liquid chromatography-mass spectrometry.

Reaction progress was monitored using a combination of analytical thin-layer chromatography (TLC) and LC-MS. TLC Silica gel 60 F_{254} aluminium-backed, pre-coated silica gel plates were purchased from Merck. Spots were visualized using ultra-violet (UV) light at 254 or 366 nm and non-UV-absorbing TLC spots were visualized using ninhydrin or anisaldehyde spray. TLC plates were developed to monitor reaction progress and accurately determine retardation factor values (R_f) in a 100-mL beaker covered with a watch glass. Silica gel column chromatography was performed using Merck Kieselgel 60: 70-

230 mesh (gravity column or flash chromatography) on a Biotage Isolera™ system (Biotage, AB, Uppsala, Sweden).

6.2.4 Synthesis and characterization

General procedure for the synthesis of SAR 1 compounds 1.1-1.11

The relevant aldehyde (1.0 equiv) was dissolved in 2-4 mL of methanol. The solution was heated under reflux at 65 °C for 5 min. Subsequently, a suspension of D-cycloserine (1.5 equiv) in 5 mL methanol was added to the solution and left to reflux until the solution became milky white/turbid. The solution was rapidly cooled down and left to stir under ice for 2-3 h until a precipitate form. The precipitate was filtered, triturated with hot methanol, and dried *in vacuo* to furnish the required Schiff base D-isoxazolidone derivative.

Compound 1.1: (4R,4'R)-4,4'-(((1E,1'E)-1,4-phenylenebis(methaneylylidene))bis(azaneylylidene))bis(isoxazolidin-3-one)

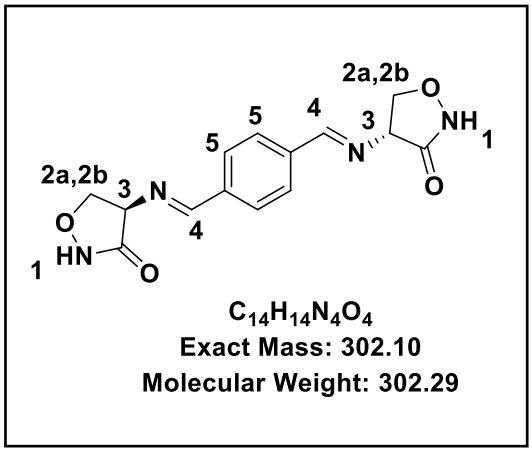

Obtained from terephtalaldehyde (0.250 g, 1.86 mmol, 1.0 equiv) and D-cycloserine (0.383 g, 3.72 mmol, 3 equiv) as a white solid (0.221 g, 88%); m.p 264.2-265.1 °C; δ_H (400 MHz, DMSO-d_6): 11.42 (s, 2H, 2x NH-1), 8.51 (s, 2H, 2x H-4), 7.84 (s, 4H, 4x H-5), 4.66 (dd, *J* = 8.57, 7.35 Hz, 2H, 2x H-2a), 4.55 (t, *J* = 7.28 Hz, 2H, 2x H-3), 4.39 (dd, *J* = 8.58, 7.12 Hz, 2H, 2x H-2b); δ_c (101 MHz, DMSO-*d_6*) 170.54 (2C), 164.70 (2C), 138.37 (2C), 128.95 (4C), 74.56 (2C), 70.18 (2C).

Compound 1.2: (R, E)-4-(benzylideneamino)isoxazolidine-3-one

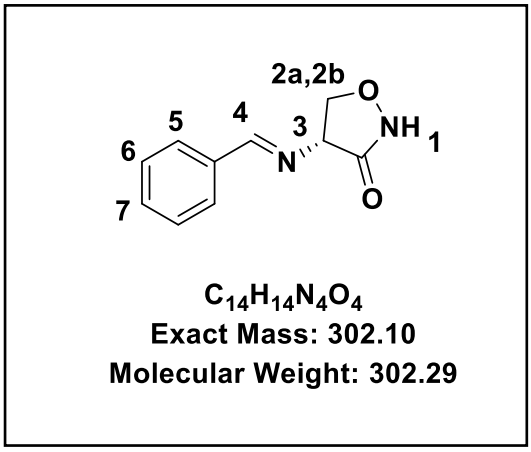

Obtained from benzaldehyde (0.200 g, 1.87 mmol, 1.0 equiv) and D-cycloserine (0.290 g, 2.83 mmol, 1.5 equiv) as a white solid (0.070 g, 20%); m.p 209.1-210.1 °C; δ_H (400 MHz, DMSO-d_6), δ 8.34 (s, 1H, NH-1), 8.25 (s, 1H, H-4), 7.62-7.50 (m, 2H, 2x H-5), 7.43-7.38 (m, 3H, 2x H-6, H-7), 4.46-4.30 (m, 2H, H-2a, H-2b); δ_C (101 MHz, DMSO-*d_6*) δ 165.41, 150.26, 132.16, 130.57, 129.24 (2C), 127.48 (2C), 75.54, 55.11.

Compound 1.3: (R, E)-4-((4-methylbenzylidene)amino)isoxazolidine-3-one

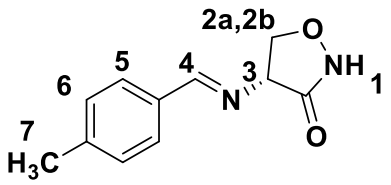

$C_{11}H_{12}N_2O_2$
Exact Mass: 204.09
Molecular Weight: 204.23

Obtained from *p*-tolualdehyde (0.250 g, 2.08 mmol, 1.0 equiv) and D-cycloserine (0.321 g, 3.12 mmol, 1.5 equiv) as a white solid (0.150 g, 35%); m.p 262.20-264.8 °C; δ_H (400 MHz, DMSO-d_6): 8.18 (s, 1H, NH-1), 8.14 (s, 1H, H-4), 7.47 (d, *J* = 8.13 Hz, 2H, 2x H-5), 7.20 (d, *J* = 8.1 Hz, 2H, 2x H-6), 4.40-4.30 (m, 2H, H-2a,H-2b), 4.18-4.13 (m, 1H, H-3), 2.31 (s,3H, 3x H-7); δ_C (101 MHz, DMSO-d_6): 165.46, 150.18, 140.33, 133.40, 129.78 (2C), 127.46 (2C), 75.37, 55.27, 21.38

Compound 1.4: (R, E)-4-(((3-oxoisoxazolidin-4-yl)imino)methyl)benzonitrile

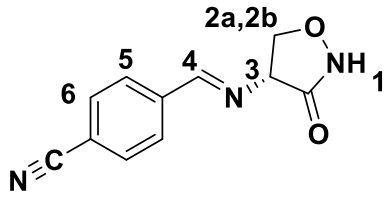

$C_{11}H_9N_3O_2$
Exact Mass: 215.07
Molecular Weight: 215.21

Obtained from 4-cyanobenzaldehyde (0.250 g, 1.90 mmol, 1.0 equiv) and D-cycloserine (0.294 g, 2.85 mmol, 1.5 equiv) as a white solid (0.031 g, 9.5%); m.p 221.9-226.8 °C; δ_H (400 MHz, DMSO-d_6): 8.40 (s, 1H, NH-1), 8.34 (s, 1H, H-4), 7.86 (d, *J* = 8.40 Hz, 2H, 2x H-5), 7.79 (d, *J* = 8.39 Hz, 2H, 2x H-6), 4.4-4.38 (m, 2H, H-2a, H-2b), 4.22-4.18 (m, 1H, H-3); δ_C (101 MHz, DMSO-d_6): 165.31, 149.05, 136.62, 133.15 (2C), 128.10 (2C), 118.96, 112.65, 75.65, 55.06.

Compound 1.5: (R, E)-4-((4-methoxybenzylidene)amino)isoxazolidine-3-one

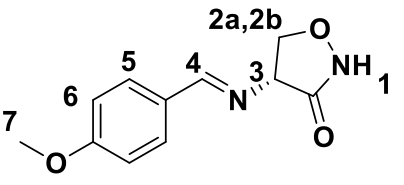

$C_{11}H_{12}N_2O_3$
Exact Mass: 220.08
Molecular Weight: 220.23

Obtained from *p*-anisaldehyde (0.200 g, 1.46 mmol, 1.0 equiv) and D-cycloserine (0.226 g, 2.20 mmol, 1.5 equiv) as a white solid (0.023 g, 7.5%); m.p 303.0-305.7 °C; δ_H (400 MHz, DMSO-d_6): 8.31 (s, 1H, NH-1), 8.18 (s, 1H, H-4), 7.54 (d, *J* = 8.85 Hz, 2H, 2x H-5), 6.96 (d, *J* = 8.78 Hz, 2H, 2x H-6), 4.38-4.32 (m, 2H, H2a, H-2b), 4.18-4.14 (m,1H, H-3), 3.78 (s,3H, 3x H-7); δ_C (101 MHz, DMSO-d_6): 165.31, 149.05, 136.62, 133.15 (2C), 128.10 (2C), 118.96, 112.65, 75.65, 55.06.

Compound 1.6: (R, E)-4-((3-methoxybenzylidene)amino)isoxazolidine-3-one

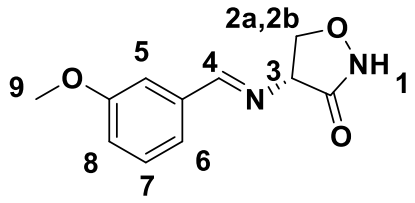

$C_{11}H_{12}N_2O_3$
Exact Mass: 220.08
Molecular Weight: 220.23

Obtained from *m*-anisaldehyde (0.200 g, 1.46 mmol, 1.0 equiv) and D-cycloserine (0.226 g, 2.20 mmol, 1.5 equiv) as a white solid (0. 014 g, 4.3%); m.p 303.1-305.7 °C; δ^H (400 MHz, DMSO-d_6): 8.34 (s, 1H, NH-1), 8.21 (s, 1H, H-4), 7.34-7.32 (m, 1H, H-6), 7.18-7.16 (m, 2H, H-5, H-6), 6.98 (ddd, *J* = 8.26, 2.60, 1.70 Hz, 1H, H-8) 4.44-4.39 (m, 2H, H-2a, H-2b), 4.18-4.16 (m, 1H, H-3), 3.76 (s, 3H, 3x H-9); δ_C (101 MHz, DMSO-d_6): 175.00, 163.84, 159.93, 133.51, 130.34, 120.07, 116.57, 112.26, 75.66, 55.65, 55.09.

Compound 1.7: (R, E)-4-((2-methoxybenzylidene)amino)isoxazolidine-3-one

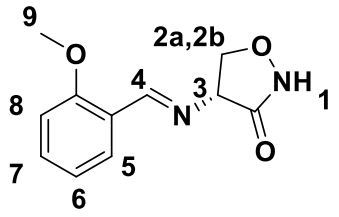

$C_{11}H_{12}N_2O_3$
Exact Mass: 220.08
Molecular Weight: 220.23

Obtained from *o*-anisaldehyde (0.200 g, 1.46 mmol, 1.0 equiv) and D-cycloserine (0.226 g, 2.20 mmol, 1.5 equiv) as a white solid (0.151 g, 46%); m.p 339.7-340.2 °C; δ_H (400 MHz, DMSO-d_6): 8.38 (s, 1H, NH-1), 8.35 (s, 1H, H-4), 7.63 (dd, *J* = 7.66, 1.72 Hz, 1H, H-5), 7.40 (ddd, *J* = 8.35, 7.52, 1.81 Hz, 1H, H-7), 7.06 (d, *J* = 8.35 Hz, 1H, H-8), 6.95 (dd, *J* = 8.79, 7.66 Hz, 1H, H-6), 4.38-4.28 (m, 2H, H-2a, H-2b), 4.18-4.13 (m, 1H, H-3), 3.76 (s, 3H, 3x H-9); δ_C (101 MHz, DMSO-d_6) 165.85, 165.37, 157.76, 145.69, 132.20, 126.48, 121.10, 112.32, 75.36, 56.16, 54.32

Compound 1.8: (R,E)-4-((4-fluorobenzylidene)amino)isoxazolidin-3-one

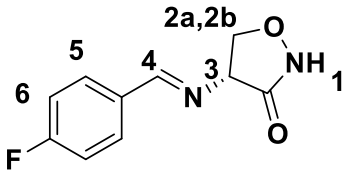

$C_{10}H_9FN_2O_2$
Exact Mass: 208.06
Molecular Weight: 208.19

Obtained from 4-flurobenzaldehyde (0.200 g, 1.61 mmol, 1.0 equiv) and D-cycloserine (0.248 g, 2.41 mmol, 1.5 equiv) as a white solid (0.138 g, 41%); m.p 263.4-266.0 °C; ^{1}H-NMR (400 MHz, DMSO-d_6) δ 8.33 (s, 1H, NH-1), 8.25 (s, 1H, H-4), 7.65 (ddd, *J* = 8.71, 5.40, 2.58 Hz, 2H, 2x H-5), 7.23 (ddd, *J* = 8.89, 5.32, 2.58 Hz, 2H, 2x H-6), 4.43-4.32 (m, 2H, H2a, H2b), 4.17-4.13 (m, 1H, H3); δ_C (101 MHz, DMSO-d_6): 174.98, 165.40, 164.80, 149.21, 129.69 (d, *J* = 8.50 Hz, 2C), 116.31 (d, *J* = 22.01 Hz, 2C), 75.53, 55.09; δ_F (377 DMSO-d_6): -110.54

Compound 1.9: (R, E)-4-((3-fluorobenzylidene)amino)isoxazolidine-3-one

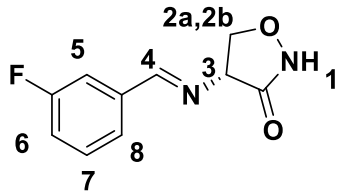

$C_{10}H_9FN_2O_2$
Exact Mass: 208.06
Molecular Weight: 208.19

Obtained from 3-flurobenzaldehyde (0.200 g, 1.61 mmol, 1.0 equiv) and D-cycloserine (0.248 g, 2.41 mmol, 1.5 equiv) as a white solid (0.016 g, 4.95%); m.p 240.2-242.4 °C; δ_H (400 MHz, DMSO-d_6): 8.38 (s, 1H, NH-1), 8.35 (s, 1H, H-4), 7.50-7.38 (m, 2H, H H-7, H-8), 7.43-7.39 (m, 1H, H5), 7.30-7.22 (m, 1H, H-6), 4.45-4.31 (m, 2H, H-2a, H-2b), 4.20-4.16 (m, 1H, H-3); δ_C (101 MHz, DMSO-d_6): 163.91, 161.49, 134.61 (d, *J* = 8.29 Hz), 131.32 (d, *J* = 8.34 Hz), 123.80, 117.33 (d, *J* = 21.37 Hz), 113.66 (d, *J* = 22.69 Hz), 75.49, 55.08; ^{19}F (377 DMSO-d_6) δ -112.74.

Compound 1.10: (R,E)-4-((2-fluorobenzylidene)amino)isoxazolidin-3-one

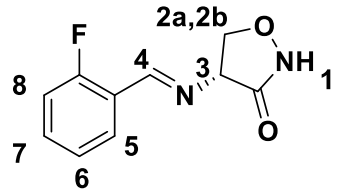

$C_{10}H_9FN_2O_2$
Exact Mass: 208.06
Molecular Weight: 208.19

Obtained from 2-flurobenzaldehyde (0.200 g, 1.61 mmol, 1.0 equiv) and D-cycloserine (0.248 g, 2.41 mmol, 1.5 equiv) as a white solid (0.151 g, 49%); m.p 235.2-237.1 °C; δ_H (400 MHz, DMSO-d_6) 8.39 (s, 1H, NH-1), 8.32 (s, 1H, H-4), 7.72 (dd, *J* = 7.60, 1.83 Hz 1H, H-5), 7.52-7.43 (m, 1H, H-7), 7.27 (dd, *J* = 7.87, 7.35 Hz, 1H, H-6), 7.22 (d, *J* = 6.90 Hz, 1H, H-8) 4.44-4.32 (m, 2H, H-2a, H-2b), 4.24-4.15 (m, 1H, H-3); δ_C (101 MHz, DMSO-d_6) 165.85, 161.81, 159.32, 132.68 (d, *J* = 8.58 Hz), 127.68, 125.29, 119.61 (d, *J* = 10.67 Hz), 116.52 (d, *J = 20.68* Hz), 76.87, 55.07; δ_F (377 DMSO-d_6) δ -118.60.

Compound 1.11: (R,E)-4-((4-bromobenzylidene)amino)isoxazolidin-3-one

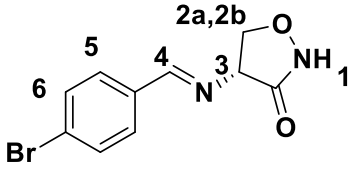

$C_{10}H_9BrN_2O_2$
Exact Mass: 267.98
Molecular Weight: 269.10

Obtained from 4-bromobenzaldehyde (0.200 g, 0.74 mmol, 1.0 equiv) and D-cycloserine (0.114 g, 1.11 mmol, 1.5 equiv) as a white solid (0.082 g, 28%); m.p 282.2-283.4 °C; δ_H (400 MHz, DMSO-d_6) 8.26 (s, 1H, NH-1), 8.24 (s, 1H, H-4), 7.61 (d, *J* = 8.65 Hz, 2H, 2x H-5), 7.54 (d, *J* = 8.50 Hz, 2H, 2x H-6), 4.47-4.31 (m, 2H, H-2a, H-2b), 4.19-4.16 (m, 1H, H-3); δ_C (101 MHz, DMSO-d_6) 167.3, 165.38, 149.32, 132.24 (2C), 129.35 (2C), 123.83, 75.56, 55.23.

General procedure for compounds 3.1 and 3.6

For compound **3.1**, a solution containing D-CS (1.2 equiv) was added to the relevant acyl chloride (1.0 equiv) and was treated with triethylamine (1.5 equiv) in N-methyl-2-pyrrolidone (NMP). For compound **3.6**, twice the equivalence of D-CS and triethylamine was used. The reaction was left to stir at room temperature (18–20 °C) for 1–1.5 h. The solvent was removed using a GeneVac evaporator. The crude product was then purified via column chromatography on silica gel using 80% EtOAc/Hex to produce a white solid.

Compound 3.1: (R)-N-(3-oxoisoxazolidin-4-yl)benzamide

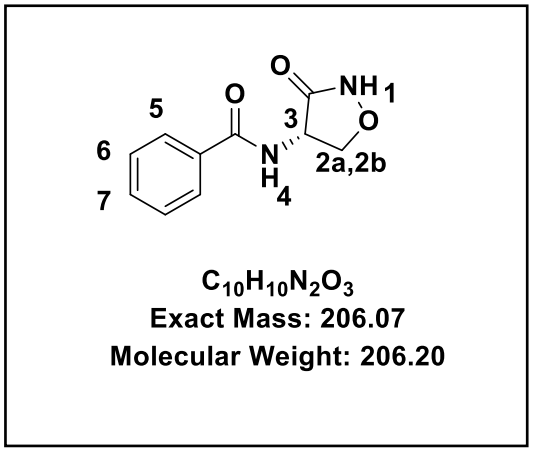

Obtained from benzoyl chloride (0.300 g, 2.13 mmol, 1.0 equiv), D-cycloserine (0.264 g, 2.56 mmol, 1.2 equiv) treated with triethylamine (0.44 mL, 1.5 equiv) as a white solid (54.7 mg, 19%); m.p. 187.3–186.6 °C; R_f (EtOAc: Hex, 8:2) 0.13; δ_H (400 MHz, DMSO-d_6): 11.49 (s, 1H, H-1), 8.92 (d, *J* = 8.21 Hz, 1H, H-4), 7.87 (dd, *J* = 7.06, 1.42 Hz, 1H, 2x H-5), 7.54 (dd, *J* = 6.90, 1.42 Hz, 1H, 2x H-7), 7.48 (dd, *J* = 8.32, 6.90 Hz, 2H, 2x H-6), 5.04 (q, *J* = 9.23 Hz, 1H, H-3), 4.57 (t, *J* = 8.53 Hz, 1H, H-2b), 4.11 (dd, *J* = 10.36, 8.28 Hz, 1H, H-2a); δ_C (101 MHz, DMSO-d_6): 170.54, 166.38, 133.50, 131.51, 128.26 (2C), 127.29 (2C), 71.70, 51.44; HPLC-MS (APCI/ESI): purity = 96%, t_R = 0.45 min, m/z $[M+H]^+$= 207.07.

Compound 3.6: N^1-((R)-3-oxoisoxazolidin-4-yl)-N^4-((S)-3-oxoisoxazolidin-4-yl)terephthalamide

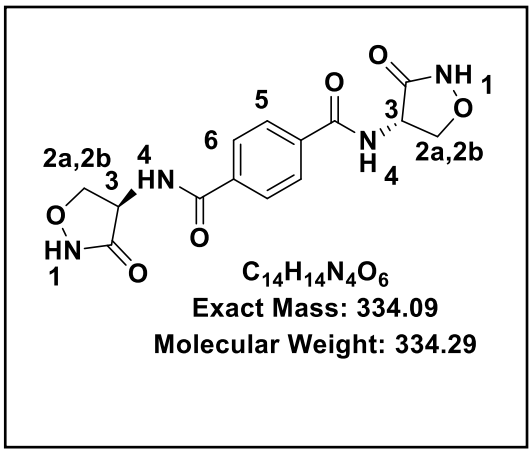

*Please see chapter 2 for spectrum and more in detailed analysis.

Obtained from terephthaloyl dichloride (0.200 g, 0.99 mmol, 1.0 equiv), D-cycloserine (0.201 g, 1.97 mmol, 2.0 equiv) treated with triethylamine (0.41 mL, 3 equiv) as a white solid (47.2 mg, 14%); m.p. 366.1–368.2 °C; R_f (MeOH: DCM) 0.08; δ_H (400 MHz, DMSO-d_6): 11.51 (s, 2H, H-1), 9.08 (d, *J* = 8.21 Hz, 2x H-4), 7.97 (s, 4H, 4x H-5), 5.05 (q, *J* = 9.06 Hz, 2H, 2x H-3), 4.58 (t, *J* = 8.57 Hz, 2H, 2x H-2b), 4.12 (dd, *J* = 10.23, 8.36 Hz, 2H, 2x H-2a); δ_C (101 MHz, DMSO-d_6) 170.88 (2C), 166.40 (2C), 136.76 (2C), 127.88 (4C), 72.43 (2C), 52.28 (2C); HPLC-MS (APCI/ESI): purity > 99%, t_R = 0.29 min, m/z $[M+H]^+$ = 335.09.

General procedure for compounds 3.2 and 3.3

The relevant carboxylic acid was solubilized in thionyl chloride (3.0 equiv). The solution was heated under reflux at 85.5 °C and the solvent was removed under reduced pressure, yielding the relevant crude acyl chloride, which was used without purification. The relevant acyl chloride (1.0 equiv) was solubilized into a solution of D-CS (1.2 equiv) and triethylamine (1.5 equiv) in DMF. The reaction was left to stir at room temperature (18–20 °C) for 1–1.5 h. DMF was removed *in vacuo* and the resulting crude mixture was purified via silica gel chromatography using the relevant solvent system. Combined fractions were concentrated *in vacuo* and dried under the vacuum to yield the relevant target compounds 3.2-3.3**.**

Compound 3.3: (R)-4-bromo-N-(3-oxoisoxazolidin-4-yl)benzamide

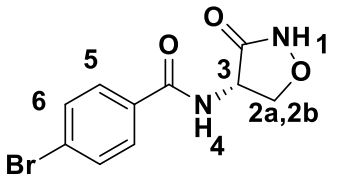

$C_{10}H_9BrN_2O_3$
Exact Mass: 283.98
Molecular Weight: 285.10

Obtained from 4-bromobenzoyl chloride (0.300 g, 1.37 mmol, 1.0 equiv), D-cycloserine (0.168 g, 1.64 mmol, 1.2 equiv) treated with triethylamine (0.38 mL, 1.5 equiv) using 80% EtOAc/Hex as a eluent to afford a white solid (20.8 mg, 5.33%); m.p 317.4–313.8 °C; R_f (EtOAc: Hex, 8:2) 0.14; δ_H (400 MHz, DMSO-d_6) 11.49 (s, 1H, H-1), 9.02 (d, *J* = 8.19 Hz, 1H, H-4), 7.82 (d, *J* = 8.63 Hz, 2H, 2x H-5), 7.70 (d, *J* = 8.57 Hz, 2H, 2x H-6), 5.05-4.99 (m, 1H, H-3), 4.57 (t, *J* = 8.6 Hz, 1H, H-2b), 4.10 (dd, *J* = 10.2, 8.4 Hz, 1H, H-2a); δ_C (101 MHz, DMSO-d_6): 166.03, 133.16, 131.94 (2C), 129.98 (2C), 125.87, 72.25, 52.07; HPLC-MS (APCI/ESI): purity = 96%, t_R = 0.75 min, m/z $[M+H]^+$ = 284.9, 285.9, 286.9, 287.9.

Compound 3.2: (R)-4-methoxyl-N-(3-oxoisoxazolidin-4-yl)benzamide

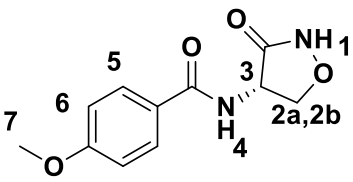

$C_{11}H_{12}N_2O_4$
Exact Mass: 236.08
Molecular Weight: 236.23

Obtained from 4-methoxybenzoyl chloride (0.300 g, 1.758 mmol, 1.0 equiv), D-cycloserine (0.217 g, 2.113 mmol, 1.2 equiv) treated with triethylamine (0.61 mL, 1.5 equiv) using 90% EtOAc/Hex as a eluent to afford a white solid (20 mg, 21%); m.p 315.2–317.8 °C; R_f (EtOAc: Hex, 8:2) 0.13; δ_H (400 MHz, DMSO-d_6), 11.44 (s, 1H, H-1), 8.74 (d, *J* = 8.08 Hz, 1H, H-4), 7.87 (d, *J* = 8.88 Hz, 2H, 2x H-5), 7.02 (d, *J = 8.87* Hz, 2H, 2x H-6), 5.06-4.93 (m, 1H, H-3), 4.54 (t, *J* = 8.6 Hz, 1H, H-2b), 4.20-4.08 (m, 1H, H-2a), 3.81 (s, 3H, 3X H-7); δ_C (101 MHz, DMSO-d_6): 166.37, 165.40, 162.36, 159.68, 129.75 (2C), 114.05 (2C), 72.33, 55.86, 55.10; HPLC-MS (APCI/ESI): purity > 99%, t_R = 0.57 min, m/z $[M+H]^+$ = 237.38.

General procedure for compound 3.4

Pyrazine-2-carboxylic acid (1 equiv) was solubilized in thionyl chloride (3.0 equiv). The solution was heated under reflux at 85.5 °C. Thionyl chloride was removed under pressure, yielding pyrazine-2-carbonyl chloride, which was used without further purification. Pyrazine-2-carbonyl chloride was solubilized into a solution of D-CS (1.2 equiv) and triethylamine (2.5 equiv) in DMF. The reaction was left to stir at room temperature (24–26 °C) for 1–1.5 h. DMF was removed *in vacuo* and the resulting crude mixture was dry-loaded on ISOLUTE® and purified using a reversed-phase ISCO CombiFlash system eluting with a gradient (0 to 10%, 0.1% formic acid in acetonitrile and 0.1% trifluoroacetic acid (TFA) in water). The combined pure fractions were concentrated *in vacuo* and dried under vacuum to yield the relevant target compound 3.4.

Compound 3.4: (R)-N-(3-oxoisoxazolidin-4-yl)pyrazine-2-carboxamide

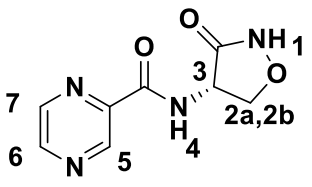

$C_8H_8N_4O_3$
Exact Mass: 208.06
Molecular Weight: 208.18

*Please see chapter 2 for spectrum and more in detailed analysis.

Obtained from pyrazine-2-carboxylic chloride (0.800 g, 5.61 mmol, 1.0 equiv), D-cycloserine (0.686 g, 6.73 mmol, 1.2 equiv) treated with triethylamine (1.19 mL, 1.5 equiv) as a white solid (247.0 mg, 21%); m.p. 313.5–318.2 °C; R_f (EtOH: DCM, 1:9) 0.63; δ_H (400 MHz, DMSO-d_6) 11.55 (s, 1H, H-1), 9.32 (d, *J* = 8.3 Hz, 1H, H-4), 9.20 (d, *J* = 1.46 Hz, 1H, H-5), 8.90 (d, *J* = 2.43 Hz, 1H, H-6), 8.77 (dd, *J* = 2.43, 1.63 Hz, 1H, H-7), 5.06 (dt, *J* = 11.05, 8.57 Hz, 1H, H-3), 4.57 (t, *J* = 8.48 Hz, 1H, H-2b), 4.25 (dd, *J* = 11.06, 8.17 Hz, 1H,H-2a); δ_C (101 MHz, DMSO-d_6) 170.65, 163.08, 148.34, 144.69, 144.02 (2C), 71.78, 51.75; HPLC-MS (APCI/ESI): purity > 99%, t_R = 0.17 min, m/z $[M-H]^+$ = 207.10.

General procedure for compound 3.5

5-((Tert-butoxycarbonyl)amino)picolinic acid (1 equiv) was added to a solution of 1,1'-carbonyldiimidazole (CDI, 2.5 equiv) in DMF and the resulting mixture was stirred for 1 h at 18 °C. In a separate round-bottom flask, D-CS (2.5 equiv) was added to a catalytic amount of 4-dimethylaminopyridine (DMAP) in DMF and the resulting mixture was left to stir for 5 min. The solution containing D-CS was added dropwise to the flask containing the acid and the resulting mixture was stirred at 18–20 °C for 20 h. After completion of the reaction (monitored via TLC), DMF was removed *in vacuo* and the resulting crude mixture was purified via column chromatography (15% MeOH/DCM) to produce compound 3.5.

Compound 3.5: Tert-butyl (R)-(6-((3-oxoisoxazolidin-4-yl)carbamoyl)pyridin-3-yl)carbamate

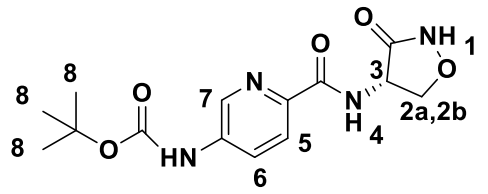

$C_{14}H_{18}N_4O_5$
Exact Mass: 322.13
Molecular Weight: 322.32

White solid (10.0 mg, 10%); m.p. 323.2–325.1 °C; R_f (EtOH: DCM, 1:9) 0.54; δ_H (400 MHz, DMSO-d_6) 9.91(s, 1H, H-1), 8.66 (d, *J* = 8.3 Hz, 1H, H-4), 9.20 (d, *J* = 1.46 Hz, 1H, H-5), 8.90 (d, *J* = 2.66 Hz, 1H, H-6), 8.05 (dd, *J* = 8.48, 2.63 Hz, 1H, H-7), 4.98 (dt, *J* = 11.04, 8.05 Hz, 1H, H-3), 4.57 (t, *J* = 8.48 Hz, 1H, H-2b), 4.20 (dd, *J* = 11.13, 8.09 Hz, 1H,H-2a); δ_C (101 MHz, DMSO-d_6) 170.50, 166.91, 160.74, 152.29, 149.72, 138.50, 132.42, 123.35, 88.92, 67.52, 64.75, 59.30, 26.91 (3C); HPLC-MS (APCI/ESI): purity > 99%, t_R = 0.17 min, m/z $[M-H]^+$ = 322.13

6.3 Methods: Biology

6.3.1 Turbidimetric solubility

The turbidimetric method described by Bevan and Lloyd[1] was adapted to estimate the aqueous solubility of the final target compounds at pH 7.4. Stock solutions (10 mM) of target and control compounds (reserpine and hydrocortisone) were prepared in HPLC-grade DMSO. Subsequently, stock solutions were serially diluted in triplicate by first pipetting 20 µL DMSO into row G and 50 µL DMSO in the rows above (**Figure 5.1**). Next, 80 µL of the 10 mM stock solutions was pipetted into row G and mixed to obtain a starting concentration of 8 mM (100 µL). This solution was serially diluted by transferring 50 µL from row F through to row B. The final pre-dilution concentrations obtained ranged from 0.25 mM (row B) to 8.0 mM (row G). The wells in row A contained only DMSO, while those in row H contained the undiluted 10 mM stock solution.

		Compound 1 (triplicate)			Compound 2 (triplicate)			Compound 3 (triplicate)			Compound 4 (triplicate)		
Conc. (mM)		**1**	**2**	**3**	**4**	**5**	**6**	**7**	**8**	**9**	**10**	**11**	**12**
0	**A**												
0.25	**B**												
0.5	**C**												
1.0	**D**												
2.0	**E**												
4.0	**F**												
8.0	**G**												
10.0	**H**												

Figure 6.1: Layout of the turbidimetric solubility assay compound pre-dilution plate

From each pre-dilution solution, secondary dilutions were prepared in DMSO and 0.01 M phosphate buffered saline (PBS, pH 7.4) in a second 96-well microtiter plate in triplicate (**Figure 5.2**). Wells in columns 1-6 contained the test compound dissolved in DMSO while those in columns 7-12 contained the same compound dissolved in PBS. The final volume in each well was 200 µL, prepared by pipetting 4 µL of each solution from the pre-dilution plate to the corresponding well into both DMSO and PBS (196 µL each). The final concentration of DMSO in the PBS aqueous buffer preparations was therefore 2% v/v. Test compounds in DMSO served as controls to determine potential false turbidimetric absorbance readings arising from the compounds in solution absorbing radiation at the analysis wavelength.

		DMSO						0.01 M PBS (pH 7.4)					
		Compound 1 (triplicate)			Compound 2 (triplicate)			Compound 1 (triplicate)			Compound 2 (triplicate)		
Conc. (µM)		**1**	**2**	**3**	**4**	**5**	**6**	**7**	**8**	**9**	**10**	**11**	**12**
0	**A**												
5	**B**												
10	**C**												
20	**D**												
40	**E**												
80	**F**												
160	**G**												
200	**H**												

Figure 6.2: Turbidimetric solubility assay plate layout

The plates were covered and left to equilibrate for 2 h at room temperature. UV-VIS absorbance values were then recorded at 620 nm using a SpectraMax 340PC384 microplate reader (Molecular Devices, Sunnydale, CA, USA). The wells containing only DMSO and 2% v/v DMSO in PBS (0 µM in plate layout, row A) served as controls and blanks. At concentrations above the solubility limit, undissolved particles precipitated out of solution, occluding incident radiation and resulting in increased apparent absorbance. Therefore, the concentration at which increased absorbance was recorded was considered to be the approximate solubility of the compounds. Reserpine and hydrocortisone were used as minimum and maximum solubility standards respectively, as established by previous reports.[9]

6.3.2 HPLC-based solubility

Kinetic solubility measurements were obtained by Nina Lawrence at the Holistic Drug Discovery and Development centre (H3D). Aqueous solubility was measured using the DMSO dry-down method, adapted from Zhou et al.[2,3] Briefly, the high and medium calibration standards (220 and 100 µM, respectively) were added in duplicate and samples (200 µM) were added in triplicate to a 96-well plate from a 10 mM stock solution in DMSO. DMSO was then evaporated in a MiVac sample concentrator (SP Scientific, Cape Town, South Africa) operated at full vacuum at 37 °C for 2 h. DMSO was then added to the standards and after vortexing the plate, the high standard was used to prepare a low (11 µM) calibration standard in DMSO. PBS (pH 7.4) was added to the sample wells and the plate was incubated for 24 h at 25 °C with shaking. The plate was then centrifuged at 2500 × *g* for 30 min and the supernatants were transferred to another plate for analysis. Aqueous solubility was determined from the UV peak areas of the samples relative to those of the standards using best-fit calibration curves in Microsoft Excel 2013. HPLC-DAD analysis was performed using an Agilent 1200 Rapid Resolution HPLC instrument, coupled with an Agilent 1200 diode array detector (ABSciex, Johannesburg, South Africa). For elution, 0.1% formic acid in water and 0.1% formic acid acetonitrile were used as mobile phases A and B, respectively. A Kinetex C18 (50 mm x 2.1 mm) column packed with 2.6-µM fused-core particles (Separations, Johannesburg, South Africa) was used for chromatography. Agilent Chemstation for used for instrument control and data processing.

6.3.3 Bacterial strains and growth conditions

For all antimycobacterial experiments carried out, *M. smegmatis* (Mc^2155)[4] (Msm) and *M. tuberculosis* H37Rv[5] (Mtb) strains from stocks maintained at H3D at -80 ^oC were used. In the case of Msm, the stocks were stored in 33% glycerol (v/v). All culturing and manipulations of Mtb were performed by Tb biology team in a Biosafety Level 3 laboratory at IDM. For experiments carried out using ESKAPE pathogens, strains of *Staphylococcus aureus, Acinetobacter baumannii, Klebsiella pneumoniae,* and *Escherichia coli* from stocks maintained by H3D at -80 ^oC were used (**Table 5.1**).

Table 6.1 : Bacterial strains used in this study

Bacterial species strain	Strain
Mycobacterium smegmatis	Non-virulent reference laboratory of *Msm* Mc^2 155
Mycobacterium tuberculosis	Virulent reference laboratory strain of *Mtb* H37Rv ATCC 27294
Staphylococcus aureus	ATC 25923
Acinetobacter baumannii	ATCC 19606
Klebsiella pneumoniae	ATCC BAA-1705
Escherichia coli	ATCC 25922

Mtb and ESKAPE Pathogens was cultured in Middlebrook 7H9 (Difco™) broth enriched with 10% oleic acid-dextrose-catalase (OADC), 0.5% glycerol, and 0.05% Tween® 80. Growth medium was were filtered using filtration flasks fitted with 0.22-µm filter membranes. M. smeg was cultured in liquid broth (LB) and were sterilized by autoclaving at 121 ^{o}C for 15 min.

6.3.4 Antimycobacterial screening: minimum inhibitory concentration (MIC) of target compounds in *Msm*, *Mtb*, and ESKAPE pathogens

The MICs of synthesized compounds were determined via broth microdilution method using the microplate Alamar Blue assay (MABA). This method allows determination of the MICs of compounds over a range of concentrations in a single 96-well microtiter plate.[6] In the MABA assay, the metabolic activity of the cell is correlated with Alamar Blue reduction and the resulting change in colour from blue to pink and fluorescent allows for visual detection and fluorometric or colorimetric quantification. For the experiments reported here, growth and growth inhibition were assessed visually. Prior to the addition of Alamar Blue (at day 3 for Msm and day 7 for Mtb), growth and inhibition were assessed via visual inspection for pellet formation, while growth and inhibition were assessed via visual inspection for pellet formation only for the ESKAPE pathogens.

As described in Standard lab operating protocols (SOPs), a 10-mL Mtb culture was grown to reach an OD_{600} of 0.6–0.7 and diluted to 1:500 (in the case of Mtb) and/or 1:1000 (in case of Msm or ESKAPE pathogens) in the relevant medium. In a 96-well microtitre plate, 50 µL of the relevant medium was added to all wells in rows 2–12. Target compounds were added to row 1 at a final concentration of 8 × MIC_{90} (for compounds with pre-determined or estimated MIC values) and serially diluted (two-fold). This was achieved by transferring 50 µL of the liquid in row 1 to row 2 using a multichannel pipette and mixing. Subsequently, 50 µL of the liquid in row 2 was transferred to row 3 and mixed. The procedure was repeated until row 11, from which 50 µL was discarded to bring the final volume in these wells to 50 µL. In row 12, the relevant control (1 mg/mL) was added for maximal inhibition

before adding 50 µL diluted culture was added to all wells. The microtitre plate was stored in a secondary container and incubated at 37 °C for 24 h (Msm) or 14 days (Mtb). On Day 1 (Msm) and Day 14 (Mtb), Alamar Blue (BUF012B, Celtic Molecular Diagnostics) was added to each well and plates were incubated at 37 °C for 6 and 24 h, respectively. Post incubation, the MIC results were visually scored and calculated. MIC are defined as the lowest concentration of compound that inhibited visible growth. The lowest concentration of drug that prevented the colour change from blue to pink) was recorded as the MIC inhibiting >90% of the bacterial population.

6.3.5 *In vitro* cytotoxicity assay

The *in vitro* cytotoxicity of target compounds was tested against mammalian cell-lines (Chinese Hamster ovarian (CHO) cells and HepG2 cells) in a 3-(4,5-dimethylthiazol-2-yl)-2,5-diphenyltetrazoliumbromide (MTT) assay at the Division of Clinical Pharmacology, University of Cape Town. The MTT assay is a colorimetric assay used to assess cellular growth and survival.[7,8] Reduction of the tetrazolium salt MTT to a formazan salt was used to measure all growth and chemosensitivity. The final target compounds were tested in triplicate. Stock solutions of the target compounds (20 mg/mL) were prepared in 10% methanol or 10% DMSO and were used as a suspension if not properly dissolved. Final target compounds were stored at -20 ºC until further use. Emetine was used as the control drug in all experiments. The initial concentration of each compound was 100 µg/mL, which was serially diluted in complete medium with 10-fold dilutions to obtain six concentrations, the lowest being 0.001 µg/mL. Plates were developed after 44 h exposure to the drug by the addition of a solution of MTT. After 4 h incubation at 37 ºC, the supernatant was removed via suction and DMSO was added to each well to dissolve the reduced dye crystals. The absorbance was measured at a wavelength of 540 nm using a spectrophotometer to determine the relative amount of formazan in each well. The 50% inhibitory concentration (IC_{50}) values were obtained from full dose-response curves via non-linear dose-response curve fitting analysis using GraphPad Prism v.4 software.

6.3.6 *In vitro* metabolic stability studies

The metabolic stability of compounds was assessed in mouse, rat, and human liver microsomes at the pre-clinical pharmacology laboratory at Groote Schuur Hospital. All compounds were prepared as 10-mM stock solutions in DMSO. Test compounds (1 µM) were incubated at 37 °C in a solution containing 0.35 mg/mL microsomes (mouse liver microsomes (MLM), male mouse BALB/c, Xenotech; rat liver microsomes (RLM), male rat IGS, Xenotech; human liver microsomes (HLM), mixed gender, Xenotech) and NADPH (1 mM) in phosphate buffer (100 mM, pH 7.4) for 30 min while shaking. The samples were then precipitated out of solution using cold-ice acetonitrile containing 0.1 µM carbamazepine (internal

standard), centrifuged, and filtered for LC-MS analysis. The experiments were performed in triplicate and three controls (propranolol, midazolam, and MMV390048) were also included. Results are reported as percentage drug remaining unchanged after 30-min incubation and predicted half-life estimated using Obach's formula.

LC-MS/MS analysis was performed on a 4000 Q-TRAP (AB SCIEX) instrument with a Turbo V® ion source coupled to an Agilent 1200 Rapid Resolution (600 bar) HPLC system. ESI mode was used for assessment of all synthetic compounds. Analyst 1.5.1 software was used for instrument control and data acquisition. Metabolic stability analysis was performed using a Kinetex PFP column (2.1 mm × 50 mm, 2.6 µm; Phenomenex) or a Kinetex C18 column (2.1 mm × 50 mm, 2.6 µm; Phenomenex) with a gradient of 0.4 mL/min (mobile phase A, 0.1% formic acid; B, 0.1% formic acid in acetonitrile) at 40 °C. The sample tray temperature was 8 °C and the injection volume used was 2 µL. Multiple reaction monitoring (MRM) mode was used for quantification of the parent compound before and after incubation in liver microsomes.

6.4 References

(1) Bevan, C. D.; Lloyd, R. S. A High-Throughput Screening Method for the Determination of Aqueous Drug Solubility Using Laser Nephelometry in Microtiter Plates. *Anal. Chem.* **2000**, *72* (8), 1781–1787.

(2) Zhou, L.; Yang, L.; Tilton, S.; Wang, J. Development of a High Throughput Equilibrium Solubility Assay Using Miniaturized Shake-Flask Method in Early Drug Discovery. *J. Pharm. Sci.* **2007**, *96* (11), 3052–3071.

(3) Hill, A. P.; Young, R. J. Getting Physical in Drug Discovery: A Contemporary Perspective on Solubility and Hydrophobicity. *Drug Discov. Today* **2010**, *15* (15–16), 648–655.

(4) Snapper, S. B.; Melton, R. E.; Kieser, S. M. T. Isolation and Characterization of Efficient Plasmid Transformation Mutants of Mycobacterium Smegmatis. *J. Bacteriol.* **1990**, *4*, 1911–1919.

(5) Ioerger, T. R.; Feng, Y.; Ganesula, K.; Chen, X.; Dobos, K. M.; Fortune, S.; Jacobs, W. R.; Mizrahi, V.; Parish, T.; Rubin, E.; et al. Variation among Genome Sequences of H37Rv Strains of Mycobacterium Tuberculosis from Multiple Laboratories. *Antimicrob.Agent Chemother* **2010**, *192* (14), 3645–3653.

(6) Collins, L. A.; Franzblau, S. G. Microplate Alamar Blue Assay versus BACTEC 460 System for High-Throughput Screening of Compounds against Mycobacterium Tuberculosis and Mycobacterium Avium. *Antimicrob.Agent Chemother* **1997**, *41* (5), 1004–1009.

(7) Mosmann, T. Rapid Colorimetric Assay for Cellular Growth and Survival: Application to Proliferation and Cytotoxicity Assays. *J. Immunol. Methods* **1983**, *65*, 55–63.

(8) Shoemaker, L. V. R. R. H.; Paull, K. D.; Simon, R. M.; Tosini, S.; Skehan, P.; Scudiero, D. A.; Monks, A.; Boyd, M. R. Comparison of In Vitro Anticancer-Drug-Screening Data Generated With a Tetrazolium Assay Versus a Protein Assay Against a Diverse Panel of Human Tumor Cell Lines. *J. Natl. Cancer Inst.* **1990**, *82*, 1113–1118.

(9) Bevan, C. D.; Lloyd, R. S. *Anal. Chem.* **2000**, *72* (8), 1781–1787.